DISSERTATION

submitted to the

Faculty of Chemistry and Earth Sciences

of the University of Heidelberg, Heidelberg, Germany

in partial fulfilment of the requirements for the degree of

Doctor of Natural Sciences (Dr. rer. nat.)

submitted by

Xin Du (M.Sc. polymer science)

born in Ganzhou, China

Supervisors: Dr. Pavel A. Levkin and Prof. Dr. Michael Grunze

Oral examination: May 29th, 2015

DISSERTATION

Zur Erlangung der Doktorwürde

Der Naturwissenschaftlich-Mathematischen

Gesamtfakultät der

Ruprecht-Karls-Universität Heidelberg

vorgelegt von

Xin Du (M.Sc. Polymerwissenschaft)

Geboren in Ganzhou, China

Betreuer: Dr. Pavel A. Levkin und Prof. Dr. Michael Grunze

Tag der mündlichen Prüfung: 29. Mai 2015

Surface functionalization and surface patterning based on UV-induced dopamine polymerization and disulfide exchange strategies

This dissertation was carried out at the

Department of Applied Physical Chemistry

Heidelberg University

Referees:

Prof. Dr. Michael Grunze

Prof. Dr. Michael Zharnikov

Abstract

Surface functionalization methods are very important for modern science and technology in order to endow surfaces with various novel and unique properties. Examples include slippery property, antibacterial and antifouling properties, superhydrophobicity and superhydrophilicity, biocompativity and conductivity. As an important branch of surface functionalization, surface patterning has attracted a lot of attention. Patterned surfaces can find a wide range of applications in various fields such as microfluids, printing devices, sensors and diagnose devices to name a few. Photo-based surface functionalization is one of the most powerful surface modification and patterning methods due to its controllability both spatially and temporally. Different goals could be achieved by surface modification, for example, addition or remove of functionalities and formation of 3D morphologies. This thesis contains three parts, which deal with different topics related to surface functionalization.

Part I demonstrates the method of UV control of dopamine (DA) polymerization and polydopamine (PD) deposition. PD coating is a recent surface modification strategy inspired by the adhesive performance of mussels. DA is able to self-polymerize in aqueous solutions under basic conditions. The adhesive nature of the resulting PD, allows it to attach to any immersed substrates forming a PD layer. Further functionality can be introduced using the reactivity of PD layer towards thiols, amines and metal ions. The simplicity, generality, and the possibility of versatile secondary modifications have promoted the PD coating method to be a promising coating strategy in many fields. Since the first report in 2007, PD coatings have been widely applied in different fields. Currently, the main drawback of the PD coating method is the lack of spatial and temporal control during the polymerization process, limiting its applications and making the mechanism investigations difficult. On the other hand, photo-assisted methods have been widely investigated and are known to be highly controllable. The idea of introducing the control offered by photo-assisted reactions into DA polymerization might result in a more controllable PD coating strategy. In this thesis, it was shown that reactive oxygen species (ROS), formed upon UV irradiation of oxygen-containing solutions, could serve as oxidants for DA. Therefore, UV light could be used to achieve a better control over the DA polymerization. I investigated the effects of UV irradiation on DA solutions. It was found that DA polymerization was accelerated by UV irradiation, and that under neutral conditions a well-controlled DA polymerization could be achieved. By cooperation with an antioxidant, sodium ascorbic acid (SA), DA polymerization in basic solutions can also be well-controlled. UV-triggered DA polymerization could be used to

perform long term control of DA polymerization, and could be applied on PD coating to result in PD patterns. DA polymerization and PD deposition was characterized by UV-Vis spectroscopy, X-Ray photoelectron spectroscopy (XPS), ellipsometry, atom force microscopy (AFM), infrared reflective absorption specotroscopy (IRRAS), time-of-flight secondary ion mass spectroscopy (ToF-SIMS), X-ray reflectivity (XRR) and scanning electron microscopy (SEM).

In the part II, a photo based reversible surface modification strategy is demonstrated. Reversible surface modification represents a new generation of surface modification strategies because they are capable of producing reversible surfaces with reversible properties. Reversible surface exhibits significant advantages compared to normal functional surface, for example, the capability of "write and erase" process, possibility to renew and reuse the surface, formation of complex, multi-component and gradient patterns, capture-and-release properties, and the possibility of in-situ manipulation of local environments. However, currently most reported reversible surface functionalization strategies suffer from time-cost reversible cycle and non-controllable processes, which greatly limit potential applications of the method. In order to develop a smart reversible photopatterning strategy, I introduced a photodynamic disulfide exchange reaction as a method for surface modification. Surface photo-disulfide exchange was applied and characterized on a porous HEMA-EDMA surface. The results showed that reversible photopatterning could easily be achieved and that the kinetics of the exchange is extremely fast. A reversible photo functionalization/patterning strategy could also be obtained. The disulfide exchange reaction was investigated and analyzed by water contact angle (WCA) measurement, SEM, ToF-SIMS and microscopy.

The part III describes a facile method to create a superhydrophobic surface on different substrates. Superhydrophobic surfaces hold great promise in a variety of applications where extreme water repellency can lead to novel properties and functionalities. Most of the existing techniques, however, require multi-step and laborious procedures as well as only applicable to certain substrates. In the last part of the thesis, I present a facile one-step ("paint-like") method for creating superhydrophobic porous polymer coatings. The approach is based on the anionic polymerization of 2-octyl cyanoacrylate in the presence of aqueous ethanol. This leads to the formation of a highly porous superhydrophobic polymer film. The morphology of the porous structure could be controlled by varying the ethanol/water ratio. The method is fast, convenient, does not require any special equipment, and can be performed in the presence of oxygen. It was shown that the technique could be used to coat variety of materials, is applicable to three-dimensional substrates and leads to the formation of stable and strongly

adherent superhydrophobic coatings. The surface was characterized by WCA measurement, and SEM.

Abstrakt

Oberflächenmodifizierung ist ein wichtiges Thema in der modernen Wissenschaft und Technologie geworden. Der Grund dafür ist die Fähigkeit, Oberflächen mit einer Vielzahl an einzigartigen Eigenschaften, wie Superhydrophilie, Superhydrophobie, Biokompatibilität, Leitvermögen und antibakteriellen oder anwuchsverhindernden Verhalten auszustatten.

Oberflächenpatterning hat als ein wichtiger Zweig der Oberflächenmodifizierung viel Aufmerksamkeit auf sich gezogen. Oberflächen mit Patterns finden Anwendungen in vielen Bereichen, wie der Mikrofluidik, Druckern, Sensoren und diagnostischen Geräten.

Dank seiner zeitlichen und räumlichen Kontrollierbarkeit, die für die Oberflächenmodifizierung entscheidend ist, ist die photobasierende Modifizierung eine der wirksamsten Methoden. Oberflächenmodifizierung umfasst verschiedenste Strategien, wie zum Beispiel die Einführung neuer Funktionalitäten, Entfernung oder Austausch von Funktionalitäten auf der Oberfläche oder Formation von 3D Morphologien. Diese Doktorarbeit stellt die Ergebnisse dreier Projekte vor:

Part I: Kontrolle der Dopaminpolymerisierung durch UV-Strahlung. Part II: Reversible Funkionalisierung und Patterning durch photoinduzierte Disulfid-Austausch-Reaktion, und Part III: Formation einer superhydrophoben Oberfläche durch Polymerisierung von hydrophoben Cyanoacrylate.

Part I stellt die Methode der UV-kontrollierten Dopaminpolymerisierung und die Ablagerung von Polydopamin (PD) dar. Die Polydopamin Beschichtung ist eine Vorgehensweise, die von den adhäsiven Eigenschaften der Muscheln ispiriert ist. Dopamin ist in der Lage unter basischen Bedingungen eigenständig zu polymerisieren. Die adhäsive Natur des daraus resultierenden Polydopamine (PD) erlaubt es ihm, an jedes eingetauchte Substrat zu binden und somit PD Schichten zu bilden. Weiterhin kann die Oberfläche durch die Eigenschaft von PD, mit Thiolen, Aminen und Metallionen zu reagieren, funktionalisiert werden. Die Einfachheit, Allgemeingültigkeit und die Möglichkeit vielseitiger sekundärer Modifikationen der PD Beschichtung machen sie zu einer vielversprechenden Beschichtungsmethode in vielen Bereichen.

Seit der ersten Veröffentlichung 2007 wurden PD Beschichtungen breitflächig in verschiedenen Gebieten angewendet, wie zum Beispiel zur Bildung von biologischen Oberflächen oder Arrays und zur Beschichtung verschiedener Applikationen mit Nanopartikeln. Der zur Zeit größte Nachteil ist der Mangel an räumlicher und zeitlicher Kontrolle während des Ablaufs der Polymerisierung, was somit die Anwendungsmöglichkeiten einschränkt und die Untersuchung des Mechanismus erschwert.

Lichtunterstütze Methoden dahingegen wurden weitgehend untersucht und es ist bekannt, dass diese sehr gut kontrollierbar sind. Die Idee, die Kontrollierbarkeit lichtunterstützter Reaktionen bei Dopaminpolymerisierungen einzuführen, könnte den Vorgang der DP Beschichtungen beeinflussbarer machen.

In dieser Doktorarbeit kam heraus, dass die Dopaminpolymerisierung durch UV-Bestrahlung beschleunigt wird und dass selbst in saurer und neutraler Umgebung eine gut kontrollierte Polymerisierung erreicht werden kann. Der Effekt der UV-Strahlung bei PD-Polymerisierungen wurde im Detail untersucht. Es kam heraus, dass reaktive Sauerstoffspezies (ROS), die durch UV-Bestrahlung von Sauerstoff gebildet wurden, in den beobachteten Anstieg der Polymerisierungskinetik von Dopamin involviert sind. Durch Hinzugabe eines Oxidationsinhibitors, wie zum Beispiel Natriumascorbat (SA), auch unter basischen Bedingungen eine gut kotrollierbare Dopaminpolymerisierung möglich ist. Die Uv-gesteuerte Dopaminpolymerisierung konnte genutzt werden um während des Prozesses über lange Zeit eine kontrollierte Polymerisierung zu haben und konnte für Patterning mit PD-Beschichtungen angewendet werden. Dopaminpolymerisierung und PD-Ablagerungen wurden mittels UV-Vis Spektroskopie, X-Ray Photoelektronenspektroskopie (XPS), Ellipsometrie, Rasterkraftmikroskopie (AFM), Infrarot-Reflexions-Absorptions-Spektroskopie (IRRAS), Sekundärionenmassenspektrometrie (ToF-SIMS), X-Ray Reflektion (XRR) und Rasterelektronenspetroskopie charakterisiert.

In Part II wurde eine photobasierende, reversible Oberflächenmodifizierung gezeigt. Reversible Oberflächenmodifizierungen repräsentieren eine neue Generation der Oberflächenmodifizierungstrategien und weisen signifikante Vorteile, wie die Fähigkeit des „Schreiben und Löschen“-Prozesses, die Möglichkeit der Wiederverwendung der Oberfläche, Formung von Komplex- Multikomponenten- und Gradientenpatterns, Festhaltungs- und Freigabeeigenschaften und die Möglichkeit von in-situ-Manipulationen lokaler Umgebungen, auf. Jedoch bringen die meißten der derzeitig berichteten reversiblen Oberflächenfunktionalisierungen einen zeitaufwändigen reversiblen Zyklus sowie einen nicht kontrollierbaren Prozess mit sich, was die Anwendung der Methode überaus einschränkt. Um eine zügige, reversible, auf PD basierende Photopatterningmethode zu entwickeln, wurde eine photodynamische Disulfid-Tauschreaktion zur Modifikation der Oberfläche eingeführt. Diese Methode wurde zuerst auf einer porösen HEMA-EDMA Oberfläche angewendet und beschrieben. Die Ergebnisse zeigten, die Möglichkeit eines reversiblen Photopatterning auf. Die Disulfid-Tauschreaktion wurde mittels Wasserkontaktwinkelmessung (WCA), SEM, ToF-SIMS und optischer Mikroskopie untersucht und analysiert.

Part III beschreibt eine einfache Methode superhydrophobe Oberflächen auf verschiedenen Substraten zu kreieren. Superhydrophobe Oberflächen verprechen eine Vielzahl an Applikationen in denen die ausgeprägte Wasserabweisung zu neuen Eigenschaften und Funktionalitäten führen kann. Die meißten der bereits existierenden Techniken jedoch, benötigen mehrstufige, umständliche Abläufe und sind nur auf bestimmten Substraten anwendbar. Im letzten Teil der Doktorarbeit, wird eine einfache einstufige („lackierungsgleiche“) Methode für superhydrophobe, poröse Polymerbeschichtungen vorgestellt. Der Ansatz beruht auf der anionischen Polymerisierung von 2-Octyl Cyanoacrylat in der Gegenwart von flüssigem Ethanol, welches sowohl als Initiator als auch als Porenbildner dient. Dies führt zur Bildung eines höchst porösen, superhydrophoben Polymerfilms. Die Morphologie dieser porösen Struktur kann durch die Änderung des Ethanol-Wasser Verhälntisses kontorlliert werden. Die Methode ist schnell, praktisch und kann ohne spezielles Equipment und unter Sauerstoff durchgeführt werden. Die Technik kann auch für eine Vielfalt an Materialien benutzt werden, ist für dreidimensionale Substrate anwendbar und bringt eine stabile, stark anheftende und superhydrophobe Beschichtung mit sich, die Oberläche wurde mittels WCA-Messung und SEM charakterisiert.

Acknowledgement

This work was performed in the group of Dr. Pavel A. Levkin (Group of Chemical Engineering of Biofunctional Materials, Institute of Toxicology and Genetics, Karlsruhe Institute of Technology) and at the department of Applied Physical Chemistry (APC) at the University of Heidelberg. It was funded by the Helmholtz Association's Initiative and Networking Fund (Grant VH-NG-621) and CSC scholarship (2011624034). First I would like to give my special thanks to Dr. Pavel A Levkin for offering me the opportunity to perform the Ph.D. thesis in his research group, and for all the guidance and useful advices during my research. I would like to express my gratefulness to Prof. Dr. Michael Grunze for supervising and reviewing my Ph.D. work, and for all the insightful advices that he offered me. I would also like to thank Prof. Dr. Hans-Robert Volpp for kindly accepting to be my second reviewer. I am grateful to all my colleagues: Dr. Linxian Li, Dr. Junsheng Li, Wenqian Feng, Dr. Alexander Efremov, Dr. Erica Boles, Dr. Victoria Nedashkivska, Girish Shankara, Zewei Bai, and all other colleagues at APC, who continuously shared their ideas and happiness, and offered a friendly and mild environment for me to work in. I would like to thank Prof. Dr. Frank Breitling, Prof. Dr. Andrew Cato for being my TAC members and for their valuable scientific suggestions. I thank Zhi Chen, Chengwu Yang, Zhengbang Wang, Zhigang Gu, Nataliya Frenkel, Dr. Alexander Welle, Stefan Heissler and Dr. Camila Blanco-Jaimes for their great help in my experiments and paper writing. I thank Prof. Dr. Yinghan Wang, who guided and helped me in scientific research during my master period. I would like to express my sincere gratitude to my parents, who tried their best to help me with everything. I would like to thank the China Scholarship Council for the Ph.D. scholarship.

List of abbreviations

AED	2-aminoethyl disulfide (hydrochloride acid salt)
AFM	Atom force microscope
ATRP	Atom transfer radical polymerization
BP	Benzophenone
CED	Carboxyethyl disulfide
CVD	Chemical vapor deposition
DA	Dopamine
DBD	Dibutyl disulfide
DIC	*N,N'*-Diisopropylcarbodiimide
DMAP	4-(Dimethylamino)pyridine
DMF	Dimethylformamide
DMPAP	2,2-Dimethoxy-2-phenylacetophenone
DMSO	Dimethyl sulfoxide
DoD	Didodecyl disulfide
DOPA	*L*-3,4-Dihydroxyphenylalanine
DPN	Dip-pen nanolithography
DPPH	2,2-diphenyl-1-picrylhydrazyl
EDMA	Ethylene glycol dimethacrylate
FITC	Fluorescein isothiocyanate isomer I
HED	2-Hydroxyethyl disulfide
HEMA	2-Hydroxyethyl methacrylate
HEMA-EDMA	Poly(2-hydroxyethyl methacrylate-co-ethylene dimethacrylate)
IR	Infrared
IRRAS	Infrared reflection absorption spectroscopy
LBL	Layer by layer
PD	Polydopamine
PDDE	Photodynamic disulfide exchange
PDMS	Poly(dimethylsiloxane)
PET	Polyethylene terephthalate
PVD	Physical vapor deposition
RAFT	Reversible addition-fragmentation chain transfer
ROS	Reactive oxygen species

SA	Sodium ascorbate
SAM	Self-assembled monolayer
SEM	Scanning electron microscope
ToF-SIMS	Time-of-flight secondary ion mass spectroscopy
UV-Vis	Ultraviolet-visible light spectroscopy
WCA	Water contact angle
XPS	X-ray photoelectron spectroscopy
XRR	X-ray reflectivity
μCP	Micro-contact printing

List of publications

Publications related to the Ph.D. thesis:

Xin Du, Linxian Li, Junsheng, Li, Chengwu Yang, Nataliya Frenkel, Alexander Welle, Stefan Heissler, Alexei Nefedov, Michael Grunze, Pavel A. Levkin. UV-Triggered Dopamine Polymerization: Control of Polymerization, Surface Coating and Photo-Patterning. *Adv. Mater.*, **2014**, 26, 8029-8033.

Xin Du, Linxian Li, Alexandra Welle, Junsheng Li, Stefan Heiser, Pavel A. Levkin. Control of Dopamine Polymerization in Alkaline Solution by UV Irradiation: Effect of Sodium Ascorbate as Antioxidant. In preparation.

Xin Du, Linxian Li, Junsheng Li, Alexandra Welle, Stefan Heiser, Pavel A. Levkin. Reversible Surface Functionalization and Rewritable Patterning towards Photodynamic Disulfide Exchange on Disulfide Surfaces. Submitted to *Adv. Mater*.

Xin Du, Junsheng Li, Linxian Li, Pavel A. Levkin. Porous Poly(2-Octyl Cyanoacrylate): a Facile One-Step Preparation of Superhydrophobic Coatings on Different Substrates. *J. Mater. Chem. A*. **2013**, 1, 1026-1029.

Other publications:

Linxian Li, Junsheng Li, **Xin Du**, Alexander Welle, Michael Grunze, Oliver Trapp, Pavel A. Levkin. Direct UV-Induced Functionalization of Surface Hydroxy Groups by Thiol–Ol Chemistry. *Angew. Chem. Int. Ed.* **2014**, 53, 3835 –3839.

Junsheng Li, Linxian Li, **Xin Du**, Wenqian Feng, Alexander Welle, Oliver Trapp, Michael Grunze, Michael Hirtz, Pavel A Levkin. Reactive Superhydrophobic Surface and Its Photo Induced Disulfide-ene and Thiol-ene (Bio)functionalization. *Nanoletters*, in press.

Xin Du, Linxian Li, Wenqian Feng, Alexandar Welle, Zhi Cheng, Stefan Heiser, Junsheng Li Michael Grunze, Pavel A. Levkin. Disulfide-yne Chemistry: Surface Photo-Click Reaction, Acid Responsibility, and Photo Induced Reversible/Irreversible Sulfide Exchange. In preparation.

Patents

Pavel Levkin, Linxian Li, Junsheng Li, **Xin Du**, Wenqian Feng. Reactive superhydrophobic surfaces, patterned superhydrophobic surfaces, methods for producing the same and use of the patterned superhydrophobic surfaces. Submitted

Pavel Levkin, Gary Davision, Linxian Li, **Xin Du**, Girish Shankara. Cationic lipid-like molecules: their synthesis and application. Submitted

Pavel Levkin, Gary Davision, Linxian Li, Girish Shankara, **Xin Du**. Synthesis and application of cationic amino lipids. Submitted

Posters

Xin Du, Linxian Li, Junsheng, Li, Chengwu Yang, Nataliya Frenkel, Alexander Welle, Stefan Heissler, Alexei Nefedov, Michael Grunze, Pavel A. Levkin. UV-Triggered Dopamine Polymerization: Control of Polymerization, Surface Coating and Photo-Patterning. *Fourth International Conference on Multifunctional, Hybrid and Nanomaterials conference*, **2015**.

Contents

1. Introduction

1.1 Surface modification and surface patterning

Surface modification is a widely investigated and interesting topic in material sciences.[1–10] It can be used to introduce or to vary a specific functionality in a substrate. Surface modification enables a variety of interface properties, for example, hydrophobicity,[11–13] hydrophilicity,[14–16] reactivity to special molecules (acids, amines, silanes, thiols, *etc.*),[17–19] antibacterial property,[20] antifouling property,[7,21] adhesive/non-adhesive property,[22,23] biocompatible property,[4,24] conductivity,[25] stimuli-responsibility,[9,26–29] among others.

As a branch of surface modifications, surface patterning has found many applications in the past years. It is used to create well-controlled physical or chemical patterns.[30–37] Patterned surfaces are important in many fields of modern science and technology, with applications ranging from information storage devices[38] and sensors,[39] to microfluids,[40–42] bioarrays[43,44] and diffractive optical devices.[45]

1.2 Strategies for chemical modification and patterning of surfaces based on photochemistry

1.2.1 Photoreactions for surface modification

Despite the large number of strategies for surface chemical modification that have been developed, the principle has remained mostly the same. The strategy consists of the creation of reactive functional groups (such as hydroxyl and amine group) on the substrate (if no other reactive groups are present), followed by an introduction of new functionalities via reactions with the specific functional groups. Different methods have been commonly employed for the formation of functional groups on surfaces, such as plasma treatment.[46] For those surfaces which already contain reactive functional groups, different chemistries (depending on the nature of the substrates) can be used for modification, for example, self-assembled monolayer (SAM),[47] silane chemistry,[48] esterification reactions,[49] azide-yne chemistry,[50] chemical vapor deposition (CVD),[51] physical vapor deposition (PVD),[52] layer by layer (LBL),[53] electroplating,[54] reversible addition-fragmentation chain transfer (RAFT) polymerization,[55] atom transfer radical polymerization (ATRP),[56] among others. Photo-assisted surface modifications have been widely applied in the past decades in many different fields. The main advantages of the photo-reactions are (a) the possibility to perform reactions in a non-contact

fashion;[57] (b) the ability to create patterns by applying a photomask;[29,49,58–60] and (c) the ability to control the onset and termination of the reaction.

Many photo-reactions have been reported and applied for surface modifications. The most common surface photo-chemistries could be divided into three different categories:

Photo-induced radical reactions

Many well-known surface photo-reactions are directly based on radical reactions, for example, thiol-ene (Figure 1.1a)[61] and thiol-yne (Figure 1.1b) chemistry,[62] in which thiol reacts with double or triple bonds under UV irradiation; surface initiated photopolymerization (typically combined with RAFT and ATRP polymerization),[63] in which light excites monomers (often acrylates) in a solution to perform radical polymerization; Paterno-Buchi reaction,[64] in which light activates ketone or aldehyde to form radicals followed by cyclization with alkenes (Figure 1.2a); Photografting,[42] in which activated photosensitizers (typically benzophenone, BP) subtracts hydrogens from the C-H bond on the substrate and generate reactive radicals on the surface (Figure 1.2b).

There are also well-studied chemistries which are indirectly based on radical reactions. For example, photo induced Diels-Alder reaction,[65] where methylphenyl ketone is rearranged under irradiation forming hydroxyl diene, which in turn reacts with maleimides via Diels-Alder reaction (Figure 1.2c); photo induced azide-yne reaction,[66] in which Cu^{2+} is photo-reduced to Cu^{+} and then worked as a catalyst for the azide-yne reaction (Figure 1.2d).

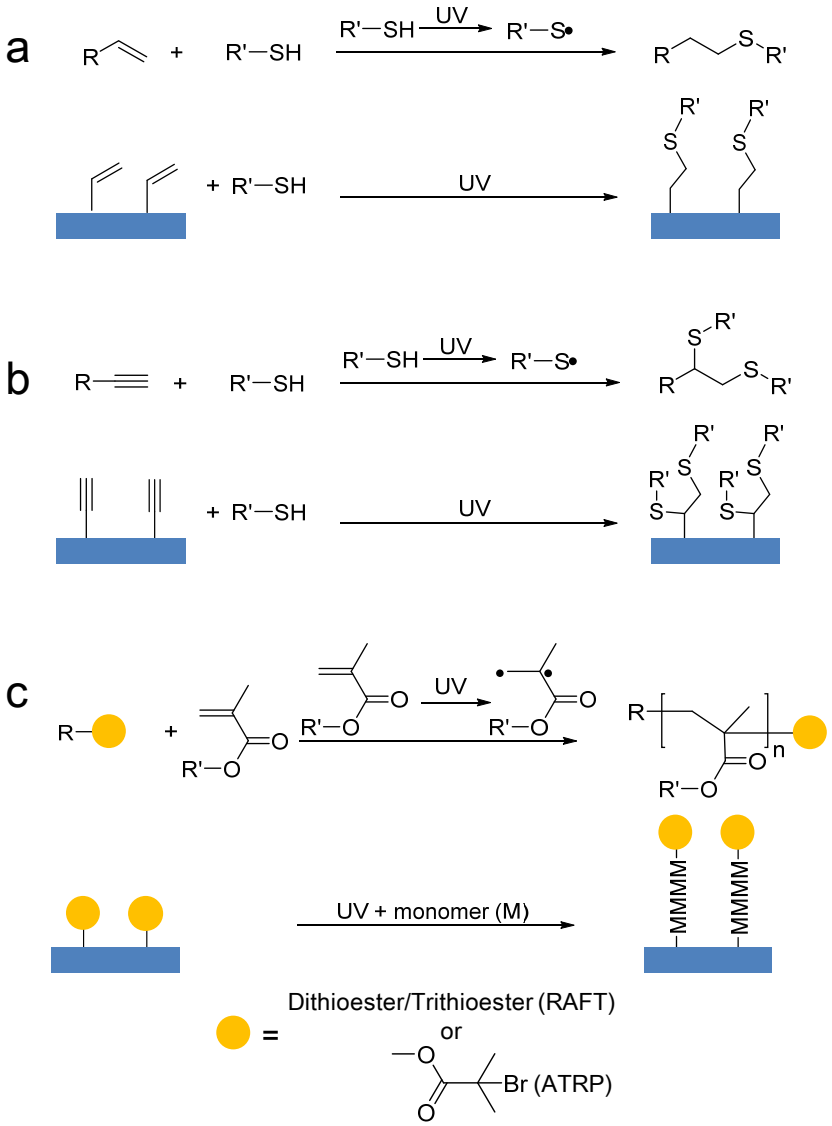

Figure 1.1: Examples of surfaces photoreactions based on radical reactions. (a) Thiol-ene chemistry (b) thiol-yne chemistry (c) Surface initiated photopolymerization.

Photo-induced decomposition

A different strategy is based on the light-induced decomposition of molecules to form functional groups, which can be involved in further modifications. Some strategies based on this route have been reported. For example, photo-induced oxime ligation,[67] where light degrades the nitrobenzyl-based structure forming a benzaldehyde group, which reacts with hydroxylamine derivatives via the Schiff base reaction (Figure 1.3a); photoactivated copper-free azide-yne chemistry,[68] in which cyclopropenone decomposes under irradiation forming a triple bond, followed by the copper-free azide-yne click chemistry (Figure 1.3b); tetrazole-based photoreactions,[69] where light leads to decomposition of tetrazole to form a

nitrile imine intermediate, which reacts with alkenes via 1,3-dipolar cycloaddition (Figure 1.3c).

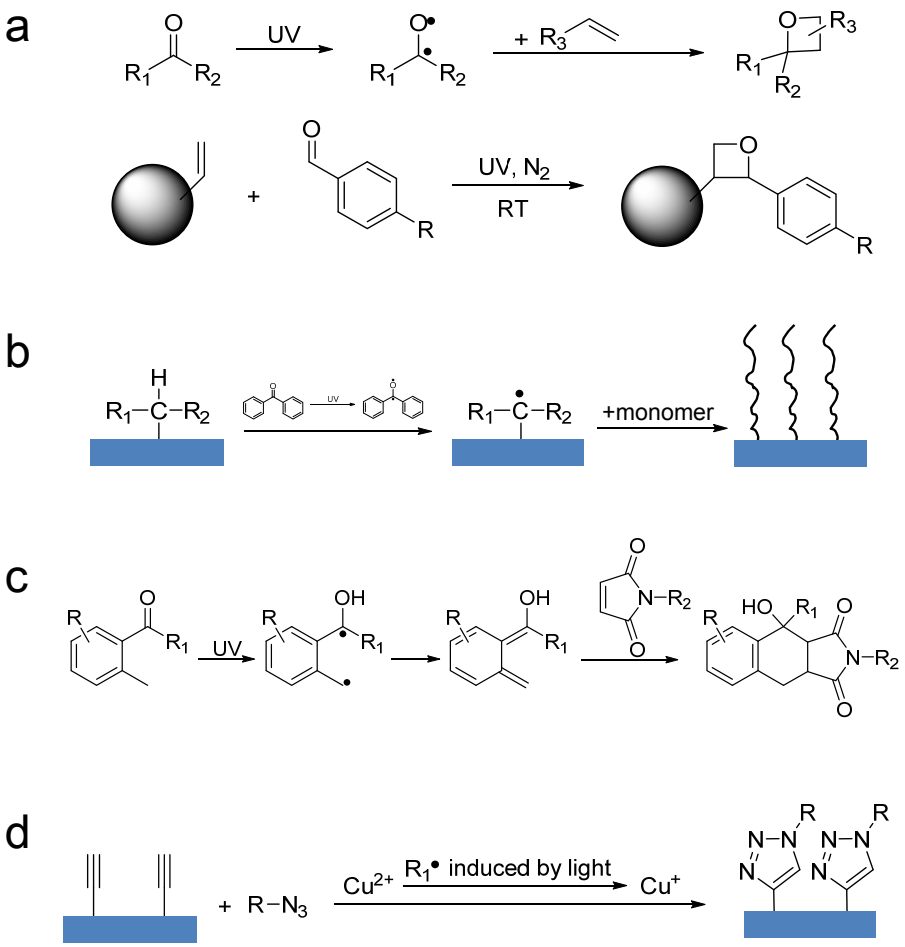

Figure 1.2: Surface photoreactions indirectly based on radical reactions. (a) Parton-Buchi reaction. The carbonyl group is activated under irradiation to form two radicals, followed by the cyclization reaction between alkene and radicals. (b) Photografting. Light activate photoinitiator (typically benzophenon) to form radicals, and the resulted radical attracts a hydrogen from the C-H bond on the organic surface, leading to a reactive radical on the surface which enables further grafting polymerization. (c) Photo induced Diels-Alder reaction. The methylphenyl ketone is activated and rearranged to an *o*-xylylene intermediate, followed by the Diels-Alder reaction with maleimides.

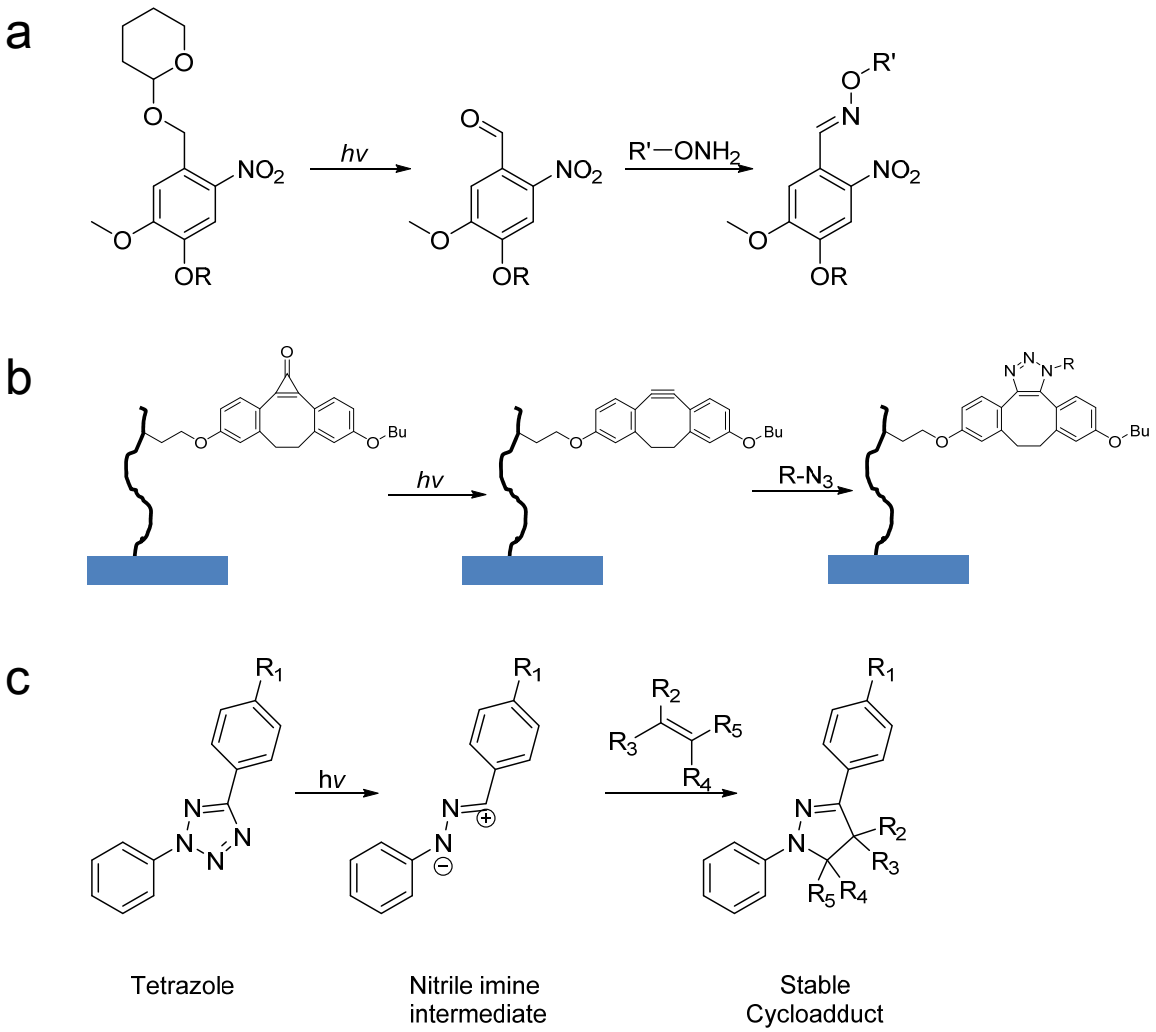

Figure 1.3: Surface photoreactions based on photo-induced decomposition. (a) Photo induced oxime ligation. Light induces the cleavage of 2-[(4,5-dimethoxy-2-nitrobenzyl)oxy] tetrahydro-2H-pyranyl derivative to form an aldehyde group, and subsequent oxime ligation occurs between the aldehyde group and the hydroxylamine derivatives. (b) Photo-activated copper-free azide-yne chemistry. The cyclopropenone decomposes under UV irradiation and results in an alkyne group. (c) Tetrazole-ene chemistry. Tetrazole decomposes under UV irradiation, the resulted nitrile imine intermediate could quickly reacts with alkenes by cycloadditon.

Photo-assisted oxidation

Light, especially UV light, is able to trigger or accelerate oxidation via the formation of reactive oxygen species (ROS).[70] For reactions requiring an oxidation process, photo-assisted oxidation is a good alternative since it increases the controllability of the reaction. UV-Ozone irradiation, which is a well-known surface modification method, follows this mechanism.[71,72] UV-Ozone irradiation is normally employed to oxidize molecules on the surface for

"detachment", for example, to remove thiols from gold surfaces by oxidation to sulfonates (Figure 1.4a).[71] However, photo-assisted oxidation could also be used to attach molecules to the surface. For example, thiol-ol chemistry[60] involve the oxidation of thiols to sulfonates, which can further react with the hydroxyl groups on the surface (Figure 1.4b).

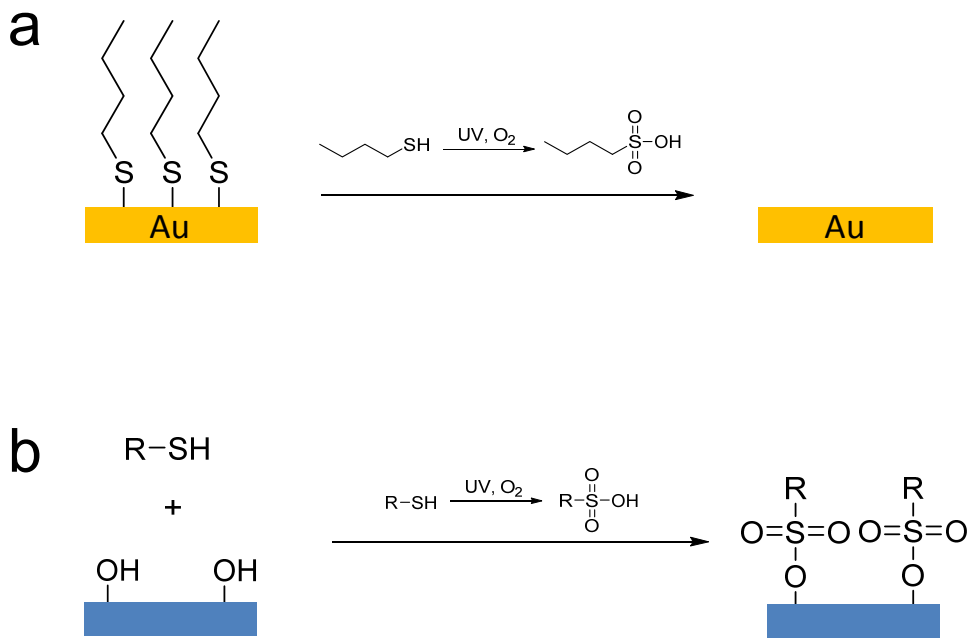

Figure 1.4: Examples of surface photoreactions based on photo-assisted oxidation. (a) UV-Ozone irradiation. UV is capable of oxidizing thiols to sulfonates, which could be washed away from gold surface. (b) Thiol-ol chemistry. UV irradiation of a hydroxyl surface in the presence of thiols and oxygen leads to the immobilization of the thiol via the sulfonate formed *in situ*.

1.2.2 Strategies of photochemical surface patterning methods

In general, surface patterning methods are based on existing surface modification strategies. Three methods have been reported to achieve the control needed during surface patterning. In the first method, the contact between a substrate and a modification solution is controlled, thus avoiding reaction where no modification solution is present. Currently most patterning strategies are based on this principle. Commonly used strategies include micro-contact printing (Figure 1.5a),[73] photolithography,[74] microfluidic patterning (Figure 1.5b),[75] dip-pen nanolithography (DPN, Figure 1.5c),[76] and inkjet printing.[77] In the second method, the initiation of the modification reaction is controlled. In this case, the whole surface is in contact with the modification solution but the reaction is only initiated in the selected

areas. Photopatterning[78–81] is the most important strategy following this method. The principle of photopatterning is that the modification reaction is initiated by light (Figure 1.5d), therefore when the area is protected by a photomask, the modification does not take place. Advantages of photopatterning are the better controllability and the possibility of *in-situ* pattern formation. The third method involves partial removal of a modified layer on the surface. AFM nanolithography is a method based on this strategy (Figure 1.5e).[82]

For surface patterning through photoreactions, photopatterning is most often used. However, other patterning strategies, such as μCP and DPN, could also be employed to avoid the use of photomasks or increase the contrast of patterns in some cases.

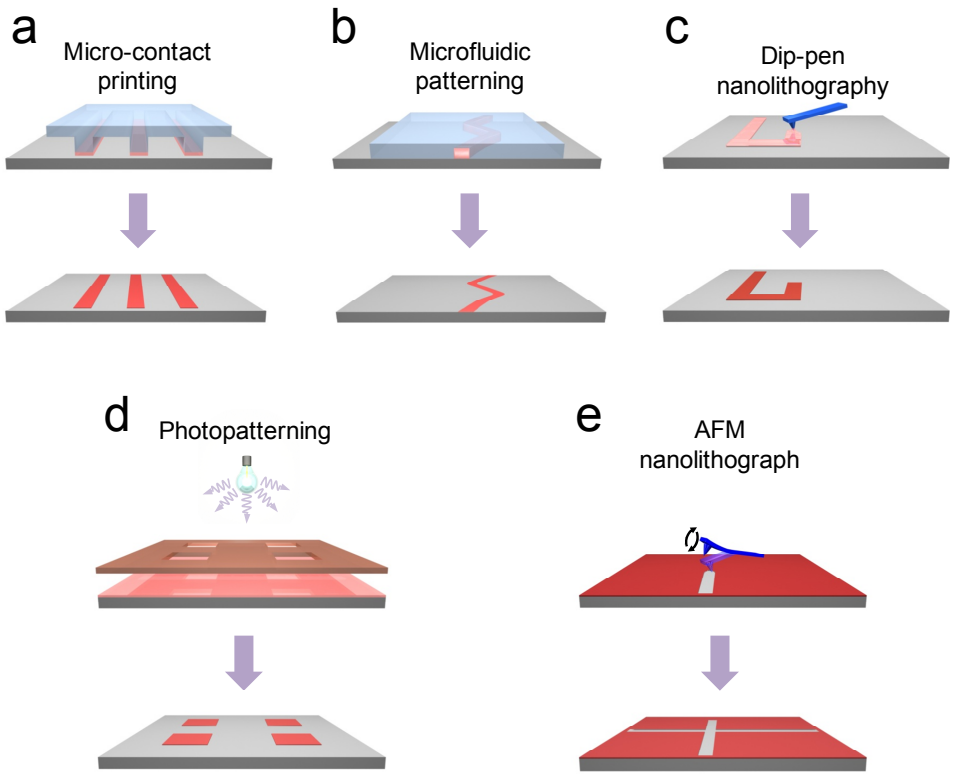

Figure 1.5: Commonly employed strategies for surface patterning. (a) Micro-contact printing. A polydimethylsiloxane (PDMS) mold is wetted by the modification solution and then printed onto the substrates. (b) Microfluidic patterning. A microfluidic stamp is added on the substrate and the modification solution is continuously injected through the microchannel. (c) Dip-pen nanolithography. An AFM tip wetted with modification solution is used as a "pen" to "write" on the substrate, the contacted area is modified. (d) Photopatterning. The substrate is completely wetted with modification solution, followed by exposure to light under a photomask. No reaction occurs in the masked area, thus obtaining a pattern. (e) AFM nanolithography. Substrate is first flood modified, and part of the surface is then removed by scratching the surface with an AFM tip.

1.2.3 Disadvantages of photo-assisted surface functionalization

Despite the advantages of photo-assisted surface functionalization, there are still some drawbacks of the current methods. The first drawback is that most photoreactions are limited to very specific functional groups. Therefore, in some cases in order to perform a surface functionalization or photopatterning, a pre-functionalization is required. The second drawback is the fact that light is very easy to be scattered and absorbed. For opaque surfaces and very thick films, photo-assisted functionalization does not work well. The third drawback is that light is a single-direction wave, thus sometimes the modification of 3D objects can be problematic.

1.3 Polydopamine coating: an inspiration from the sea

For decades mussels have attracted attention of scientists due to their strong attachment skills that allow them to adhere to all kinds of solid surfaces. In the sea they can attach to a variety of marine surfaces in order to survive in a dynamic and harsh marine environment, or attach to the bottom of ships. The understanding of the secret of mussel adhesion is not only necessary for the research in antifouling materials, but is also important for the development of new adhesives. Modern technologies point out that mussel foot proteins play a very important role on the strong adhesion performance of mussels. Investigations on the *Mytilus edulis* foot proteins indicate a high concentration of 3,4-dihydroxyphenylalanine (DOPA), which is believed to be the main reason for mussel adhesion.[6,83,84] The broad research on the adhesive performance of mussels led to the idea of using polydopamine (PD) to create a new coating material. The PD coating, inspired by mussels, was reported in 2007 by P. B. Messersmith *et.al.* (Figure 1.6).[85]

PD coating is based on the fact that dopamine (DA) can be polymerized in aqueous solutions under basic conditions, and the resulted polydopamine is an adhesive material which can be deposited onto virtually any substrate immersed in the solution. Therefore, after polymerization, a PD layer is formed on the surfaces of immersed objects.[85] PD is a reactive polymer which can react with thiols,[85] amines[86,87] and metal ions,[85,88] to introduce further functionalities. In other words, PD coating is a surface-independent coating method which can lead to a reactive layer on any substrate.

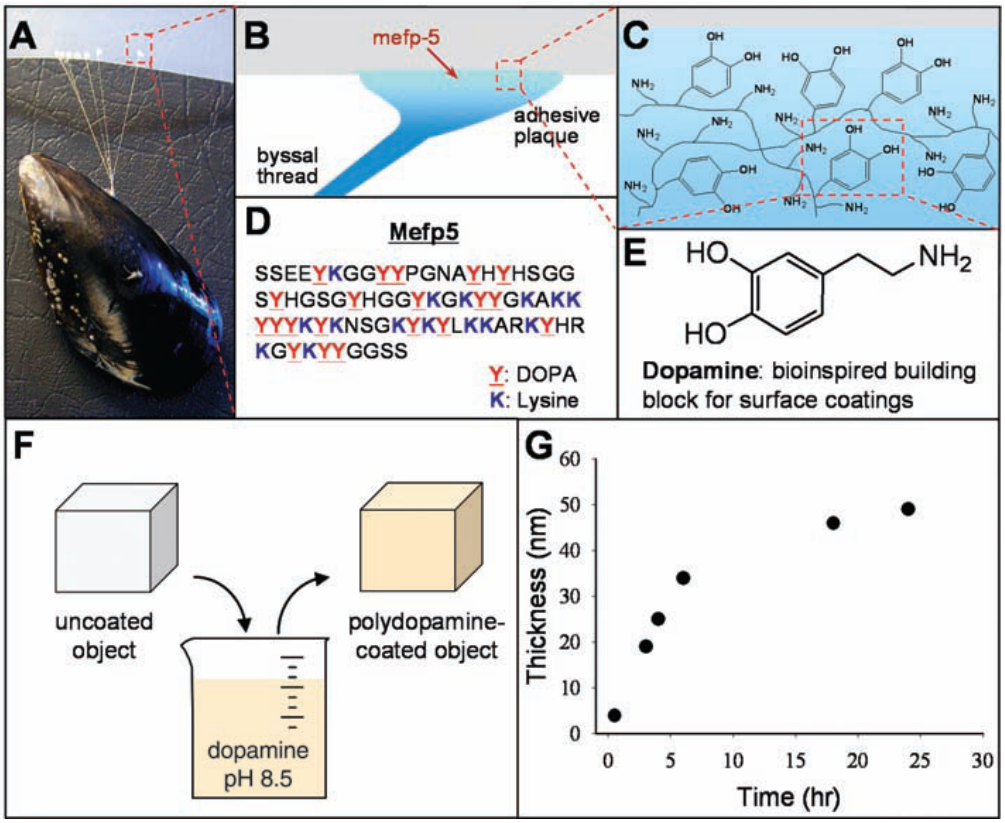

Figure 1.6: Mussel-inspired PD coatings.[85] (A) Photograph of a mussel attached to commercial PTFE. (B and C) Schematic illustrations of the interfacial location of Mefp-5. Simplified molecular representation of the characteristic amine and catechol groups. (D) The amino acid sequence of Mefp-5. (E) DA contains both amine and catechol functional groups found in Mefp-5. It was used as a molecular building block for polymer coatings. (F) A schematic illustration of thin film deposition of polydopamine by dip-coating an object in an alkaline DA solution. (G) Thickness evolution of polydopamine coating on Si as measured by AFM of patterned surfaces.

1.3.1 Mechanism of PD coating

1.3.1.1 Mechanism of DA polymerization under basic conditions

The question of how DA polymerizes is not only of interest for PD coating research, but also for melanin chemistry. PD is believed to have a similar structure as eumelanin.[89] Currently the mechanism of DA polymerization is not fully understood, it is believed to be similar to the pathway from DOPA to melanin in the biosynthesis of melanin. For the early stage of investigation (2007-2009), DA was proposed to be a polymer of poly(3,4-dihydroxyl indole). The mechanism of DA polymerization was believed to involve first the oxidation of DA and rearrangement to 3,4-dihydroxy indole, followed by further oxidation and

polymerization (Figure 1.7).

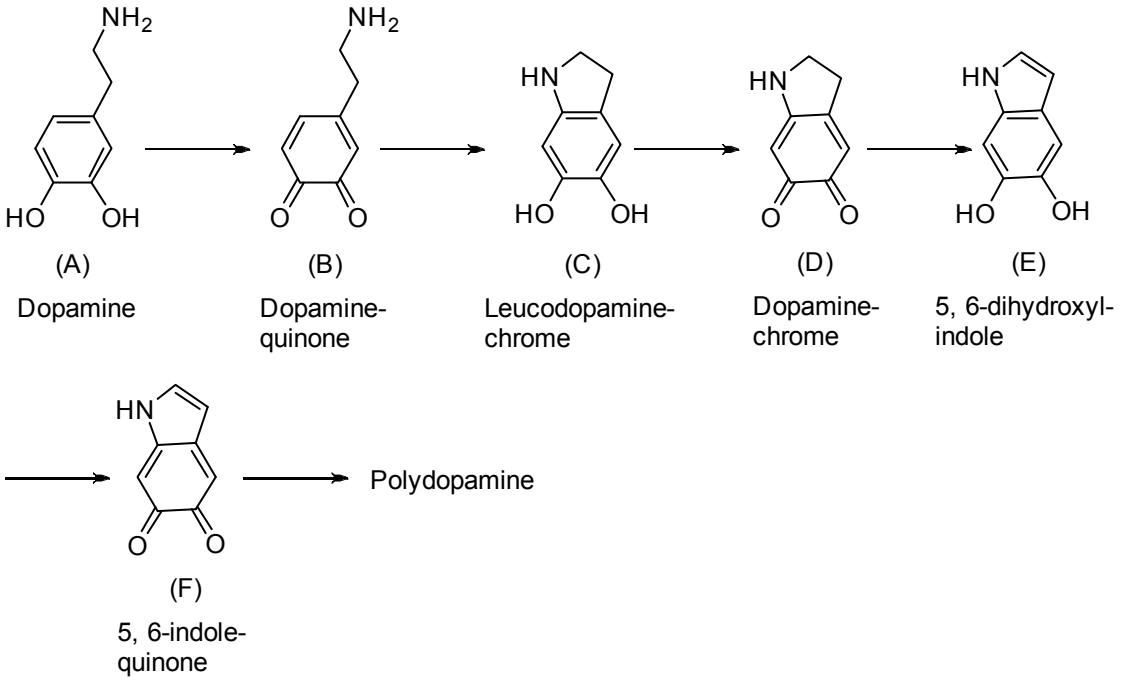

Figure 1.7: Proposed mechanism for DA polymerization.[90] DA (A) is first oxidized by oxygen to form quinone (B) (DA to dopamine quinone + $2H^+$ $+2e^-$), followed by an intramolecular Michael addition leading to (C). Further oxidation and rearrangement lead to the formation of indole-quinone (F) followed by a polymerization step.

However, different hypotheses have been proposed in the following years. J. A. Swift proposed that Diels-Alder reaction occur between indole quinones, resulting in polyindoles after further cleavage reactions (Figure 1.8a).[91] Dreyer et al. proposed that polydopamine structure is based on H bonding rather than C-C linkages (Figure 1.8b).[92] Hong et al. reported that a large amount (~18% wt) of DA physical trimers are presented in polydopamine layers (Figure 1.8c). More recently, a more complicated hypothesis for PD structures was proposed. Liebscher et. al proposed that PD is a copolymer of DA, leucodopamine chrome, 3,4-dihydroxyl indole, and 3,4-dihydroxyl indole quinone (Figure 1.8d).[93] Vecchia et al. reported similar results, but in their hypothesis the linkage of catechol units may occur at different positions on the benzene ring, and the partial oxidative cleavage might occur during the polymerization.[94]

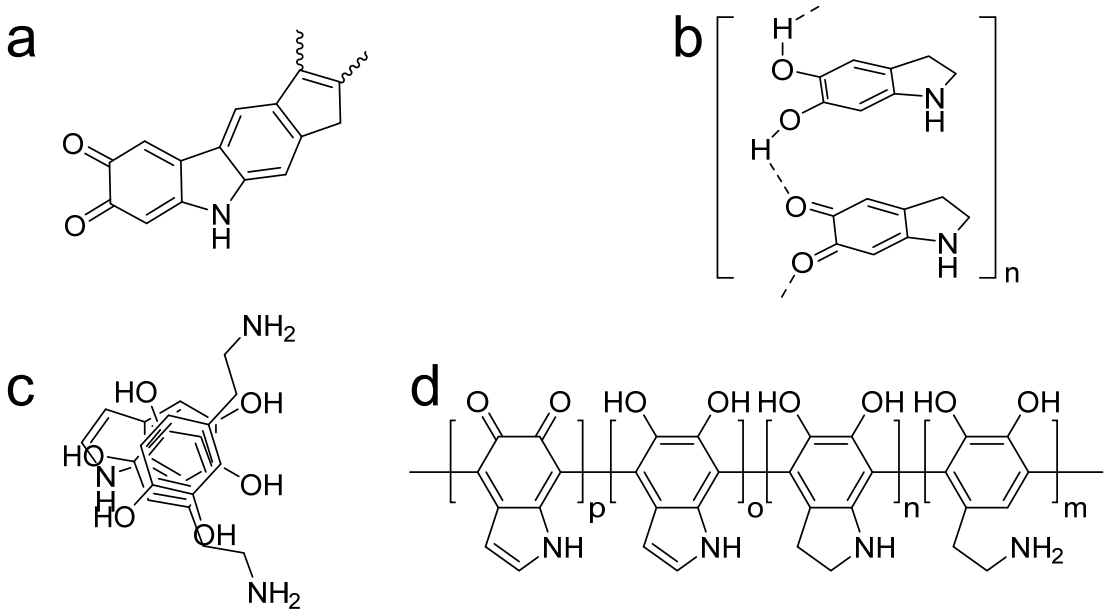

Figure 1.8: Schematic illustration showing the different proposed structures of PD. (a) polyindole structure based on Diels-Alder reaction and further cleavage reactions. (b) PD structure based on H bonding. (c) Proposed structure of DA physical trimer. (d) PD structure based on DA with different oxidation states.

Oxygen plays a very important role as oxidant during DA polymerization. Its effect has been proved by experiments in both oxygen-rich[95] and oxygen-poor solutions.[85] Interestingly, it has been reported that DA polymerization can only occur under basic conditions, because neutral and acidic solutions would strongly inhibit the first step of DA oxidation (Figure 1.7, A→B).[85,90] However, it has also been demonstrated that by adding strong oxidants, DA polymerization can occur in neutral and acidic conditions.[96,97]

1.3.1.2 Mechanism of adhesion of polycatechols

Although not well understood yet, some investigations have been done on the mechanism of adhesion of catechols.[98–101] Different interactions are believed to be involved in this process. For adhesion on metal or metal oxide surfaces, the proposed mechanism includes:

Coordination bonding

Moser *et al.* investigated the surface complexation of TiO_2 with catechol, and reported that the binding reaction involves the replacement of a hydroxyl group on TiO_2 surface by deprotonated ligand (Figure 1.9a).[102] The very stable nature of these chelates makes the complexation of titanium ions located at the surface of TiO_2 feasible.[6,102]

Bidentate chelating bonding

Rajh *et al.* proposed that the adhesion depends on the chelating interactions. They believed that for the binding of catechol to Fe_2O_3 and TiO_2 surfaces, two oxygen atoms of the catechol bind to a single metal center of Fe (Figure 1.9b) or Ti (Figure 1.9c). [103,104]

Bridged bidentate bonding

Messersmith *et al*. did a series of investigations on the adhesive performance of catechol structures[105] and reported a bridged bonding mechanism. In their hypothesis, on TiO_2 surface, the Ti-OH groups were depleted upon the adsorption of catechol. The hypothesis was also confirmed by other investigations (Figure 1.9d)[106,107].

For the adhesion on organic substrates, Lee *at al.* investigated the catechol adhesion on a molecular level by grafting a single DOPA residue to an AFM cantilever and measuring the force required to pull the molecule from contact with a substrate.[98] They reported that the strong interaction between DOPA and organic surfaces could be attributed to the covalent reactions (probably Michael addition or Schiff base reactions) between quinines and nucleophiles present on organic surfaces (Figure 1.9e).

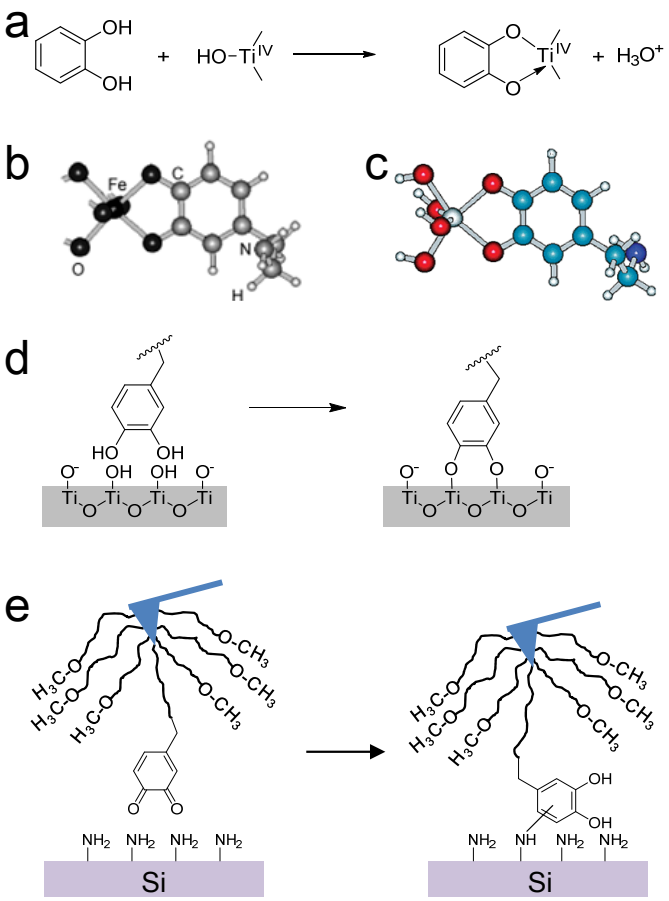

Figure 1.9: Proposed mechanism for PD adhesion. (a) Complexation reaction of catechol with hydroxylated TiO_2.[102] (b) Structures of DA-binding configurations with Fe_2O_3 nanoparticles.[103] (c) Structures of DA-binding configurations with TiO_2 nanoparticles.[104] (d) Bidentate bonding of catechol with TiO_2 surface. The phenol group covalently binds to the metal atoms on the surface.[105] (e) Adhesion of catechol to organic surfaces. The quinone groups react with the nucleophiles on the surface forming covalent bonds.[98]

1.3.1.3 Mechanism of PD deposition

Only few investigations have been done on the mechanism of PD deposition.[108–112] A simple explanation of the mechanism would be that PD nanoparticles are aggregated during the polymerization and then attached onto the substrates. However, the real mechanism and kinetics of PD deposition might be much more complex. Bernsmann *et al.* found that no PD deposition could occur if DA is allowed to first polymerize for 4.5h and then immerse the substrate.[112] Likewise, it was observed that, after a typical PD coating process, the substrate is covered by a layer of PD particles, which could easily be washed away by rinsing with water.[108] Therefore, the adhesive performance of PD polymer should not be the key reason for

the formation of a PD layer on the substrate. It has been proposed by Ball *et al.* that the PD deposition process may present strong analogy with the deposition of polyaniline films.[112] In this case, the formation of the polymer layer is due to the adsorption of oligoaniline cations on the surface, followed by radical polymerization. However, this hypothesis has not been proved yet.

1.3.1.4 Mechanism of PD secondary modification

PD can react with thiols, amines and metal ions allowing the introduction of different functionalizations. For the reaction with thiols and amines, the mechanism is believed to be similar to the DA polymerization mechanism.[85] As shown in Figure 1.10a, under basic conditions, the catechol group on the PD surface is oxidized and rearranged to quinone, and thiols or amines can be added via Michael addition. For the secondary modification with amines, Schiff base reaction is also proposed to be involved.[85] The catechol group is also capable of reacting with metal ions such as copper and silver ions, leading to metallization (Figure 1.10b).[86,113,114]

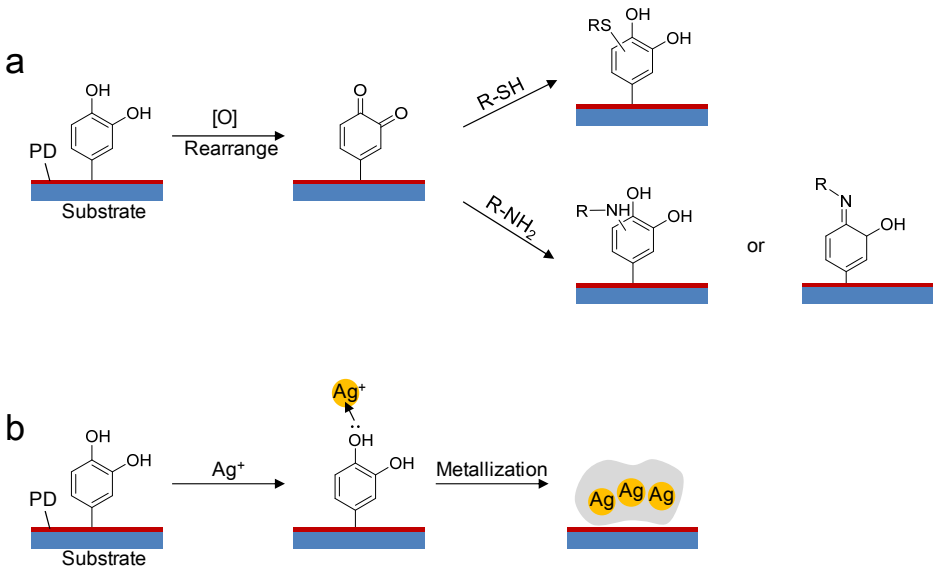

Figure 1.10: Proposed mechanism for secondary modification reactions on PD surface. (a) PD reacts with thiols and amines through Michael addition or Schiff base reaction. (b) Metal deposition on PD surface through electroless metallization.

1.3.2 Applications of PD coatings

PD coatings exhibit many advantages compare to the existing surface functionalization strategies. The first advantage is the generality. PD is adhesive to virtually all kinds of materials regardless of their nature, including low surface energy (Teflon) and soft biological

surfaces, such as tomato surface.[115] Another advantage is the simplicity of the coating procedure, which allows PD coating to be a not substrate-shape selective method. A PD layer can be formed on large flat, curved, or rough substrates as well as on small 3D objects. Finally, both PD coating and secondary modifications can be carried out in aqueous solutions, making the procedure economical and pro-environmental.

PD coating offers an ideal solution for surface functionalization in many cases. Due to its advantages, PD coating has been widely applied in many different fields. The most common applications are listed below.

1.3.2.1 Applications for surface functionalization

The most common application for PD coating is to work as a general reactive coating for further functionalization (Figure 1.11). Many functional surfaces formed by PD coating were reported, for example, antibacterial surface,[86,116–120] peptide surface,[87,121–123] superhydrophobic surface,[124] and specific chemical functionalized surfaces (Figure 1.11a).[125–127] With the combination of patterning strategies, PD patterns could be formed on substrates and microarrays could be formed after further functionalization (Figure 1.11b). Different PD-based bioarrays, such as cell arrays, peptide arrays and metal arrays, have been reported.[43,44,85,128–130]

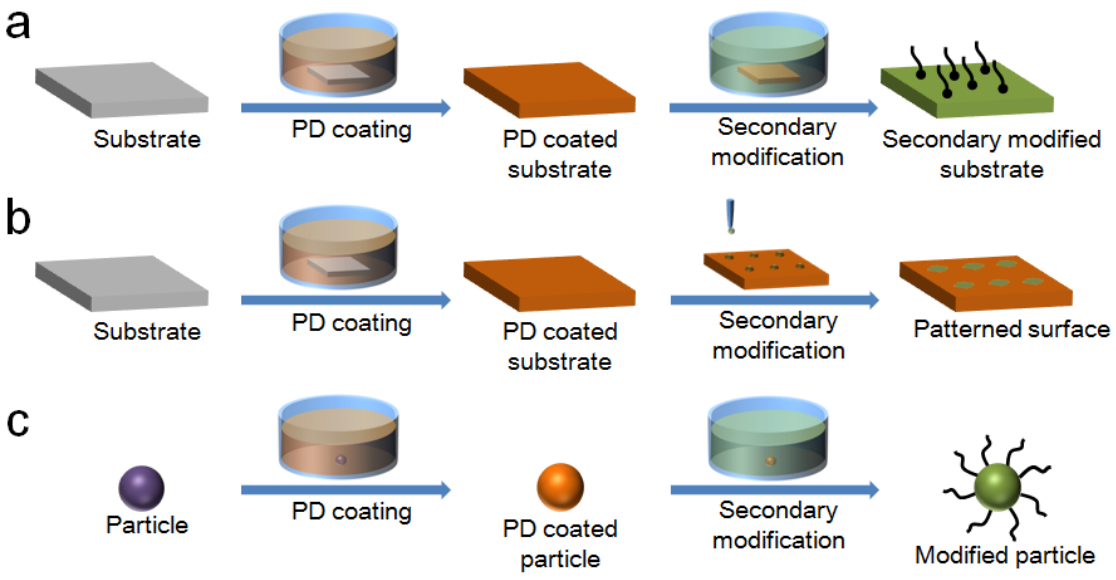

Figure 1.11: Schematic illustration of the application of PD as functionalization platform. (a) PD as a platform for surface functionalization. (b) PD as a platform for surface patterning. (c) PD as a platform for nanoparticle functionalization.

Since PD deposits over all the immersed substrate, the modification of nanoparticles was

achieved by PD coating (Figure 1.11c). Superhydrophobic nanoparticles and magnetic drug carriers were reported.[88,131]

1.3.2.2 Applications as adhesives

The adhesion properties of the PD polymer have been employed to form adhesives. For example, DA modified poly(acrylic acid) and alginate were used as adhesive links for silicon nanoparticles in the Lithium-ion batteries (Figure 1.12a);[132] by combining gecko foot structure and PD coating, an adhesive surface in both dry and wet conditions was obtained (Figure 1.12b).[22] DA can be used to modify polymers and small molecules, and the obtained catechol-containing molecules can attach to substrates in the same way as PD coatings.[133–135] PD was also used to coat graphenes and worked as adhesives for graphene paper.[136]

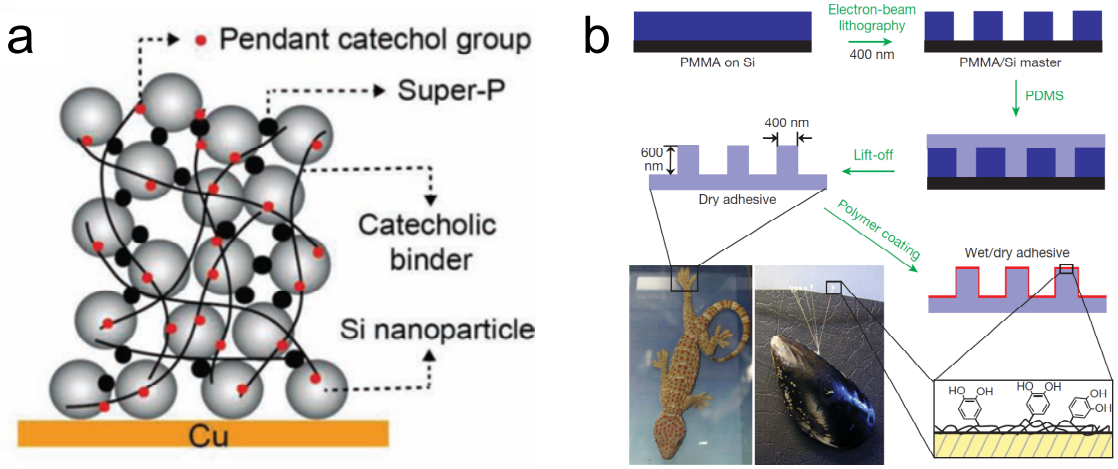

Figure 1.12. Examples for PD applications as adhesives. (a) DA modified alginate and poly(acrylic acid) was used as a linker for silicon nanoparticles in lithium batteries.[132] (b) PD is coated onto a substrate which has morphology similar to gecko foot, and an adhesive surface in both dry and wet conditions could be obtained.[22]

1.3.3.3 Other applications of polydopamine coatings

Some other applications for PD coatings have been also reported:

PD coated electrodes

Coated PD layer on a polyethylene terephthalate (PET) surface could be transformed to transparent conductive electrodes by pyrolysis at 1000 °C under hydrogen atmosphere (Figure 1.13a).[137]

PD as a free radical scavenger

PD is highly reactive to free radicals and therefore could be used as a free radical

scavenger.[138] Ju et al. synthesized PD nanoparticles and demonstrated that the obtained nanoparticles were capable of reducing 2,2-diphenyl-1-picrylhydrazyl (DPPH), which suggests the free radical scavenging activity of the material.[139]

PD as templates for nanostructures

Lee et al. synthesized mono-dispersed PD spheres with tunable diameters and used them as templates for the convenient synthesis of various nanostructures, e.g., MnO_2 hollow spheres or PDA/Fe_3O_4 and PDA/Ag core/shell nanostructures. They demonstrated that these complex nanostructures could be used as fillers in nano-composites for high performance capacitors.[114]

PD as high efficiency catalysts

Lu et al. synthesized mono-disperse PD nanoparticles and then transformed them to carbon particles by thermal treatment at 700 °C. They found that the obtained sub-micrometer carbon spheres are highly suitable nonprecious metal catalyst for oxygen reduction reaction.[140]

PD for water purification

Since PD is reactive to many metal ions, it can be employed to trap the metal ions in the water. Voelcker et al. prepared PD nanoparticles and found that PD particles could be used to remove the copper (II) ions from aqueous solutions.[141]

PD as drug carriers

PD capsules were used as drug carriers in some reports. The PD capsule was prepared by DA polymerization in emulsion, or by using SiO_2 nanoparticle as template. After further functionalization with pH responsive polymers, the PD capsules were capable to release drugs under specific pH (Figure 1.13b).[142,143]

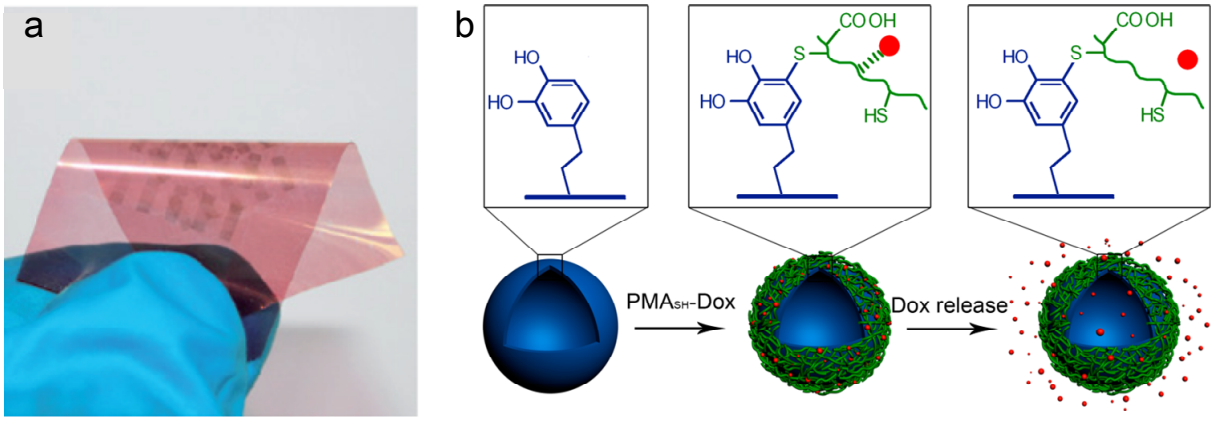

Figure 1.13: Examples of PD applications in other fields. (a) Conductive electrodes on surface formed by pattern PD coating on PET film.[137] (b) PD capsules for drug release. PD capsules were formed by performing DA polymerization in emulsions, followed by the

removal of emulsion templates by ethanol. A pH-response polymer, polymethacrylate acid (partly modified with thiol groups, conjugated with doxorubicin, PMA_{SH}-Dox), was conjugated to the capsules by secondary modification. The modified PD capsules are then capable of releasing Dox under acidic pH.[143]

1.4. Reversible surface functionalization

Reversible surface functionalization methods are becoming more and more attractive. Reversible nature of such methods allows the functionalization step to be carried out by "write and erase" procedure,[144] which is very controllable and convenient; due to the reversible properties, the substrate can be reused for many times;[145] complex, multi-component and gradient surface patterns could be easily made by using reversible strategies;[146,147] reversible surface can trap and release molecules through reversible reactions, thus controlled surface transportation and controlled surface release are possible; [148,149] *in-situ* manipulation of local environment are also possible for reversible surface.[146]

During the last decade, reversible surfaces have been reported,[34,144–147,149–158] the chemistries employed included electrically assisted ionoprinting,[34] Schiff-base reaction,[144] DNA hybridization,[151] Diels-Alder reactions,[152] cyclodextrin-based host-guest interaction,[153,157] and alkoxyamine-based chemistry,[158] *etc*.

Here I would like to propose three types of reversible surface functionalization strategies In the first type, the reversible modification procedure can be separated into two steps, the first step is to turn a surface back to the original, and the second step is to modify this original surface again with a different reagent (Figure 1.14a). The two steps are completely separated and cannot be carried out together. Currently most of the reported strategies are following this type. In the second type, the reversible chemistries are highly dynamic, which means the modification and recovery steps are not separated but done as a "one-pot" procedure. However, the reaction is poorly controllable. An example of this strategy is the alkoxyamine surface (Figure 1.14b).[158] Alkoxyamine forms radicals under heat, and dynamic exchange reaction could occur if another alkoxyamine is present in the solution. Since this process depends on heating, it is difficult to control this process. The third type of the reversible reactions includes highly dynamic reversible reactions which at the same time can be well controlled. To my best knowledge, only two methods of this type have been report. The first one is thiol-naphthoquinone methide reaction (Figure 1.14c), which is based on a photo reversible reaction between a thiol and 2-naphthoquinone-3-methide (σNQM). The second

one is Addition-Fragmentation Chain Transfer chemistry, which is based on the reversible reaction between thiols and allyl sulfides.

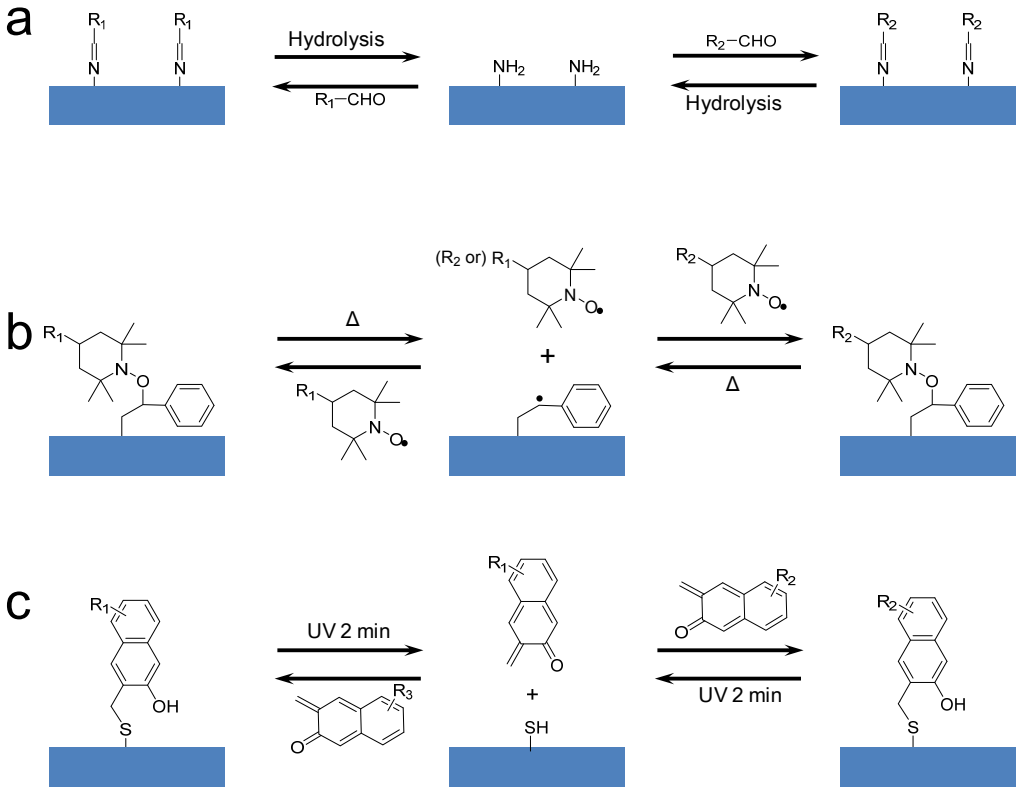

Figure 1.14: Examples of reversible surface modification strategies. (a) Schiff-base strategy. The modification-recovery cycle contains two separated steps, first is hydrolysis of imine to amine, followed by the Schiff-base reaction to form imine again. (b) Strategy based on the alkoxyamine exchange reaction. (c) Thiol-σNQM reaction for reversible surface modification.

1.5 Superhydrophobicity and superhydrophobic surfaces

Superhydrophobicity refers to a property of a surface which is extremely hydrophobic and highly water repellent.[159–163] For a superhydrophobic surface the water contact angle (WCA) is higher than 150º (Figure 1.15a), and the rolling angle of the surface is below 10º, indicating that water droplets can easily roll off the surface. Superhydrophobic surfaces are attractive for their unique water repellent and self-clean properties,[164–169] which can potentially find numerous applications in a variety of industrial and research fields ranging from coatings for solar cells and biotechnological reactors to coatings for microfluidic devices and microarrays.

Superhydrophobicity is a result of a combination of hydrophobicity of the material and surface roughness.[170] Figure 1.15b shows a SEM image of a well known natural

superhydrophobic surface, lotus leaf. The surface is very rough and contains micro-nano hieratical structures, leading to the entrapment of air and formation of an air-solid compositte interface between the surface and a water droplet. Thus to make a superhydrophobic surface, the key is to increase hydrophobicity of the material and produce highly rough structures on the surface. During the past decade, a number of methods for the fabrication of superhydrophobic surfaces have been reported. [171–184] However, despite a lot of research, most reported methods exhibit significant drawbacks. For example, most of the methods still require multi-step procedures,[181] which is not convenient and time consumable. Many methods require harsh conditions,[182] and most strategies use the specific interactions between the substrate and the reactants,[58] which means the preparation methods are limited to specific substrates. A more general and convenient strategy is still demanded in this field.

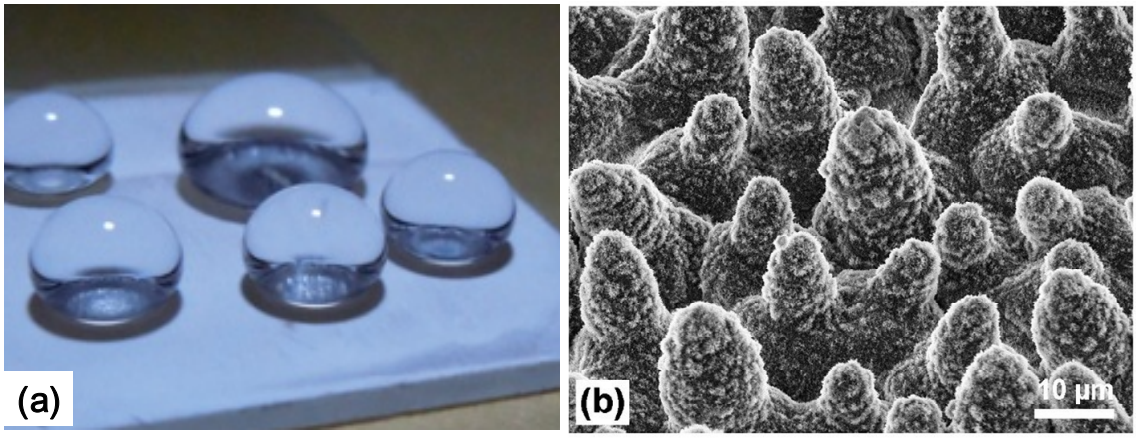

Figure 1.15: (a) Water droplets on a superhydrophobic surface.[185] (b) SEM image of the lotus leaf surface showing its micro-nano hieratical structure.[186]

2. Materials and methods

2.1 Chemicals and materials

Dopamine hydrochloride was purchased from Sigma-Aldrich (Germany). Acetone, ethanol, cyclohexanol, decanol, 4-(Dimethylamino) pyridine (DMAP), dichloromethane (DCM) and other solvents were obtained from Merck KGaA (Germany). The glass plates used in the experiments were Nexterion B glass from Schott AG (Germany). Silicon wafers (CZ-Si-wafer 4 inch) were obtained from MicroChem GmbH (Germany). Dibutyl disulfide (DBD), 2-hydroxyethyl disulfide (HED), 2-carboxyethyl disulfide (CED), 2,2-dimethoxy-2-phenylacetophenone (DMPAP), fluorescein isothiocyanate isomer I (FITC), N,N′-diisopropylcarbodiimide (DIC), cystamine dihydrochloride (aminoethyl disulfide dihydrochloride, AED), 2-hydroxyethyl methacrylate (HEMA), hydrogen peroxide (30% wt. in water) and ethylene glycol dimethacrylate (EDMA) were obtained from Sigma-Aldrich (Germany). Dimethyl sulfoxide (DMSO) and dimethylformamide (DMF) were obtained from Roth GmbH (Germany). Ethyl cyanoacrylate (containing 5-10% PMMA) and butyl cyanoacrylate (98%) were obtained from WPI Inc (Europe). 2-Octyl cyanoacrylate was obtained from GluInc (Canada). Didodecyl disulfide (DoD) was synthesized according to the literature.[187]

An OAI model 30 deep-UV collimated light source (San Jose, CA, USA) fitted with a 500 W HgXe lamp was used for UV irradiation. The lamp was calibrated to 7.5 mW/cm^2 at 260 nm with the OAI 306 UV power meter. UV-Vis spectroscopy was performed with a HR2000+ high resolution spectrometer (Ocean Optics Inc., USA) with DH-2000-BAL light source (Mikropack GmbH, Germany). The microscopy images were obtained by a BIOREVO BZ-9000 microscope (Keyence GmbH, Germany).

2.2 Description of experiments and preparation techniques

2.2.1 Dopamine polymerization under UV irradiation

Dopamine (DA, 2 mg/mL) Tris buffer solution (10 mM, pH at 2.0, 3.0, 4.0, 5.0, 6.0, 7.0, and 8.5, respectively) was filled into cuvettes and irradiated under UV for predetermined time. The UV-Vis absorbance (300-1000 nm) of the solution was measured at different time points (0, 5, 10, 20, 30, 45, 60, 90 and 120 min, air as the reference).

2.2.2 Polydopamine deposition on silicon wafers

The setup used in this experiment is described in Figure 2.1. The silicon wafers were cleaned by an UV-Ozone cleaner (UVO Cleaner Modell 42-220, Jelight Company Inc., USA) to reduce any organic contamination. DA solutions (2 mg/mL, in 10 mM Tris buffer pH 7.0 and pH 8.5) were filled into the setup, and the samples were irradiated under UV light for 2 h. For each time point, samples were taken out from the UV lamp, opened, washed with water and acetone, dried with nitrogen and the thickness of PD layer was measured by ellipsometry. The same experiments were carried out in dark environment. For the UV-induced PD coating on other substrates, the same procedure was used. For patterning polydopamine, a photomask was added above the device.

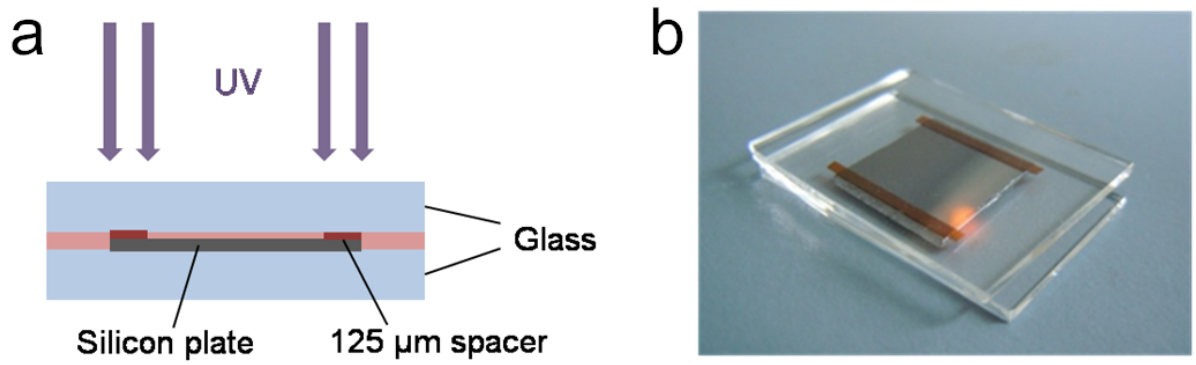

Figure 2.1. The device used for PD deposition on silicon wafer. (a) Scheme of the device structure. (b) Photo of the device used in the experiment.

2.2.3 Formation of porous HEMA-EDMA surface

Poly(butyl methacrylate-co-ethylene dimethacrylate) (HEMA-EDMA) polymer surfaces were prepared as follows: for nanoporous HEMA-EDMA, 2-hydroxyethyl methacrylate (HEMA, 24% wt.), ethylene glycol dimethyacrylate (EDMA, 16% wt.), 1-decanol (12% wt.), cyclohexanol (48% wt.) and 2,2-dimethoxy-2-phenylacetophenone (DMPAP, 1% wt. with respect to monomers) were injected into mold made of two glass plates separated with 12.5 µm polyimide film. The mold was then placed under UV lamp for 15 min. After irradiation, the glass slides were carefully opened with a scalpel. The polymer surface on the upper glass plate was ready for use after washing extensively with methanol (immersing into methanol overnight, and then drying with a nitrogen gun). For macroporous HEMA-EDMA, the procedure was similar, with a different porogen (1-decanol 40% wt., cyclohexanol 20% wt.), and a different spacer (25 µm polyimide film).

2.2.4 Formation of carboxyethyl disulfide (CED) surface

The CED surface was formed by esterification of HEMA-EDMA hydroxy groups with CED (Figure 2.2). 240 mg (1.14 mmol) CED was added into a 50 ml Falcon tube containing 45 ml acetone, followed by the addition of 176.5 μL DIC (1.14 mmol). Then porous HEMA-EDMA surface was placed into the tube, and the solution was stirred with a small magnetic stirrer for 7h after the addition of 56 mg (0.46 mmol) DMAP. The HEMA-EDMA surface was then washed with ethanol and acetone and dried by N_2.

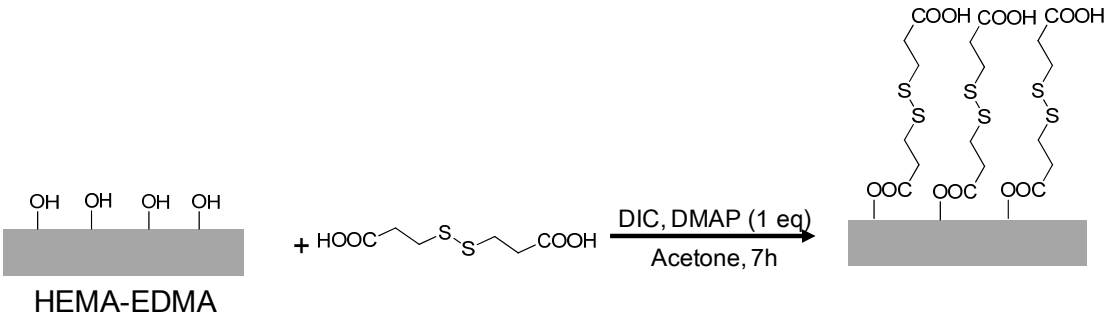

Figure 2.2: Scheme representing the formation of a CED disulfide surface.

2.2.5 Modification of disulfide surface

Disulfide surface can be modified by different molecules, such as thiols, alkenes, and disulfides. The procedure of the modifications is as follows: a few drops of a modification solution (20% wt in DMF, containing 1% wt DMPAP as photoinitiator) were applied on CED surface, then the surface was covered by a quartz slide and irradiated under UV for 2 min. After washing with acetone and drying under a stream of N_2, a new disulfide surface was obtained.

2.2.6 Photopatterning on disulfide surface

A few drops of disulfide solution (20% wt. in DMF with 1% wt. DMPAP, for FITC-disulfide is 10 mg/mL in DMSO containing 0.5 mg/mL DMPAP) were added to a disulfide surface, then the surface was covered by quartz glass and irradiated under UV for 2 min through a photomask (for FITC-disulfide, 5 min). The surface was then washed with acetone and dried under a stream of N_2.

For the reverse patterning of FITC-disulfide, the disulfide surface was first flood irradiated by UV for 5 min, followed by a washing process. Then, a few drops of DBD solution were applied on the surface and it was irradiated under UV for 2 min through a photomask. Afterwards the surface was washed with acetone overnight and dried under a stream of N_2.

2.2.7 Formation of rewritable superhydrophobic-superhydrophilic (SH-SL) patterns

The SH-SL pattern was formed on a microporous HEMA-EDMA surface. To a CED surface, didodecyl thiol (DoD) solution (10 mg/mL in hexadecane, containing 0.5 mg/mL DMPAP) was added and the surface was covered by a quartz glass and irradiated under UV for 5 min through a photomask. Then, the SH-SL pattern was erased by modifying with CED solution for 5 min to form a SL surface. The SL surface was then transformed to a SH surface by modifying it with DoD solution for 5 min and the SH surface could be returned to SL surface by modification with a CED solution for 5 min.

2.3 Methods and theoretical background

2.3.1 UV-Vis spectroscopy

UV-Vis spectroscopy refers to the absorption, transmition, or reflection spectroscopy in the ultraviolet-visible light range.[188] Substances exhibit different colors because they absorb light at different wavelengths. When molecules are exposed to light with an energy that matches a possible electronic transition within the molecule, some of the light energy will be absorbed as the electron is promoted to a higher energy orbital.[189] A UV-Vis spectrometer has a light source which offers light in whole UV-Visible range, and a spectrometer which measures how much light is absorbed/transmitted/reflected at each wavelength. For the commonly used absorption spectrum, the result is presented as a graph of absorbance versus wavelength (Figure 2.3). The absorbance is a logarithmic ratio of the intensity of the emergent light to the intensity of the incident light (Equation 2.1):[190]

$$A_\lambda = \mathrm{Log}_{10} \frac{I_0}{I} \quad (2.1)$$

Where λ is the corresponding wavelength, I_0 is the intensity of incident light and I is the intensity of emergent light. Typically the absorbance is ranged between 0 and 2, in which 0 is no light absorption, and 2 is 99% absorption.

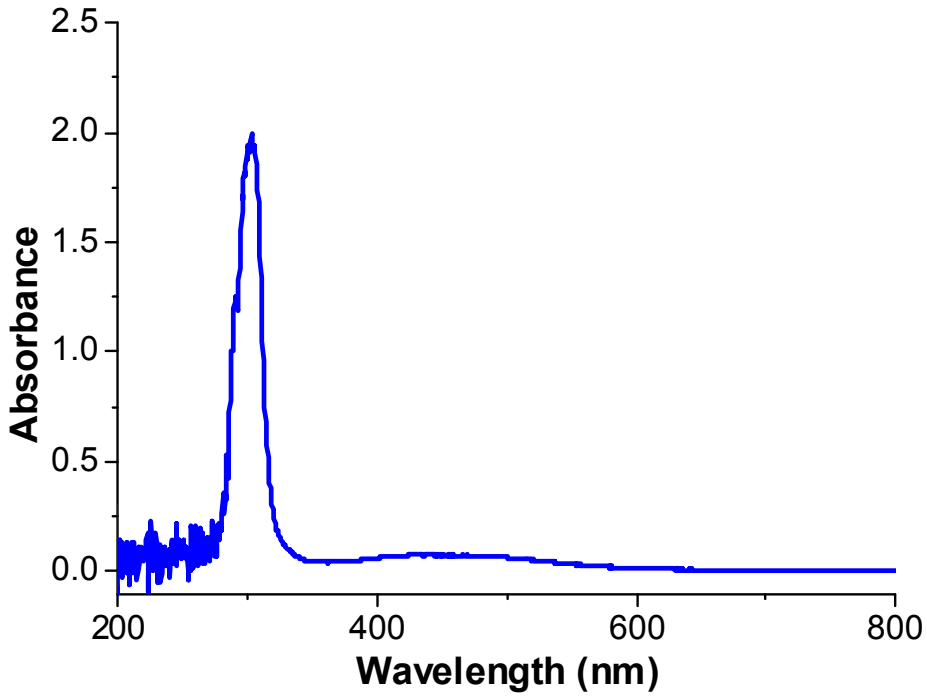

Figure 2.3: A typical UV-Vis spectrum.

In this thesis, UV-Vis spectroscopy was performed with a HR2000+ high resolution spectrometer (Ocean Optics Inc., USA) with DH-2000-BAL light source (Mikropack GmbH, Germany). The absorbance data were exported to ASC II files and the UV-Vis absorption curves were drawn by Origin 6.0.

2.3.2 Water contact angle measurement

Water contact angle (WCA) is a parameter that represents the wettability of the surface. On smooth surfaces the WCA can be determined by Young's equation (Figure 2.4a, Equation 2.2):[191]

$$0 = \gamma_{SG} - \gamma_{SL} - \gamma_{LG} cos\theta_c \qquad (2.2)$$

Where θ_c is the contact angle, γ_{SG}, γ_{SL} and γ_{LG} are the surface tensions between solid/gas, solid/liquid and solid/gas, respectively.

Typically a surface with a static water contact angle greater than 90° is defined as a hydrophobic surface (Figure 2.4b), and a surface with a static water contact angle of less than 90° is considered a hydrophilic surface (Figure 2.4c). However, according to the work from Berg et al., 65° (Berg limit) rather than 90° is the WCA limit between hydrophobicity and hydrophilicity.[192] This is confirmed by theoretical calculation and experimental report.[193–195]

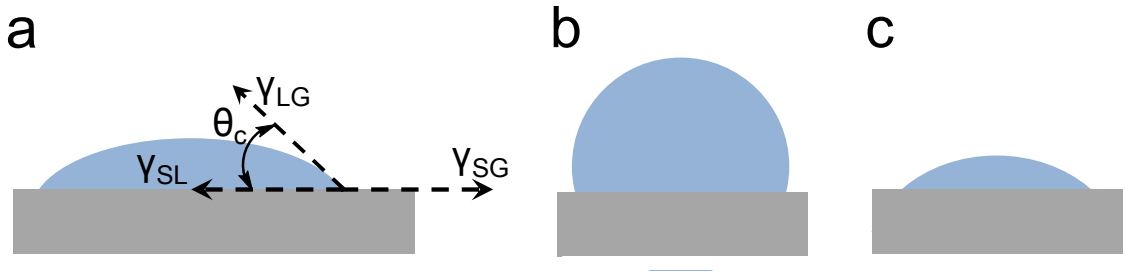

Figure 2.4: Water droplets on a smooth surface. (a) Schematic of a liquid drop showing the quantities in Young's equation. (b) A water droplet on hydrophobic surface, the WCA is higher than 65°. (c) A water droplet on hydrophilic surface, the WCA is lower than 65°.

The wettability of rough surfaces is more complicated. Typically for a water drop on the rough surface, there are two different states: Wenzel state (Figure 2.5a) and Cassie-Baxter state (Figure 2.5b). In the Wenzel model,[196] water penetrates into the space between the protrusions. In this case the WCA is calculated by equation 2.3, in which r is the surface roughness defined as the ratio of the actual surface area to the projected area. For Cassie-Baxter model,[197] air is trapped between the protrusions on the surface, therefore the interface between the water drop and the surface is a composite of air and solid. The WCA in this case is described by equation 2.4, in which f_S refers to the fraction of the solid on the surface.

$$cos\theta_W = r * cos\theta_Y \qquad (2.3)$$

$$cos\theta_B = f_S * (1 + cos\theta_Y) - 1 \qquad (2.4)$$

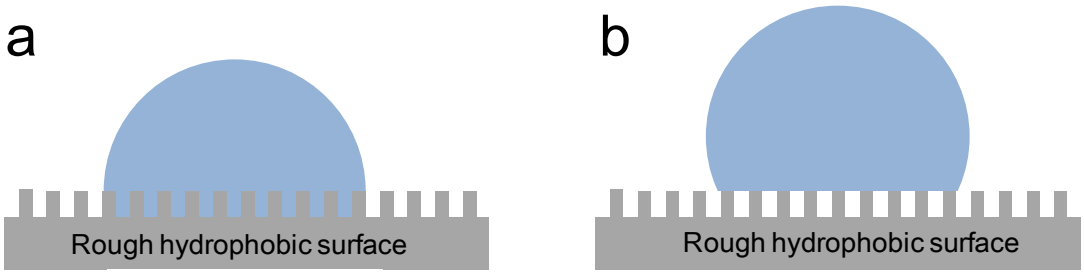

Figure 2.5: Different state of water droplet on rough surfaces. (a) Wenzel state, the gaps between the protrusions are filled by water. (b) Cassie-Baxter state, air is trapped in the gaps between the protrusions.

In this thesis, the WCA of the surfaces is measured by sessile drop method. A water drop is added onto the surface, and a photo is recorded by a camera (from a home-build device). The WCA is calculated from the image by using ImageJ with a DropSnake plugin.

2.3.3 Scanning electron microscopy

The scanning electron microscope (SEM) is used for micro and nano scale imaging measurements.[198] SEM scans the sample (in a raster way) with a focused beam of electrons, which interacts with the sample and produces various signals, such as backscattered electrons, secondary electrons, auger electrons and characteristic X-rays (Figure 2.6), which contain information about the composition and topography of the sample surface.[199] SEM can achieve a resolution better than 1 nm.

The most common mode of SEM detection is secondary electron mode, where SEM detects emitted secondary electrons coming from electron-beam-excited surface atoms. The secondary electron measurement offers the information related to the surface morphology, thus displaying the topography of the surface.

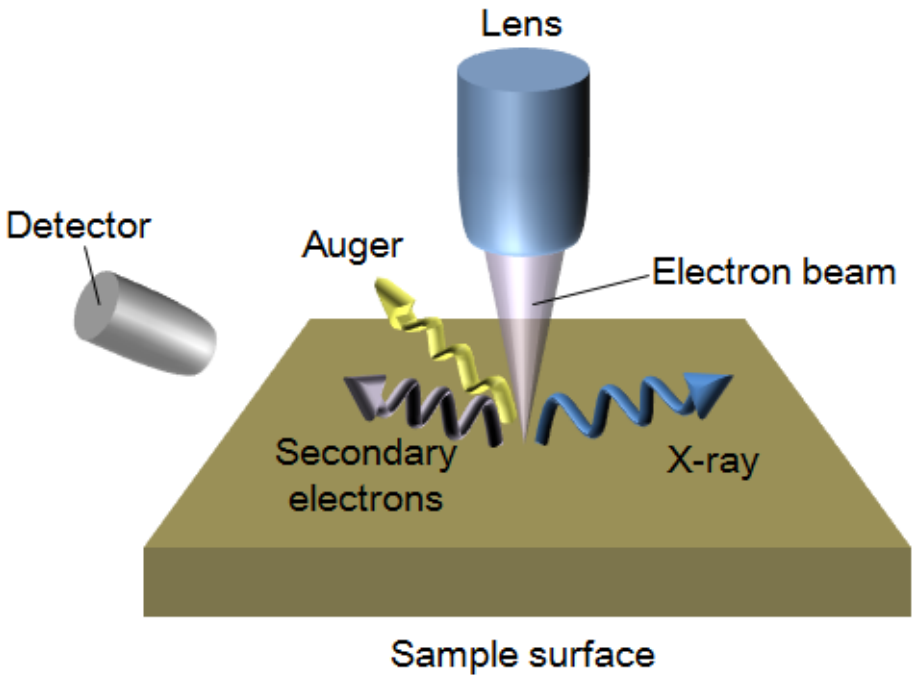

Figure 2.6: Scheme representing the main components of a SEM.

In this thesis, the SEM measurements were performed on a LEO 1530 Gemini scanning electron microscope (Zeiss, Germany). The accelerating voltage was 2 kV. The samples were sputtered with a ~ 30 nm thick gold layer using a Cressington108 auto sputter coater (Cressington Scientific Instruments Ltd. UK) before the measurements.

2.3.4 Time-of-flight secondary ion mass spectroscopy (ToF-SIMS)

ToF-SIMS is a technique used to detect the mass fragments from a surface. ToF-SIMS uses a pulsed primary ion beam to desorb and ionize species from a sample surface. The

ejected secondary ions are then collected and detected by mass spectroscopy.[200] Unlike other SIMS methods (sector and quadrupole), the time-of-flight mass analyzer separates the secondary ions in a field-free drift path according to their velocity.[201] The time of flight varies accordingly to the mass of the ions, thus all generated ions can be detected simultaneously. An illustration for a typical ToF-SIMS device is shown in Figure 2.7.

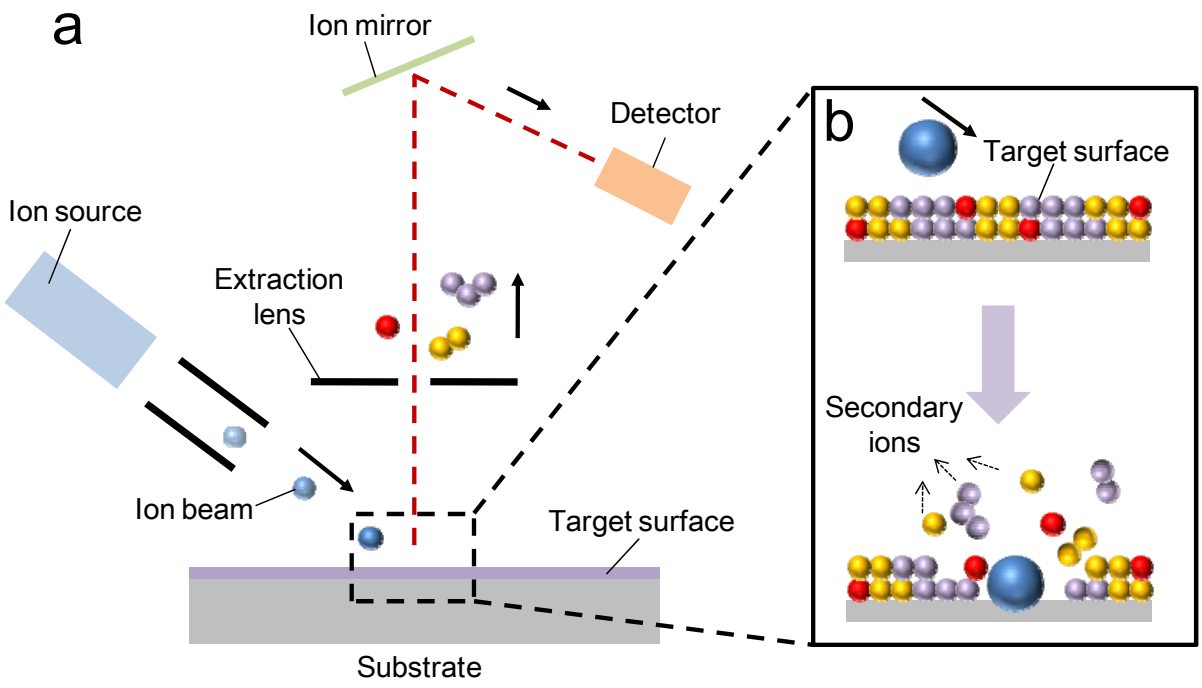

Figure 2.7: Schematic representing a typical ToF-SIMS instrument. High energy (usually several keV) ions are supplied by an ion source and focused on to the target sample, which ionizes and sputters some atoms off the surface. These secondary ions are then collected by ion lenses and filtered according to their atomic mass, then projected onto a detector.

In this thesis, ToF-SIMS measurements were done by a TOF-SIMS 5 machine (ION-TOF GmbH, Münster, Germany). The analysis chamber was held at ~8•10^{-9} mbar during the experiment. A pulsed of 25 keV Bi_1+ primary ion beam was used for all image and spectral data acquisition. All data were collected in high mass resolution bunched mode. A new sample area was used for each analysis.

2.3.5 Atomic force microscopy (AFM)

Atomic force microscopy (AFM) is a high-resolution scanning microscopy technique, which offers the topography of the sample surface.[202] The AFM test is performed through an

AFM tip consisting of a cantilever with a sharp probe (Figure 2.8a), which is used to scan the sample surface.[203] When the probe approaches the sample surface (Figure 2.8b), forces between the probe and the sample lead to a deflection of the cantilever according to Hooke's law (Equation 2.5):[204]

$$F = -k_c \delta_c \qquad (2.5)$$

Where k_c is the stiffness of the cantilever and δ_c is the deflection of the cantilever.

The deflection is measured through the movement of the laser spot reflected from the top surface of the cantilever into a photodetector. Typically, there are two modes for AFM test, the contacting mode and the tapping mode. For the contact mode, the tip is "dragged" across the surface of the sample, and the cantilever is controlled to be at a constant height position above the surface, the recorded movement of the cantilever is therefore related to the height change of the surface. For the tapping mode, the cantilever is forced to vibrate up and down around its resonant frequency, with amplitude of 100-200 nm. When the probe comes close to the surface, the interaction between the surface and the probe (Van der Waals forces, dipole-dipole interactions, electrostatic forces, etc.) decreases the amplitude of probe vibration. During the test the amplitude of the probe vibration is controlled to be constant, the movement of the AFM tip is recorded and the height change of the surface is obtained (Figure 2.8c).

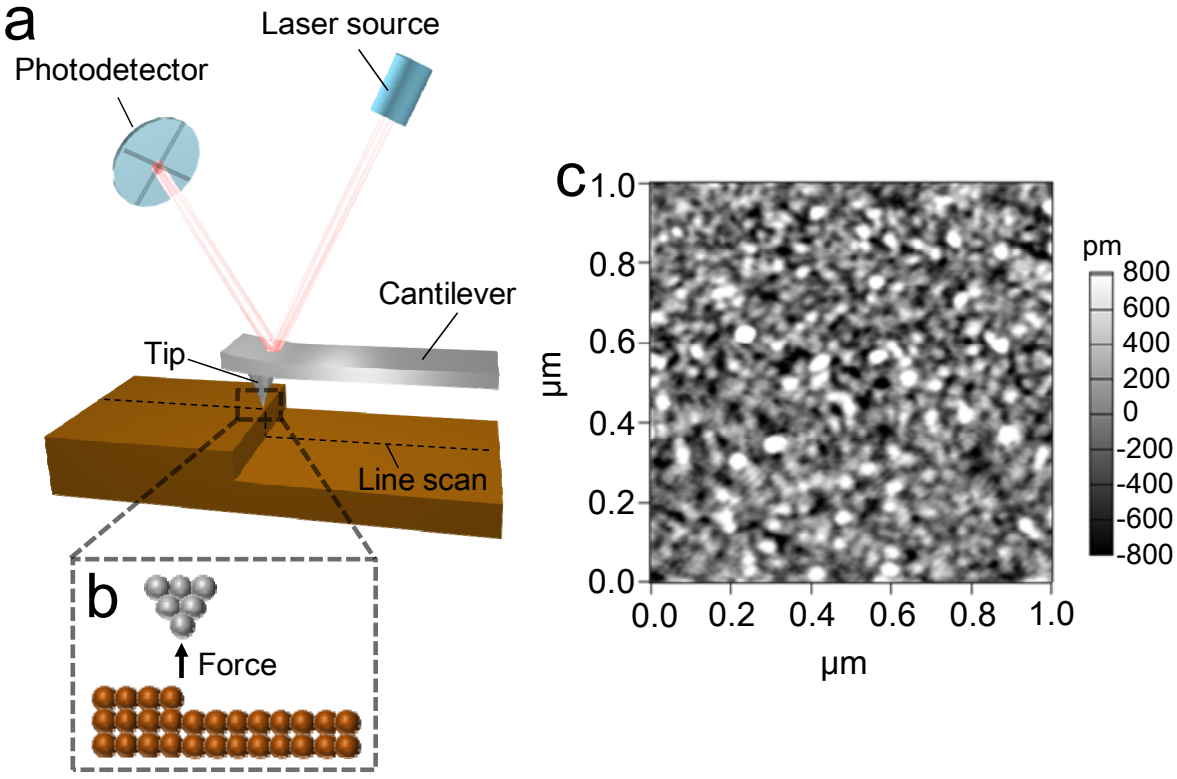

Figure 2.8: Principle of an AFM test (a) and (b). (c) A typical AFM image.

In this thesis, AFM measurements were done in the Institute of Functional Interfaces (IFG) in Karlsruhe Institute of Technology (KIT), with the help of Zhenbang Wang. The data were achieved by a Bruker Dimension Icon AFM, using a cantilever with platinum silicide probe (NanoAndMore GmbH).

2.3.7 X-ray photoelectron spectroscopy (XPS)

XPS is a surface characterization method which is based on the photoelectric effect.[205,206] The principle of XPS measurement is that electrons of an atom can absorb a photon and then be emitted as photoelectrons (Figure 2.9a). For a XPS test, the energy of the emitted electron obeys the equation 2.6:

$$E_K = E_P - (E_B + \emptyset) \qquad (2.6)$$

Where E_K is the energy of the emitted electron, E_P is the energy of each photon from the X-ray, E_B is the binding energy of electron, and $\emptyset$ is the work function of the system (which means how much energy is required for an electron to be emitted from the surface). In a typical XPS test, E_P and $\emptyset$ are known values, E_K and the corresponding amount of the emitted electrons could be measured by the detector. A spectrum of the number of the electrons (intensity) versus the binding energy of the electrons detected could be obtained (Figure 2.9b). Since binding energy is characteristic to elements, the element type and concentrations on the sample surface can be concluded from the XPS test.

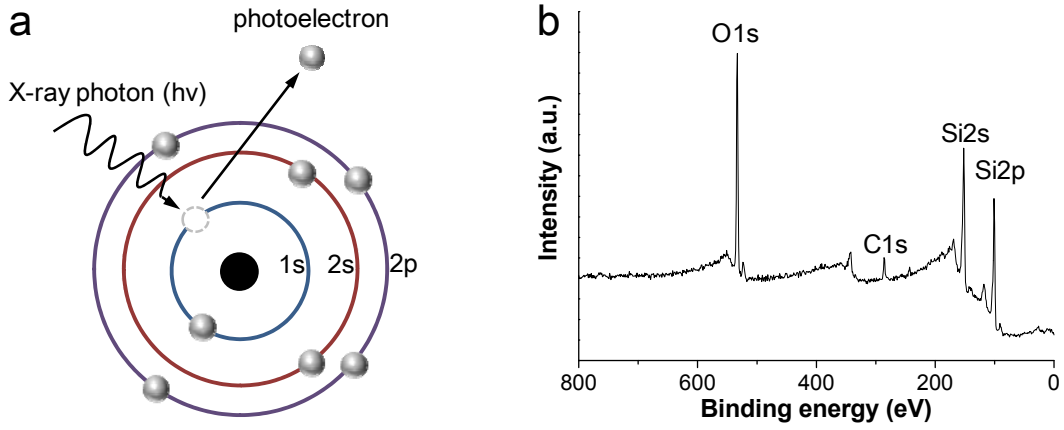

Figure 2.9: Principle of XPS test. (a) Schematic diagram of the principle of XPS test. (b) A typical XPS spectra (silicon wafer as the sample).

In this thesis, the XPS measurements were done in IFG in KIT, with the help of Chengwu Yang and Dr Nefedov. The XPS data were acquired by using a specifically designed ultrahigh vacuum Fourier transform infrared (UHV-FTIR) apparatus (Prevac, Rogów, Poland) fitting

with a hemispherical electron energy analyzer (VG-Scienta R4000) and a non-monochromatic AlKα X-ray source at pass energies (PE) of 100 eV and 200 eV for narrow scans. A Shirley background was used to fit XPS spectra using CasaXPS 2.3.16. An energy calibration was conducted by successive XPS measurement on gold and silver, using the Au 4f binding energy of 84.00 eV and Ag 3d binding energy of 368.27 eV as the reference.

2.3.8 Infrared (IR) spectroscopy

IR spectroscopy measurements are based on the fact that almost all covalent bonds in molecules vibrate.[207] The vibrating covalent bonds could be activated by absorbing radiation at specific frequencies (equation 2.7):

$$\upsilon = \frac{1}{2\pi c}\sqrt{\frac{k}{\mu}} \qquad (2.7)$$

Where υ is the frequency of the radiation, c is the speed of light in vacuum, k is the stiffness of the covalent bond, and μ is the reduced mass of the bonded atoms (equation 2.8):

$$\mu = \frac{m_A m_B}{m_A + m_B} \qquad (2.8)$$

Since k and μ are specific to different bonds, it is possible to distinguish the type of the covalent bonds by their corresponding absorption. IR test measures the light absorption (or transmission) of the molecules in the infrared range. The possible functional group in the molecules can be deduced by analyzing the peaks on the obtained spectra.[208]

Figure 2.10 shows a typical IR absorption spectrum. Normally, different vibrations might exist in one covalent bond: symmetric (sym.) stretching, asymmetric (asym.) stretching, scissoring, rocking, wagging and twisting. Therefore, one covalent bond could have several absorption peaks.

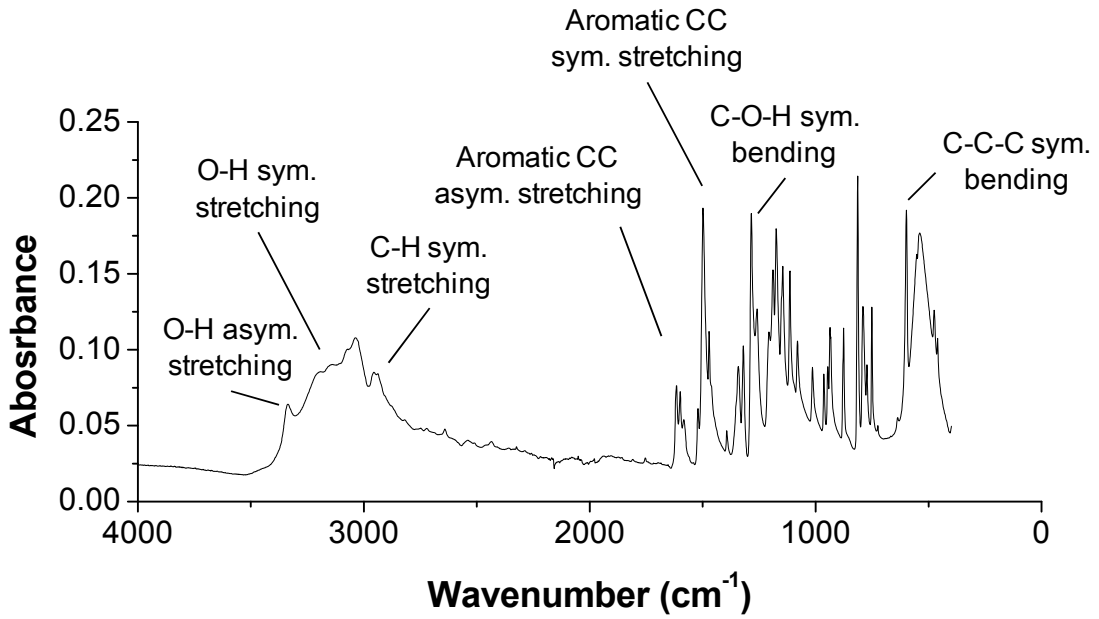

Figure 2.10: A typical IR absorption spectrum. The sample tested is dopamine hydrochloride and some peaks in the spectra are assigned.

It should be pointed out that, in order to show efficient absorption in IR spectra, changes in the dipole during the vibration are necessary. Therefore, for covalent bonds which do not have dipole change (or dipole change is very small) during the vibration (e.g., disulfide bond, triple bond), no corresponding absorbance (or very weak signals) can be found on the IR spectra.[209]

In this thesis, the IR spectroscopy measurements were done in IFG of KIT, with the help of Stefan Heisser. The IR absorption spectra were obtained using a Bruker VERTEX 80 FTIR spectrometer (Bruker Optics, Ettlingen, Germany), equipped with a liquid nitrogen cooled mercury cadmium telluride (MCT) detector and a grazing incidence external reflection accessory, at an incidence angle of 80° relative to the surface with a spectral resolution of 2 cm^{-1}. The polydopamine layers were deposit on gold substrates. Perdeuterated hexadecanethiol SAMs on a gold substrate was used as reference. Dry air was purged continuously through the spectrometer and the sample compartment. Samples were measured when the water absorption bands from ambient air disappeared. The data were processed using the Bruker OPUS® software version 7.2.

2.3.9 Raman infrared spectroscopy

Raman spectroscopy is related to IR spectroscopy. While IR spectroscopy measures the intensity change of the incident IR beam (measurement is done at same wavelength), Raman

spectroscopy measures the opposite, which means that the measurements are done at all wavelength different from the incident IR beam.[210] Raman spectroscopy is based on the "Raman effect". When an IR beam pass through a material, some of the light would be absorbed and some would be scattered. Raman effect refers to the phenomenon that the scattered light contains not only the light at the same wavelength as incident light, but also light at other wavelengths.[211] The mechanism of the phenomenon is explained in Figure 2.11a. First, a photon excites the molecule (either in ground rovibronic state or in an excited rovibronic state) to a virtual energy state; this is followed by the restoration of the rovibronic state and the emission of a new photon. In this procedure, most molecules go back to the original rovibronic state and release a photon with the frequency of the excitation photon (elastic scattering, Rayleigh scattering). However, a little amount of the molecules would not go back to the same rovibronic state, but to a different rovibronic state either in higher energy level or lower energy level (inelastic scattering), releasing a photon with lower frequency (Stokes Raman scattering) or higher frequency (anti-Stokes Raman scattering).[211] Raman scattering results into scattered lights having different wavelength shifts (or wavenumber shifts, Raman shift). The value of the shift only depends on the chemical nature of the molecules (the bonds in the molecules), therefore Raman spectra offer information about the chemical composition of the tested samples.

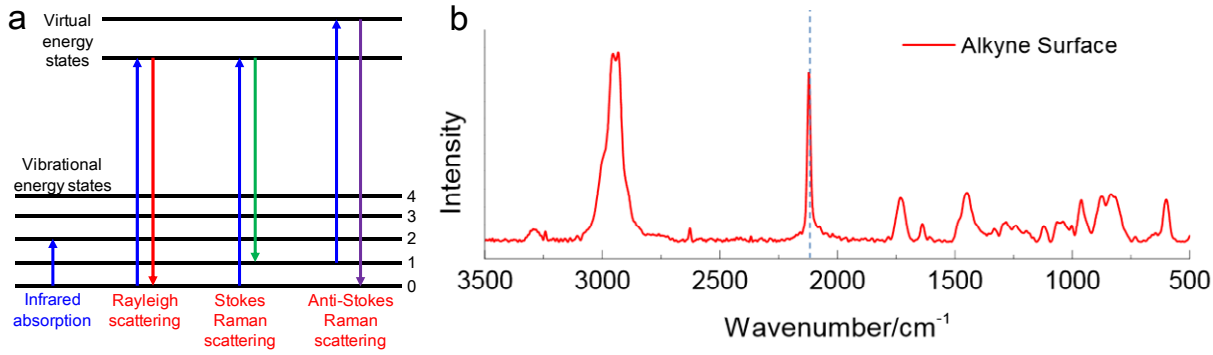

Figure 2.11: Raman scattering and Raman spectra. (a) Schematic diagram of the principle of Raman scattering. (b) A typical Raman spectrum.[212]

Raman spectroscopy allows the analysis of transitions that might not be IR active, for example, centrosymmetric structures such as alkyne and disulfide. Bands which have high intensities in Raman spectra may exhibit weak intensities in IR spectra, and vice versa. Raman spectroscopy is considered to be a complementary characterization method for IR spectroscopy.

In this thesis, Raman spectroscopy analysis were done in IFG of KIT, with the help of Stefan Heisser, by a Bruker Senterra confocal Ramanmicroscope (Bruker Optics, Ettlingen, Germany), which provides a frequency doubled NdYAG Laser = 532 nm, P = 20 mW as excitation source.

2.3.10 X-ray reflectivity (XRR)

XRR is a surface characterization method for thin films and multilayers.[213] In the XRR test, the intensity of the specular reflection of an X-ray beam on a flat surface is measured. By changing the incident angle of X-ray and measuring the corresponding specular reflection (graphic of reflectivity versus incident angle), XRR could offer physical information of the tested films, for example, refractive index, density, thickness, etc.[214]

The XRR analysis is dependent on the reflection and refraction of the X-ray. As shown in Figure 2.12a, when an X-ray is reflected by a surface, the incident X-ray normally generates 3 different waves: a specularly reflected wave, a refracted wave and a diffused reflection. X-ray undergoes total reflection when the incident angle is smaller than the critical angle for total reflection (θ_c). θ_c could be given by the equation 2.9:[215]

$$\theta_c = \sqrt{2\delta} \qquad (2.9)$$

Where δ is the density of the material, thus by measuring the total reflection angle θ_c, the density of the surface could be obtained.

When X-ray is reflected by 2 surfaces (single-layer film, Figure 2.12b), interference would occur between the reflected X-rays, and the obtained reflectivity vs incident angle curve would show oscillations (Figure 2.12c). After the Fourier transformation of the curve (Figure 2.12d), the oscillation is related to the equation 2.10:[215]

$$\rho = cos\left(\frac{4\pi d}{\sqrt{sin^2\theta - 2\delta}}\right) \qquad (2.10)$$

In which ρ is the oscillation, d is the layer thickness and δ is the density of the layer. Thus the thickness of the layer could be obtained in this case.

When a multilayer is analyzed, the conditions are much more complicated, and typically a sample model would be used to fit the results.

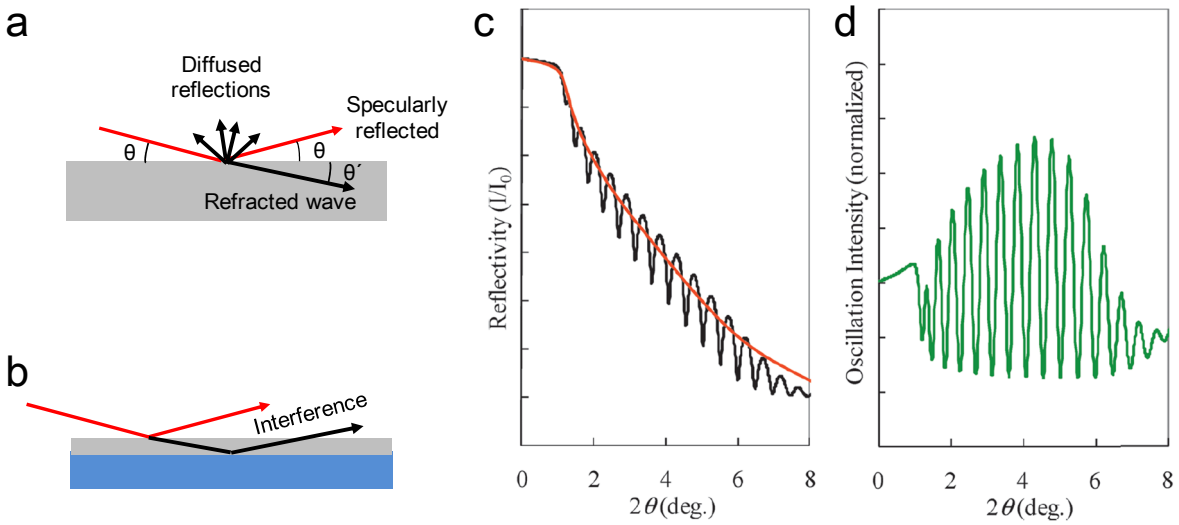

Figure 2.12: Background and principle of XRR measurement. (a) X-ray reflection and retraction on a film. (b) Interference of reflected X-rays on a single-layer surface. (c) Reflectivity vs incident angle results from a XRR measurement.[215] (d) The Reflectivity vs incident angle curve after Fourier transformation.[215]

In this thesis, XRR measurements were performed with a sealed X-ray tube (D8 Advance, Bruker, Germany), operating with Mo *K*α radiation (E = 17.48 keV, λ = 0.0709 nm) and with the help of Nataliya Frenkel. The incident beam was collimated by various slits, reducing the beam size to 200 μm in the scattering plane. Automatic attenuator settings were used to avoid radiation damage. The scans were completed in approximately 3 h. The Si wafer functionalized with PDA was placed on the sample holder horizontally. The momentum transfer perpendicular to the interface is given as a function of the angle of incidence α_i,

$$q_z = \frac{4\pi}{\lambda} \sin \alpha_i .$$

For each measurement point, the reflectivity was corrected for the beam footprint and for the beam intensity with an aid of an in-beam monitor. To minimize the artifacts from radiation damage, we carefully checked the reproducibility of the results by translating the sample position in the direction perpendicular to the beam. The data was fitted by using the Parratt formalism[216] with a genetic minimization algorithm implemented in the Motofit software package.

2.3.11 Ellipsometry

Ellipsometry is an optical method for investigating the dielectric properties of thin layers on a mirror surface.[217] Normally, ellipsometry is used to analyze the thickness and refractive

index of transparent layers. The principle of ellipsometry is shown in Figure 2.13. When polarized light is reflected by a thin film, the polarization (from linear polarized light to ellipse polarized light) and the amplitude of the light would change depending on the thickness of the layer and the optical parameters of the material. Ellipsometry measures the amplitude change ψ and the phase change Δ of the light, and setup a sample model to fit the results. Ellipsometry is a high accuracy method which can be used to measure layers with thickness down to a few atoms.[218]

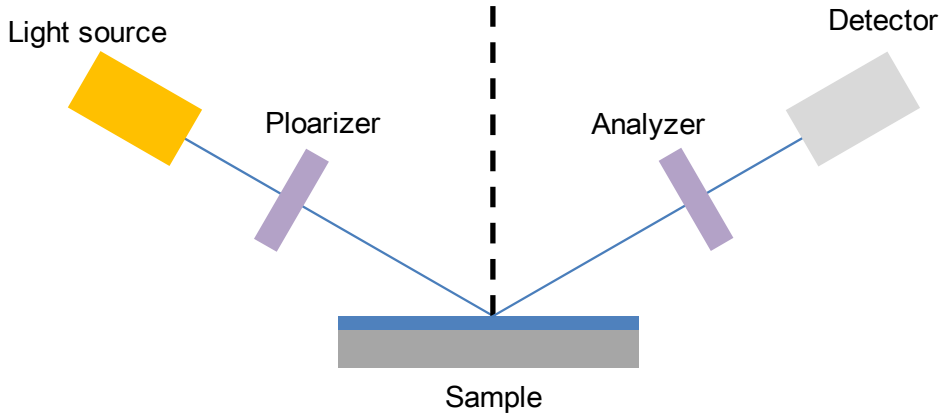

Figure 2.13: Principle of ellipsometry. The light source offers monochromatic light, and the light becomes linear polarized after passing through the polarizer. The detector is capable of recording the intensity of the reflected light at all polarization directions with the help of the analyzer (a polarizer which can rotate).

In this thesis, ellipsometric data were acquired using a SENpro ellipsometer (SENTECH Instruments, Germany) in the rotating analyzer mode at an angle of incidence of 45° in the spectral range of 370−1050 nm. The optical constants of PDA in air were taken from a previous study,[219] and the Cauchy model was used to determine the thickness of the deposited PD layer.[220]

3. Results and discussion

3.1 UV-Triggered Dopamine Polymerization: Control of Polymerization, Surface Coating and Photo-Patterning

3.1.1 Background

Efficient surface modification strategies are crucial for the development of novel functional materials, surfaces and nanoparticles.[6,23,159,221–225] Among different surface coating methods, polydopamine (PD) coatings[85] have attracted great interest due to their ease and generality, as well as their applicability to almost any substrate.[85,121,130,226,227] A typical PD coating can be performed by immersing a substrate into a DA aqueous solution at basic pH.[85] In addition, PD coatings are reactive and can be post-modified by a variety of functional molecules, such as thiols,[85] amines,[86,87] acyl halides,[228] or by metal ions such as Ag^{+} and Cu^{2+}.[85,88] Owing to these advantages, PD coatings were applied for new adhesive surfaces,[22] for surface immobilization of proteins and nucleic acids,[44,229] and for the formation of bio-arrays.[43,128,230,231] These PD coated surfaces have been exploited to create anti-bacterial surfaces,[86,229] adhesive binders,[132] conductive electrodes[137] as well as for the functionalization of nanoparticles.[88,232–234] However, the current PD coating method exhibits some critical limitations. The main drawbacks are the inability to effectively control the onset and termination of DA polymerization,[85,90,97,113] as well as the very slow kinetics of the process, which can take from several hours[95] to a few days.[85] This limits the scope of possible applications of DA polymerization and makes formation of functional PD micropatterns difficult.[43,85,128,230,231,234,235]

In this section, I describe that DA polymerization can be triggered by UV irradiation. Moreover, the polymerization can be induced or stopped using UV light as a trigger. UV-assisted PD coating and photopatterning were demonstrated on different substrates. The UV-triggered DA polymerization and deposition was investigated by ellipsometry, X-ray photoelectron spectroscopy (XPS), X-Ray Reflectometry (XRR) and Time-of-Flight Secondary Ion Mass Spectrometry (ToF-SIMS).

A possible mechanism of DA polymerization is shown in Figure 3.1. DA is first oxidized and rearranged/further oxidized into different quinone structures, which finally participate in the polymerization step. It has been shown that partial removal of oxygen by purging with argon slows down the kinetics of DA polymerization,[85] indicating an important role of oxygen in this process. In addition, basic conditions (pH 8.5) are required to promote and accelerate the dopamine-quinone oxidation and the DA polymerization (Figure S1).[97] However, strong

oxidants, such as ammonium persulfate and sodium periodate, were shown to induce DA polymerization even under neutral or acidic conditions.[90,96]

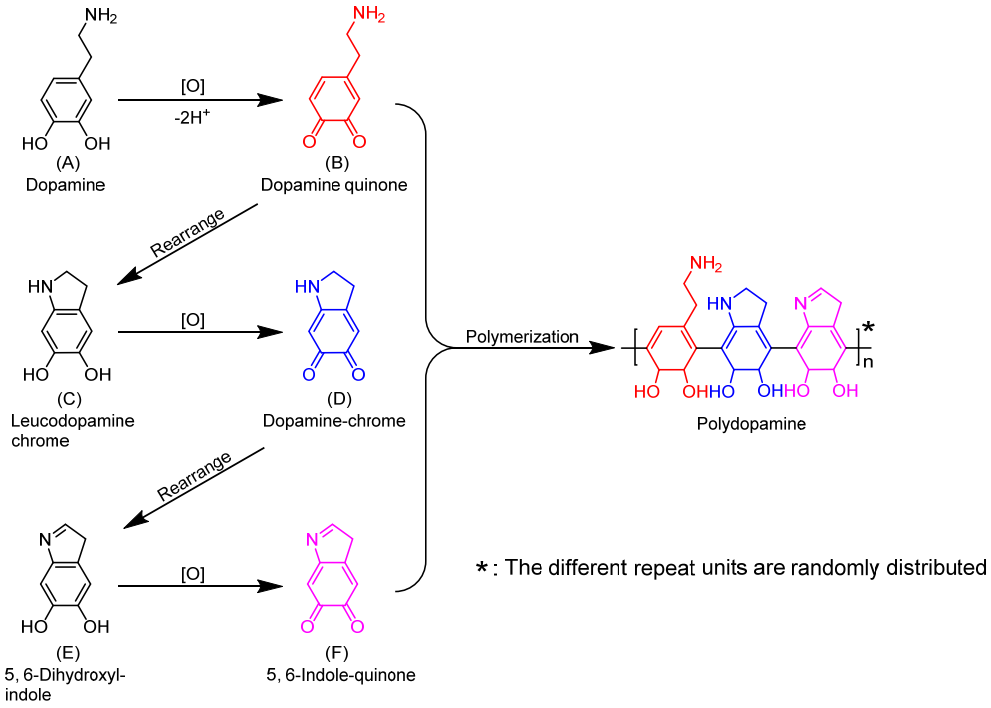

Figure 3.1: Schematic illustration of a possible mechanism of DA polymerization. DA (A) is first oxidized by oxygen to form quinone (B) (DA to dopamine quinone + $2H^+$ +$2e^-$), followed by an intramolecular Michael addition leading to (C). Further oxidation and rearrangement lead to the formation of indole-quinone (F). PD is formed from the copolymerization of (B), (D) and (F).

Reactive oxygen species (ROS), including singlet oxygen ($^1O_2$), superoxide radicals ($O_2^{-\bullet}$), or hydroxyl radicals (·OH), are more active than molecular oxygen and are known to be generated under UV irradiation.[236–239] Taking this into account, I hypothesized that ROS could play the role of the oxidant required to initiate the DA polymerization, thereby controlling the process *in situ* upon UV irradiation (Figure 3.2).

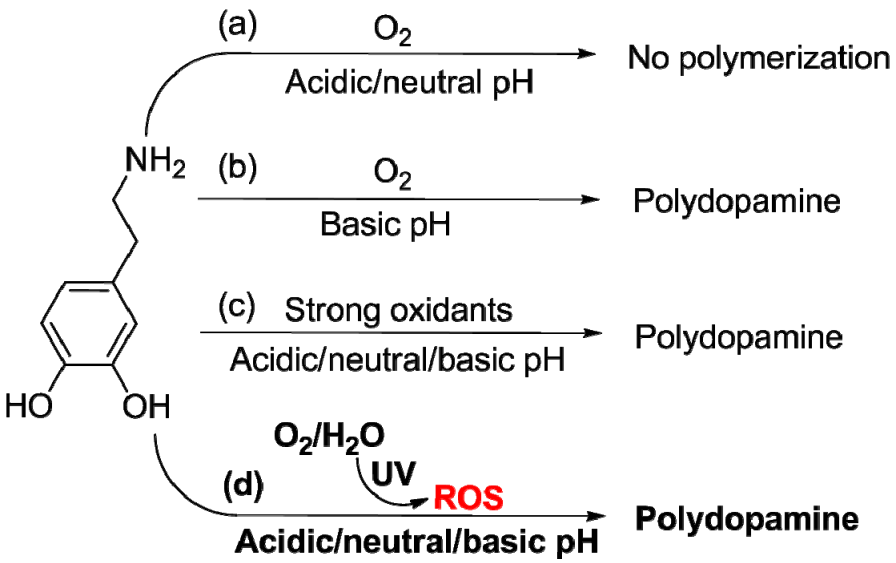

Figure 3.2: DA polymerization under different conditions. (a) Acidic conditions – no polymerization. (b) Basic conditions – fast polymerization. (c) Acidic, neutral or basic conditions, with strong oxidants – fast polymerization. d) Acidic, neutral or basic conditions, with UV irradiation – fast polymerization.

3.1.2 UV-Vis absorption test on dopamine solutions

In order to verify that DA polymerization can be initiated by UV light, the UV-Vis spectra of DA solutions (2 mg/ml) were measured after UV irradiation. The experiment was performed using Tris buffer solutions at pH 8.5 (commonly used for PD coatings[85]) and at pH 7.0 (at which DA polymerization is usually very slow). The solutions were irradiated with UV light (260 nm, 7.5 mW cm^{-2}, HgXe lamp) to achieve continuous generation of ROS. Figure 3.3 shows the time-dependent change of color (Figure 3.3a), as well as the change of absorbance at 420 nm (Figure 3.3b) of the irradiated DA solutions (open symbols), and the non-irradiated samples used as a control (filled symbols). As depicted on Figure 2a, for DA solutions at pH 7.0, UV-irradiated solutions turned dark yellow after 2 hours, while the color change was almost imperceptible in the non-irradiated solutions.

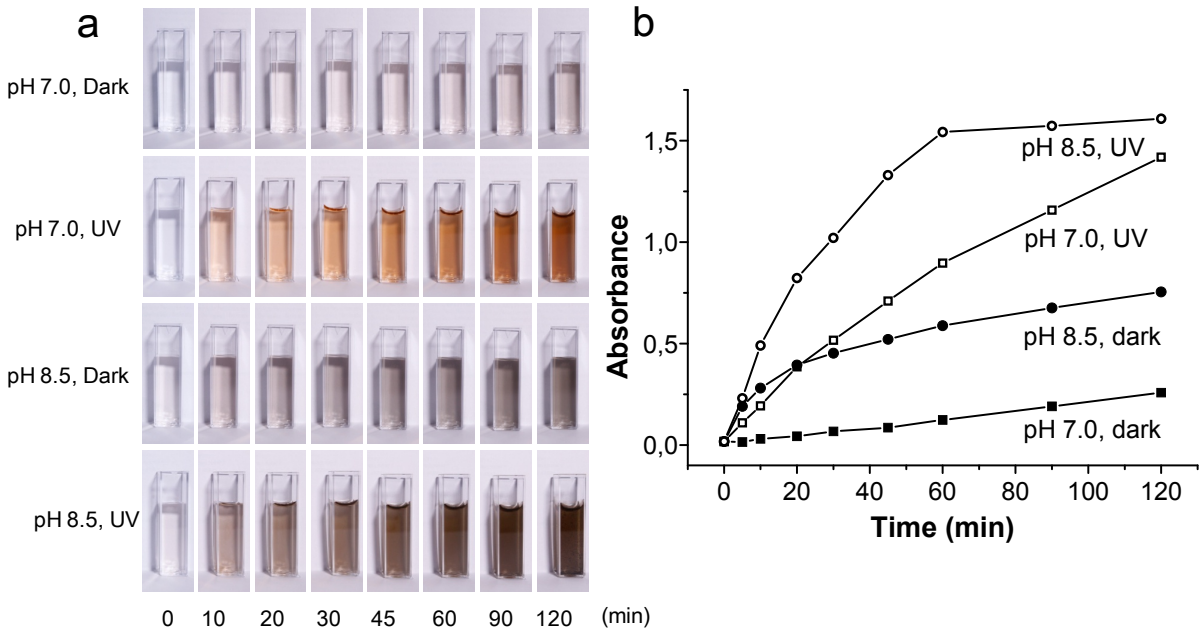

Figure 3.3: Color and absorbance change of DA solutions. (a) Photographs of the corresponding DA solutions at different time points. (b) Absorbance of the DA solution (2 mg/ml) at 420 nm as a function of time and pH.

The observed color changes were also confirmed by UV-Vis spectroscopy (Figure 3.3b and Figure 3.4). The absorbance at 420 nm of the irradiated sample increased from 0 to 1.4 after 2 hours of irradiation, while the non-irradiated solution showed only a small absorbance change from 0 to 0.26 (Figure 3.3b). The basic solutions at pH 8.5 exhibited the same tendencies. UV-irradiated solutions showed darker color (Figure 3.3a) and higher change in the UV-Vis absorbance at 420 nm after 2 hours of UV (Figure 2b, 0 - 1.6 under UV, and 0 - 0.75 in the dark). Moreover, for the DA solutions at pH 8.5, precipitation of large PD particles visible with the naked eyes was observed after 90 min of UV irradiation. On the contrary, no PD particles were observed in the non-irradiated samples after 120 min. The above experiments clearly indicate that UV irradiation accelerates DA polymerization.

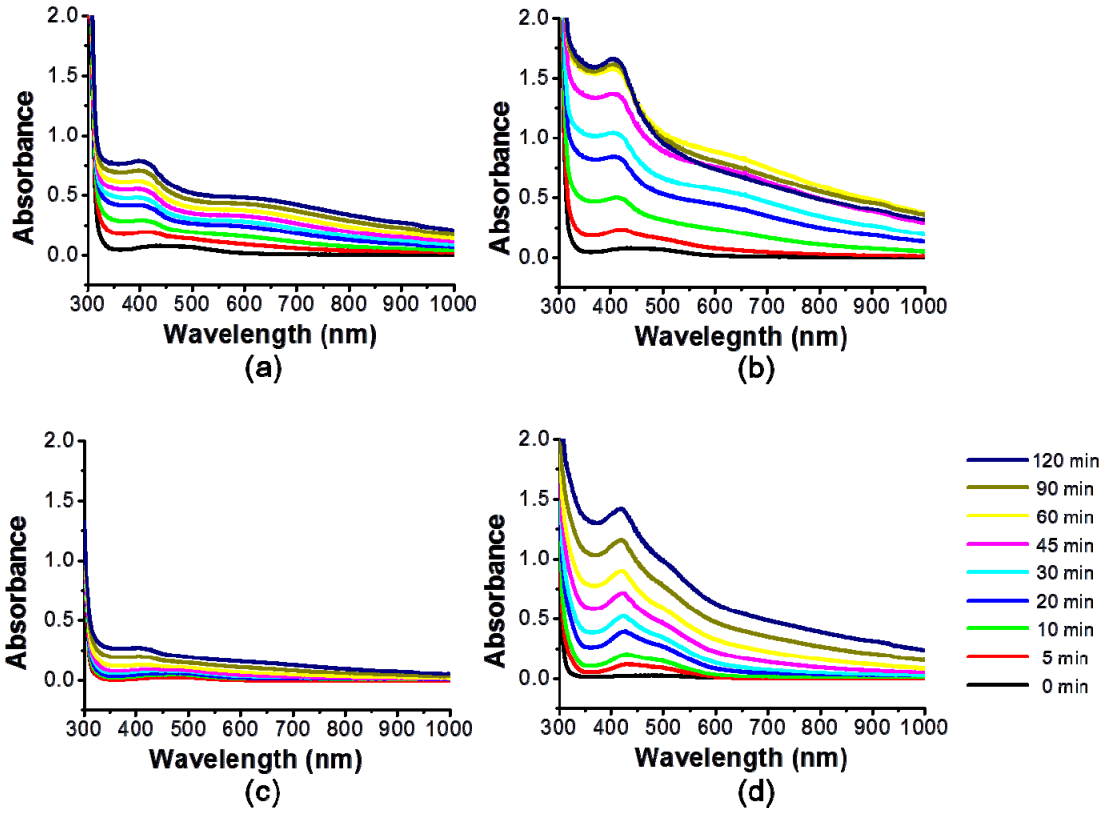

Figure 3.4: Time-dependent UV-Vis absorbance of DA in Tris buffer solutions. The DA concentration in each sample is 2 mg/mL, the concentration of Tris is 10 mM. Samples: (a) Dark environment, pH 8.5. (b) Under UV irradiation, pH 8.5. (c) Dark environment, pH 7.0. (d) Under UV irradiation, pH 7.0.

DA polymerization at different pH were also tested. To do this, DA (2 mg/mL) in buffers (10 mM) with different pH (KCl-HCl buffer pH 2, NaOAc-Acetic acid buffer pH 3/4/5/6, and Tris-HCl buffer pH 7/8.5) were irradiated under UV for 1h, and UV-Vis absorption measurements (300-1000 nm) were recorded before and after irradiation (pure buffers as reference). The same solutions in the dark environment were also used as control samples.

Previously, it was shown that polymerization of DA under acidic conditions was completely inhibited in the absence of strong oxidants,[97,110] which was confirmed by our results (Figure 3.5). However, the irradiation of the DA solution with UV light triggered the DA polymerization even under acidic conditions (Figure 3.5). On the other hand, a clear decrease of the kinetics of DA polymerization upon decrease of pH from 8.5 to 2.0 (Figure 3.5) was also observed.

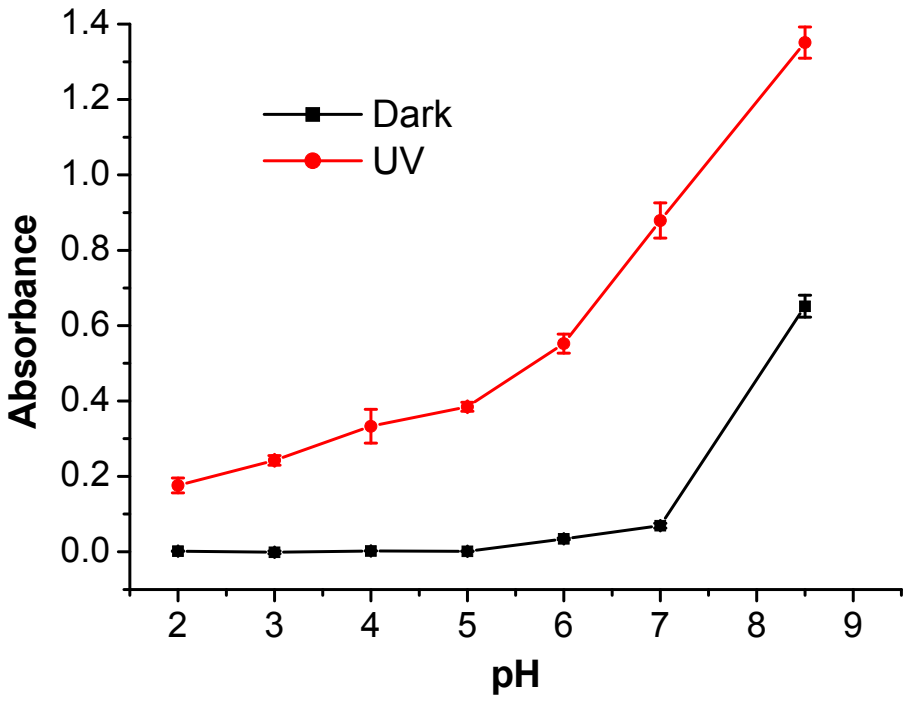

Figure 3.5: UV absorbance (λ = 420 nm) change after 1 h irradiation of DA solutions of different pH. UV-induced DA polymerization was carried out in solutions with different pH (2.0, 3.0, 4.0, 5.0, 6.0, 7.0, 8.5, respectively). UV-Vis spectra were measured (at 0 min and 60 min), and absorbance change at 420 nm was calculated for each sample.

According to the previous reports, DA polymerization under basic conditions can be slowed down by reducing the amount of O_2 in the solution, which plays the role of an oxidant in the course of DA polymerization. In order to test whether the DA polymerization under UV light is based on a possible radical mechanism, oxygen-rich and oxygen-scarce argon-purged solutions were irradiated with UV light as well as were kept in the dark. DA (2 mg/mL) Tris buffer solution (10 mM, pH 7) was filled into cuvettes and irradiated with UV for 2h, UV-Vis absorption spectra (300-1000 nm) were taken at the following time points: 5 s, 10 s, 20 s, 30 s, 1 min, 2 min, 5 min, 10 min, 15 min, 30 min, 45 min, 60 min, 90 min and 120 min. The results (Figure 3.6) showed that the reduction of oxygen in the DA solution led to a decrease in the polymerization kinetics even under UV irradiation. Since oxygen is well known for its ability to trap radicals and inhibit radical polymerization, the result confirmed that UV-initiated DA polymerization was not based on a free radical mechanism.

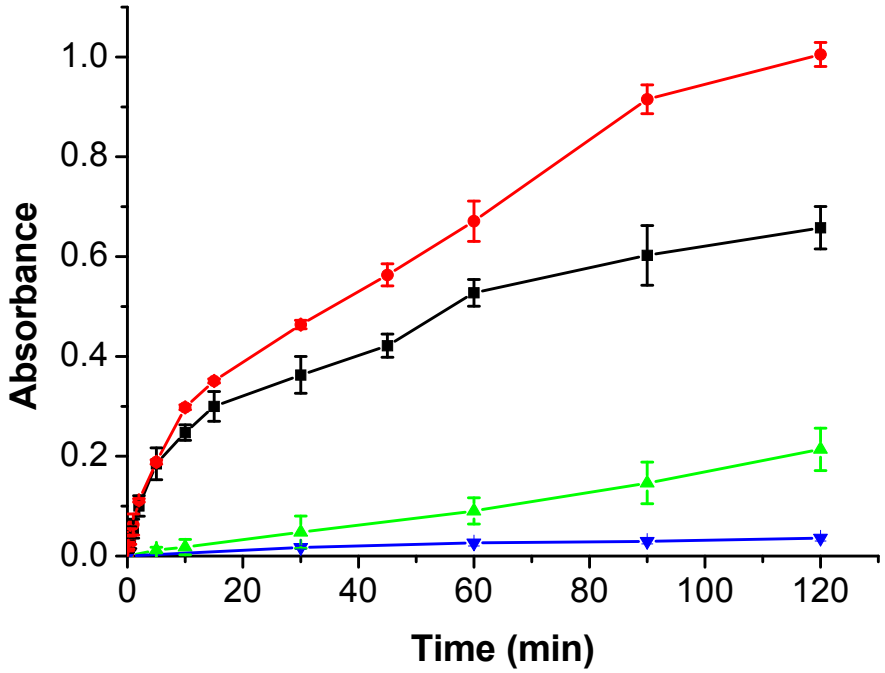

Figure 3.6: UV irradiation on deoxygenated DA solutions (pH 7.0), time dependent absorbance change at 420 nm. Samples: ■ Argon-purged solution after UV irradiation. ● Non-purged solution after UV irradiation. ▼ Argon-purged solution in the dark. ▲ Non-purged solution in the dark. The experiments were carried out using a Tris buffer (pH 7.0) purged with argon for 10 min. For the non-irradiated samples (▼), the absorbance (420 nm) of the argon-purged DA solution remained constant after 2 hours, suggesting that DA polymerization in this case is an oxygen-triggered polymerization. Under UV irradiation, the absorbance of a non-purged DA solution (●) increased faster than that of the low-oxygen-containing (■) sample, demonstrating that UV-induced DA polymerization is indeed oxygen dependent. However, the absorbance (420 nm) of UV-irradiated argon-purged DA solution still increased significantly after 2 hours, in contrast to the invariable absorbance of the non-irradiated argon-purged DA sample. This outcome indicates that UV-triggered DA polymerization can occur even in solutions where oxygen concentration is considerably low, diverging to the oxygen-rich environment needed for the conventional DA polymerization. This phenomenon can be explained by considering that ROS are the species that trigger the oxidation. Since ROS are more active than oxygen, even traces of ROS can trigger DA oxidation.

The observed acceleration of the DA polymerization under UV light may be explained by ROS, which can be generated even from traces of O_2. To confirm that UV-triggered DA polymerization is an oxidation-induced process, 2 mg/mL of sodium ascorbate (SA, an

efficient antioxidant and ROS scavenger)[236,239] was added to the DA solution in order to avoid the generation of ROS during UV irradiation. No polymerization was observed even after 2 hour UV irradiation at pH 7.0 or at pH 8.5 (Figure 3.7a). This confirms that UV-triggered DA polymerization also depends on DA oxidation which can be triggered by ROS. Additionally, I also showed that hydroxyl radicals (·OH, an active ROS), produced using the Cu^{2+}+H_2O_2 system,[240,241] could stimulate the DA polymerization at pH 7.0 without UV irradiation (Figure 3.7b).

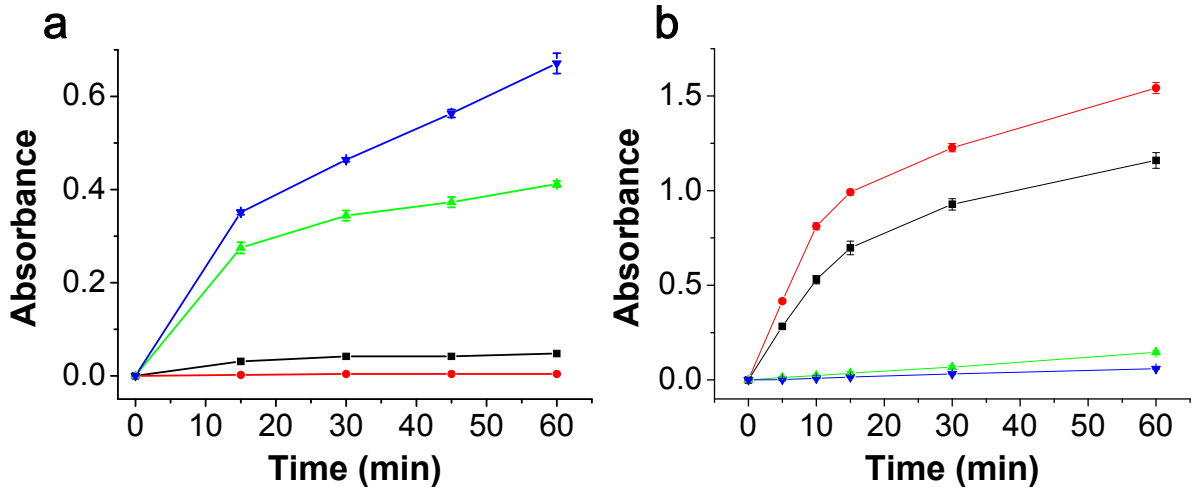

Figure 3.7: Absorbance change (at 420 nm) of DA solutions (2 mg/mL) as a function of time. (a) With and without the addition of SA (2 mg/mL) as an anti-oxidant. With the addition of SA, no polymerization occurred within 60 min. Curves: ■ pH 7.0, with SA, UV irradiated for 60 min. ● pH 8.5, with SA, dark for 60 min. ▼ pH 7.0, UV irradiated for 60 min. ▲ pH 8.5, dark for 60 min. (b) With H_2O_2 as a hydroxyl radical generator and the control sample (at pH 7.0). The solutions without hydroxyl radicals kept their absorbance almost constant, while the solutions with hydroxyl radicals (both UV- or $CuSO_4$-generated) increased their absorbance much faster. Curves: ● DA solution in the dark, with 5 mM H_2O_2 and 0.5 mM $CuSO_4$ as hydroxyl radical generator. ■ DA solution under UV irradiation, with 5 mM H_2O_2 and light as hydroxyl radical generator. ▲ DA solution in the dark with 0.5 mM $CuSO_4$ (pH 7.0, no hydroxyl radical formation). ▼ DA solution in the dark with 5 mM H_2O_2 (pH 7.0, no hydroxyl radical formation).

The half-life of the generated ROS is usually very short (e.g., ~4 μs for singlet oxygen in water, 1 μs for hydroxyl radicals).[238] Taking this into account, I hypothesized that under neutral and acidic conditions, UV triggered DA polymerization can be controlled by the UV. To investigate this, an argon-purged DA aqueous solution at pH 7.0 (Tris buffer) was irradiated with UV for 10 min (ON), followed by 30 min without UV (OFF). The ON-OFF

cycle was repeated three times and the absorbance of the solution at 420 nm was tested after each step. The result depicted in Figure 3.8 shows that absorbance of the DA solution only increases upon UV irradiation. No absorbance increment was observed when the solution was not irradiated. This phenomenon can be explained by the high reactivity and short half-life of the UV generated ROS. Thus, as opposed to the base-induced DA polymerization, the UV-triggered polymerization at neutral or acidic pH can be conveniently controlled by properly regulating the "ON/OFF" mode of the respective irradiation.

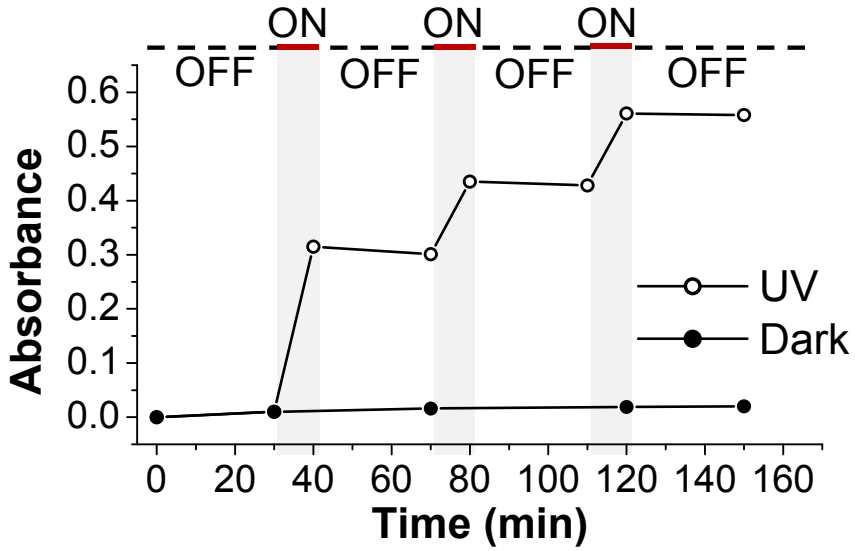

Figure 3.8: Change of absorbance (at 420 nm) of a low oxygen containing DA solution under UV irradiation at 254 nm (○) and in the dark (●). DA solution (pH 7.0, purged with argon for 10 min) was irradiated for 10 min, followed by 30 min in the dark. The cycle was repeated 3 times.

3.1.3 UV triggered polydopamine coating and patterning on different substrates

Having shown the effect of UV irradiation on triggering and controlling DA polymerization, UV-promoted formation of PD layers on silicon substrates was investigated by ellipsometry, X-ray Photoelectron Spectroscopy (XPS), X-Ray Reflectometry (XRR) and Time-of-Flight Secondary Ion Mass Spectrometry (ToF-SIMS).

Four silicon wafers coated with PD under the following conditions were studied: (a) dark, pH 8.5; (b) UV, pH 8.5; (c) dark, pH 7.0; (d) UV, pH 7.0. According to the XPS spectra (Figure 3.9a), the peak corresponding to nitrogen (N1s) was found only in samples prepared by UV-triggered DA polymerization (pH 8.5 and pH 7.0) and by non-irradiated base-catalyzed DA polymerization (pH 8.5), confirming the existence of PD on the substrates. C1s XPS data are presented in Figure 3.9b. For samples where PD coating was found ("UV, pH 8.5", "UV, pH 7.0" and "dark, pH 8.5"), the N/C ratios were 1:6, 1:8 and 1:8, respectively.

The last two N/C ratio values are the same as was previously reported for the PD structure.[2] However, the N/C ratio for the "UV, pH 8.5" sample (1:6) indicates possible binding of the Tris molecules to the PD.

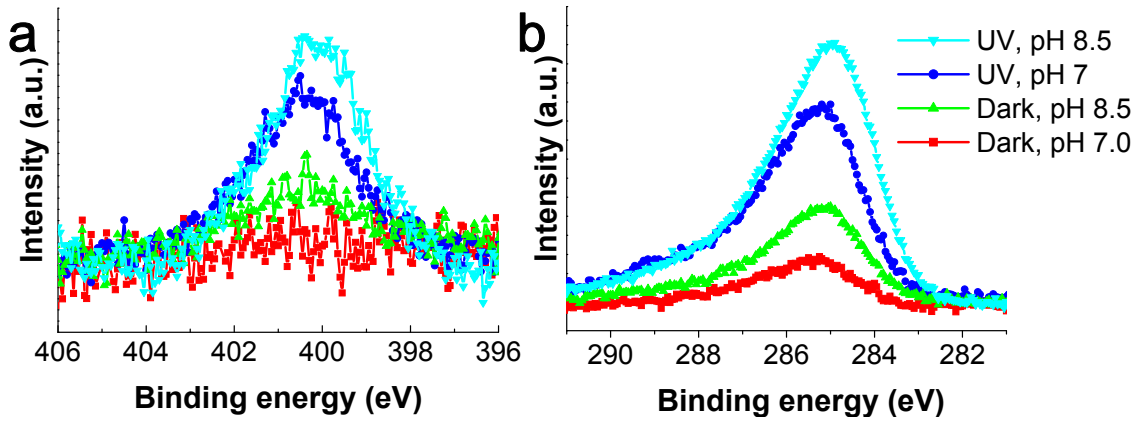

Figure 3.9: Surface characterization on surfaces coated with UV triggered PD. (a) N1s XP spectra of "UV, pH 8.5", "UV, pH 7.0", "dark, pH 8.5" and "dark, pH 7.0" samples. (b) C1s XP spectra of "UV, pH 8.5", "UV, pH 7.0", "dark, pH 8.5" and "dark, pH 7.0" samples.

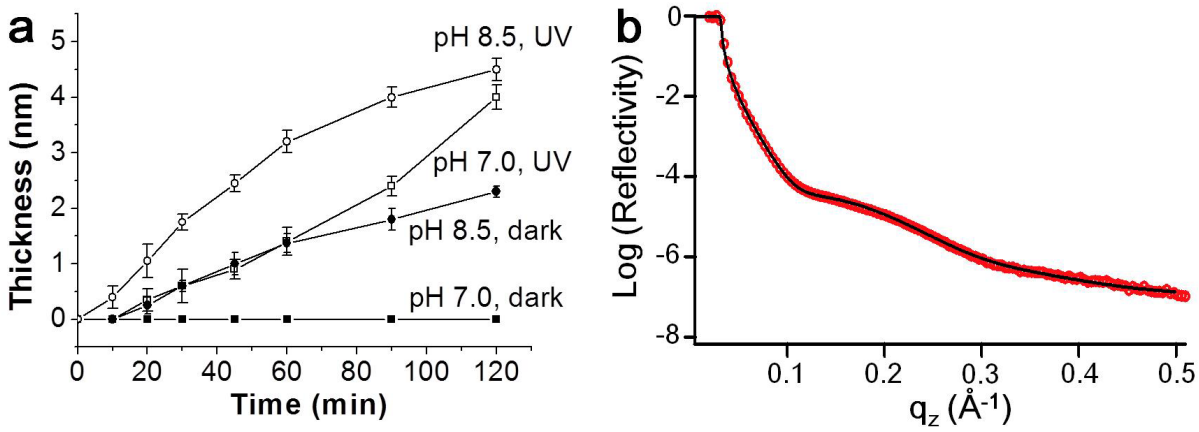

Figure 3.10: Thickness measurement on PD layer by ellipsometry and XRR. (a) Time-dependent PD thickness during the coating process, measured by ellipsometry. Samples: ○ pH 8.5, UV. ● pH 8.5, dark. □ pH 7.0, UV. ■ pH 7.0, dark. (b) XRR result of the PD layer coated on silicon wafer. The sample tested is a (UV, pH 8.5) sample at the time point of 60 min. XRR at high energy (17.48 keV), was measured at the solid/air interface on the sample "UV, pH 8.5" at 60 min time point. The thickness obtained with XRR (2.8 nm) is similar to the value acquired by ellipsometry (3.2 nm).

A time-dependent ellipsometry measurement of the PD thickness on silicon wafers is shown in Figure 3.10a. An acceleration of PD deposition under UV irradiation is clearly

observed. As shown in Figure 3.10a, for surfaces in neutral solution, without UV irradiation (dark, pH 7.0) no PD layer was formed on the wafer, while for the UV-irradiated samples (UV, pH 7.0), a PD layer of 4 nm was obtained after 2h of irradiation. Similarly, samples at pH 8.5 with UV irradiation exhibited higher PD deposition rate (~4 nm in 2h) than the non-irradiated samples (~2 nm in 2h). These results confirm that UV irradiation can accelerate both the DA polymerization and formation of PD layers on solid surfaces.

With the purpose to validate the results obtained by ellipsometry, the thickness of PD coatings obtained after 30 min in the DA solution was also characterized by XPS. From the attenuation of the Si 2p substrate signal in XPS measurements and assuming a homogeneous overlayer I estimated the PD thicknesses to be 1.3 nm, 0.4 nm and 0.8 nm for the "UV, pH 8.5", "dark, pH 8.5" and "UV, pH 7.0" samples, respectively. These values are close to those obtained by ellipsometry (1.8 nm, 0.5 nm and 0.5 nm, respectively). X-Ray Reflectivity (XRR) measurement was also employed to confirm the results of the ellipsometry measurements (Figure 3.10b). The morphology and thickness of a UV-triggered PD layer prepared on a silica surface was also measured by AFM and the result confirmed the formation of a homogeneous PD layer of several nanometer thickness with a nanostructured surface (Figure 3.11 and Figure 3.12).

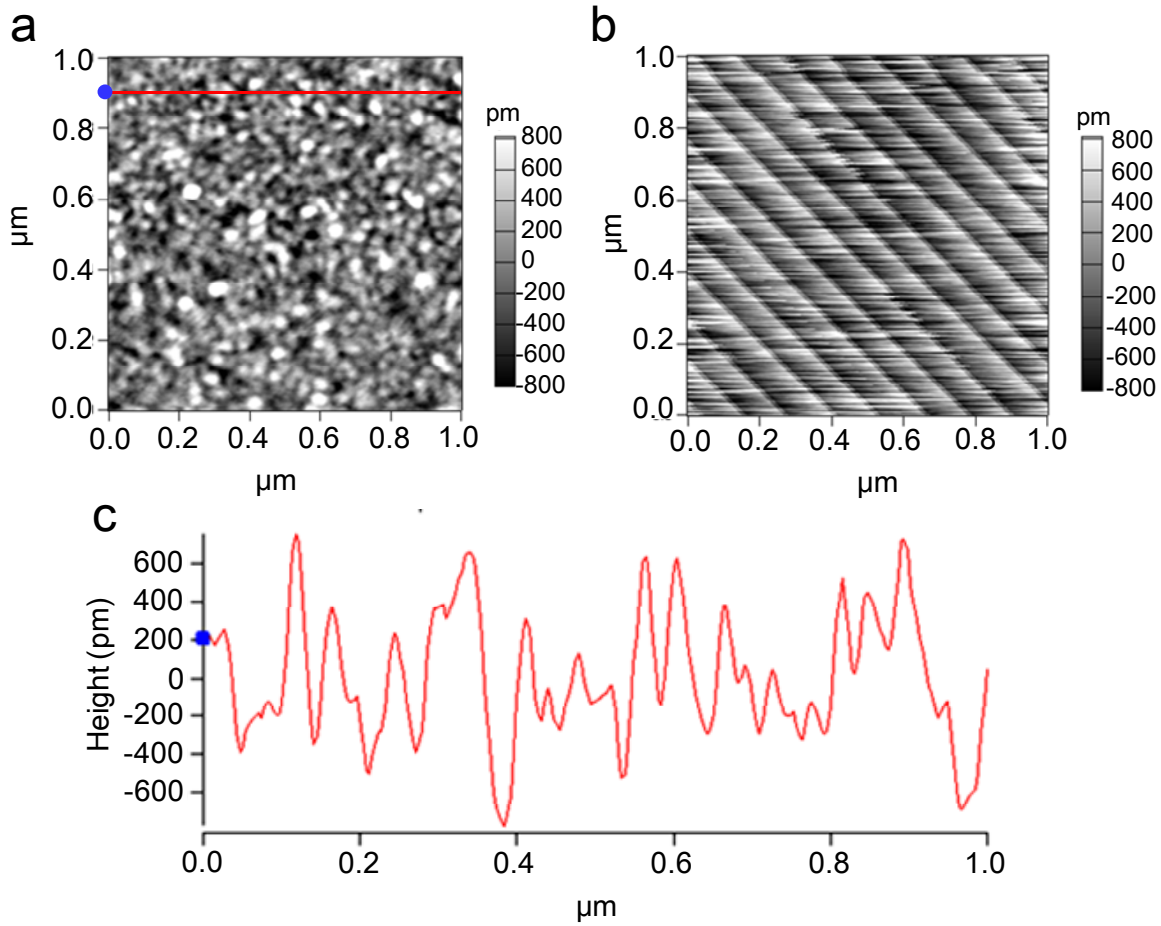

Figure 3.11: AFM of a PD coated silicon wafer (a) and a silicon wafer before PD deposition (b). The sample tested is a (UV, pH 7.0) sample after 120 min of PD deposition. (a) AFM image of the (UV, pH 7.0) PD surface. The height variation is less than 1.6 nm. (b) AFM image of a control uncoated silicon wafer. (c) Height change of the PD layer along the red line in (a).

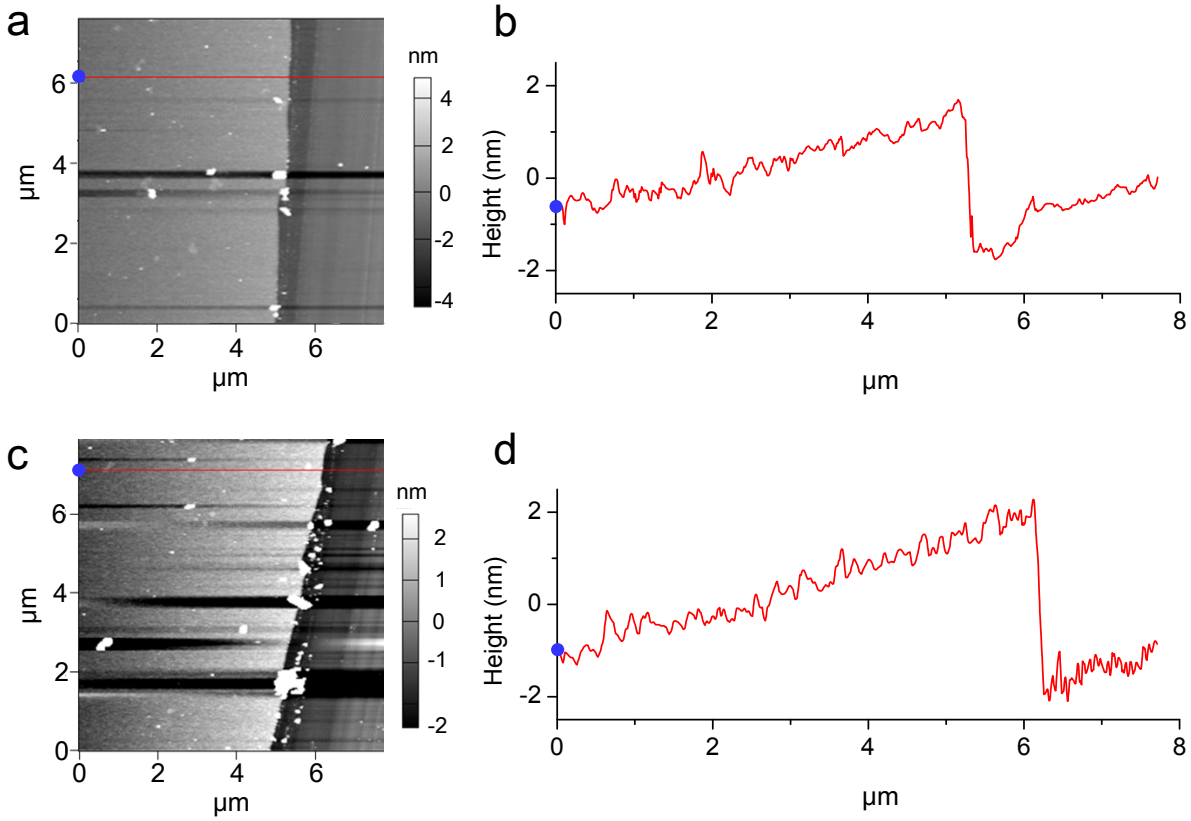

Figure 3.12. AFM scanning image on PD coated silicon wafers gently scratched by tweezers. AFM measurement was performed at the scratch site. (a) Sample: UV, pH 8.5, 60 min. (b) Height change along the red line shown on (a). The calculated thickness of the PD layer is around 3 nm and is similar to the ellipsometry result (3.2 nm). (c) Sample: UV, pH 7.0, 90 min. (d) Height change along the red line shown on (c). The calculated thickness of the PD layer is ~4 nm, which is similar to the ellipsometry result (4 nm).

The structure of UV-triggered PD was investigated by ToF-SIMS. Figure 3.13 shows the negative ion mass spectrum of the PD formed by UV-triggered polymerization (30 min UV irradiation, pH 7.0, Tris buffer). A strong signal corresponding to the DA dimer fragment can be observed at m/z 297. The results obtained by ToF-SIMS confirm that the UV-triggered PD has a similar structure to the base-triggered PD.

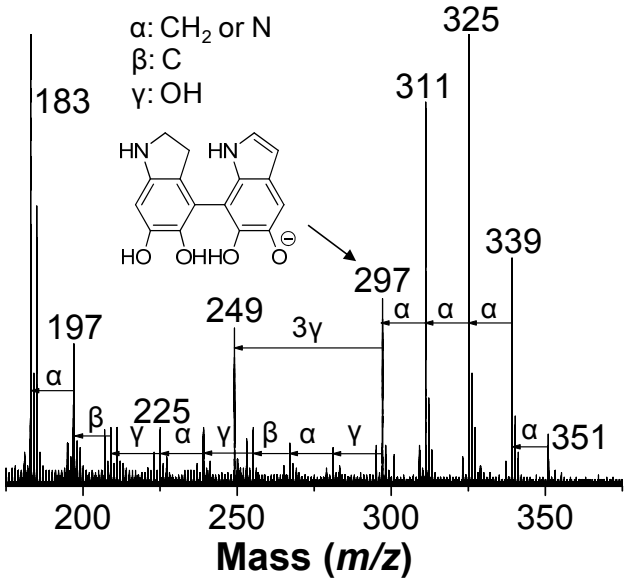

Figure 3.13: ToF-SIMS spectum obtained from the UV triggered PD surface. The mass spectrum of the coated PD (DA concentration 2 mg/mL, pH 7.0, UV for 30 min) shows a dimer structure of 5,6-dihydroxyindole, possibly fragmented from a long-chain polymer of similar composition. A series of peaks, referring to different fragments of the polymer, could be observed in the spectrum.

Considering that one of the major advantages of the base-induced PD coating is its applicability to different substrates,[85] I investigated the UV-triggered deposition of PD on glass, gold, silicon wafer and alumina surfaces (Figure 3.14). The water contact angles (WCA) on these surfaces varied from 11~64° before coating and changed to ~40° after 30 min of UV irradiation at pH 7.0, indicating coverage of the substrates with a PD layer.

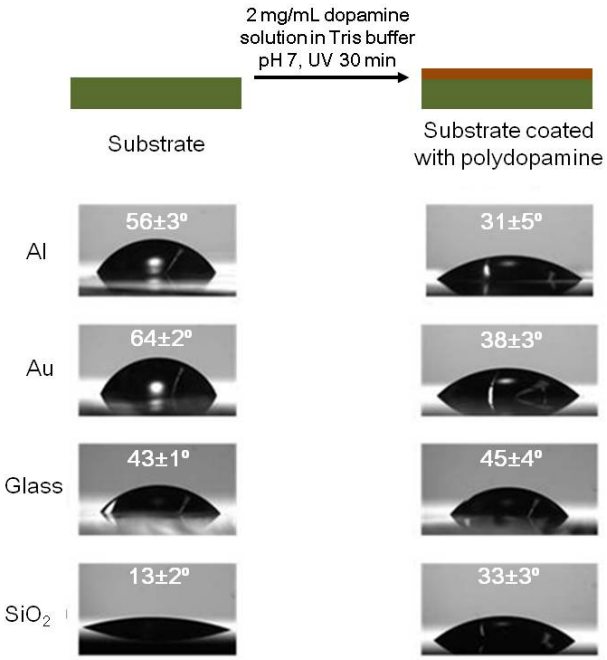

Figure 3.14: Water droplets on different substrates before and after UV-PD coating. Static water contact angles are shown on the pictures.

One of the main advantages of all photochemical surface functionalization methods is the ability to create two-dimension functional surface patterns. Formation of 2D patterns of PD using the base-catalyzed method is difficult due to the poor controllability of the polymerization. Here I show that the UV triggered PD deposition is perfectly suited for the formation of 2D PD surface patterns. As shown in Figure 3c, no PD is deposited on the silicon wafer after 120 min in neutral solution without UV light, while a 4 nm PD layer is obtained in the corresponding UV-irradiated sample. Figure 3.15a depicts the TOF-SIMS mapping results of a PD pattern prepared by irradiating a DA solution (2 mg/ml) at pH 7.0 through a photomask (see supporting information for details). Figure 3.15b shows a microscopy image of a silver nanoparticle pattern, which is formed by immersing a PD pattern, produced on a porous polymethacrylate substrate, into a 50 mM $AgNO_3$ aqueous solution for 18 hours.[85] Figure 3.15c shows a fluorescence image of a dye pattern formed by immersing the PD pattern in a Rhodamine-SH solution for 24 hours, followed by washing with acetone.

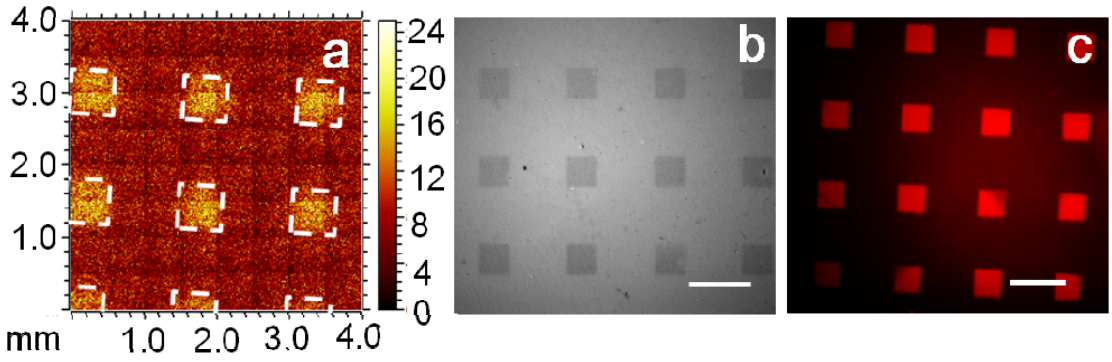

Figure 3.15: Photopatterning of PD. (a) ToF-SIMS characterization of a PD pattern produced by photopatterning on a silicon wafer surface (CN^- intensity map). (b) Bright-field microscope image of a silver nanoparticle pattern produced on a PD patterned surface. (c) Red fluorescence pattern formed by a treatment of the PD pattern with a Rhodamine-thiol solution . The scale bars are 1 mm.

3.1.4 Control of dopamine polymerization in basic solutions

From the above part, it was confirmed that it is possible to control DA polymerization by using neutral/acidic. However, this method cannot be applied in basic solutions, as in this case the polymerization can only be accelerated but not really controlled. The second problem is that, since in neutral solutions oxygen is not able to trigger DA polymerization, in order to keep the polymerization going on, a large amount of oxidants is required. Thus, in the reports where oxidants (Cu^{2+}, ammonium persulfate and sodium periodate) were added to trigger the polymerization, the amount of added oxidants was similar or even higher than that of DA;[96,97] for UV triggered DA polymerization, the solution should be continuously irradiated.

The goal of this part was to improve controllability of DA polymerization under basic conditions. Fortunately, a possible way to achieve this goal could be identified in Fig 3.7a. DA polymerization (in dark) under basic conditions could be efficiently inhibited by the addition of a large amount of an antioxidant, SA, which probably prevents DA from the oxidation by oxygen, thus inhibiting the first step of DA polymerization. Therefore, SA works as a kind of "inhibitor" for the DA polymerization. On the other hand, under UV irradiation, more of reactive oxygen species (ROS) are formed.[70] ROS plays the role of an oxidant – either to oxidize DA to trigger DA polymerization, or to oxidize the antioxidant in the solution to "consume" the inhibitor for the DA polymerization. Therefore, it's reasonable to assume that by adding a small amount of an SA as an inhibitor, it will be possible to "control" the start point of DA polymerization in basic solutions (Figure 3.16).

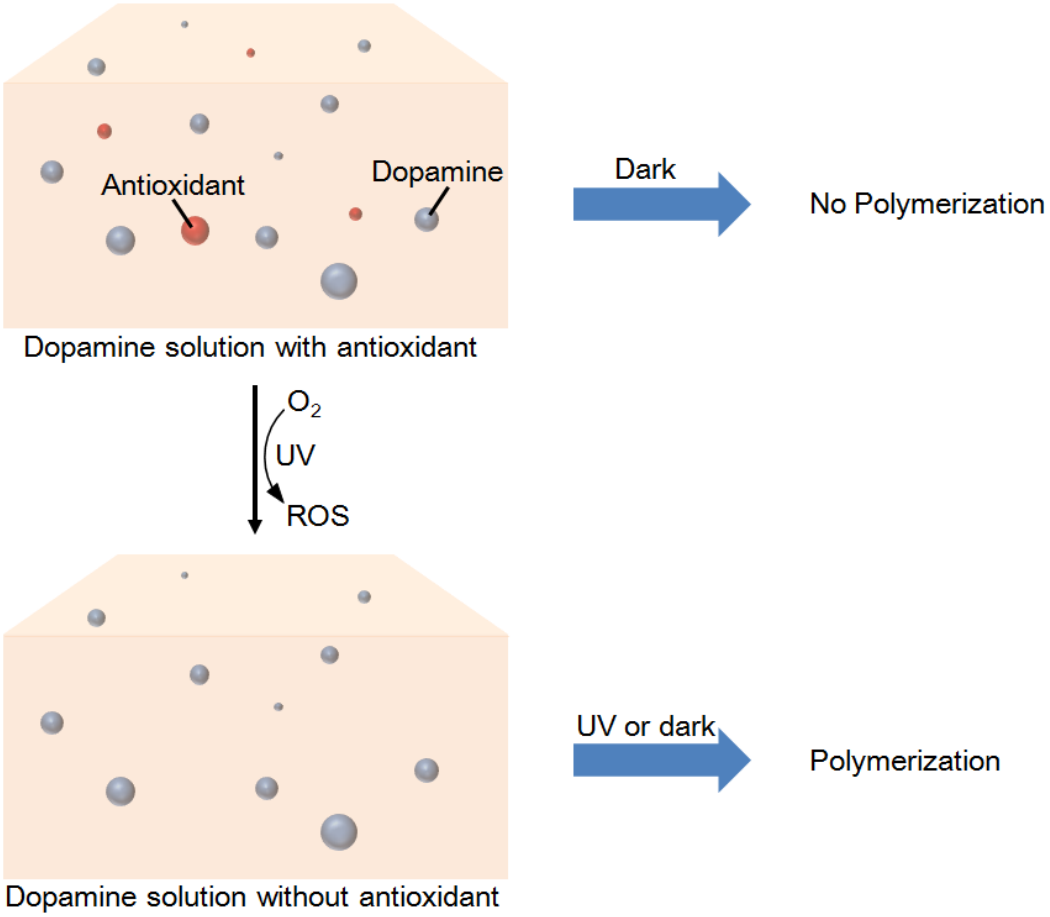

Figure 3.16: Schematic illustration for the mechanism of UV controlled DA polymerization in basic solutions. The antioxidant existing in the solution prevents the DA oxidation reaction and, therefore, inhibits the DA polymerization. After exposure to UV light, antioxidant is exhausted by the ROS generated from UV irradiation, thus DA starts to oxidize and polymerize.

To investigate the possibility of UV controlled DA polymerization in basic solutions, sodium ascorbate (SA) was used as antioxidant. The kinetics of DA polymerization in the presence of SA was first tested. DA solutions with different SA concentrations (0% to 1% wt. with respect to the DA) were prepared and tested with UV-Vis spectrometry. Both the polymerization in dark and under UV were tested for comparison. Figure 3.17 shows the UV-Vis absorption curves of the solutions at different time points. It is obviously that, for the DA solutions in the dark (Figure 3.17, a-e), with the addition of SA, kinetics of DA polymerization become slower, and an induction period could be seen. Figure 3.18 shows the time dependent absorbance change of the solutions at 420 nm, increasing for the time of induction period could be seen along with the increase of SA concentration. SA is a highly active antioxidant, while for DA polymerization, the first step is an oxidation process (DA →

dopamine quinone). Therefore, in the presence of SA, DA oxidation cannot occur (either because the oxidized dopamine quinone is reduced back to DA, or because SA consumes oxygen first), the polymerization is inhibited.

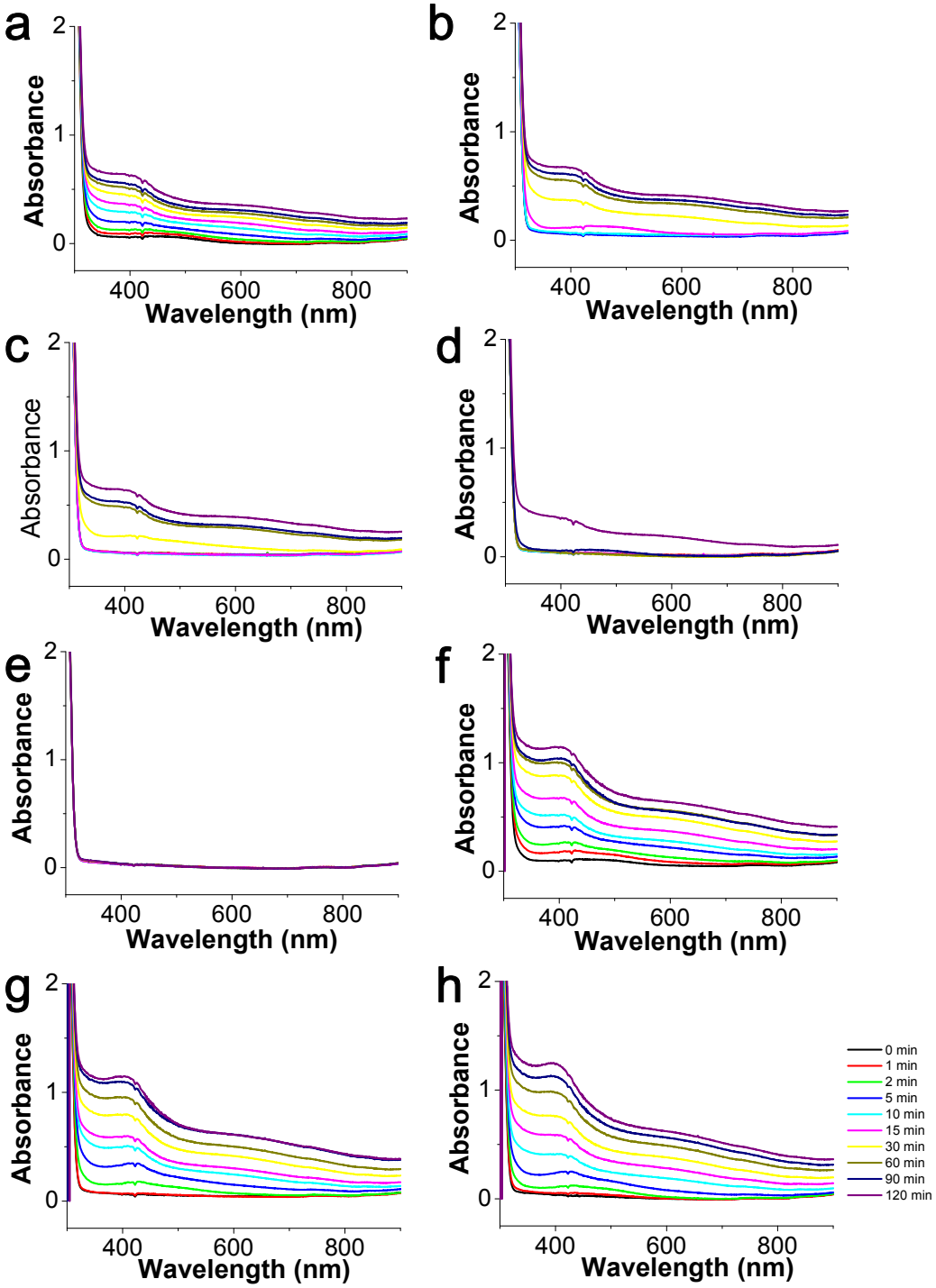

Figure 3.17: UV-Vis spectra of DA solutions (with different SA weight concentration with respect to the DA) at different time points. (a)-(e) in dark, (f)-(h) under UV. (a) without SA .(b) 0.1% wt. SA. (c) 0.2% wt. SA. (d) 0.4% wt. SA. (e) 1% wt. SA. (f) without SA. (g) 0.1% wt. SA. (h) 1% wt. SA.

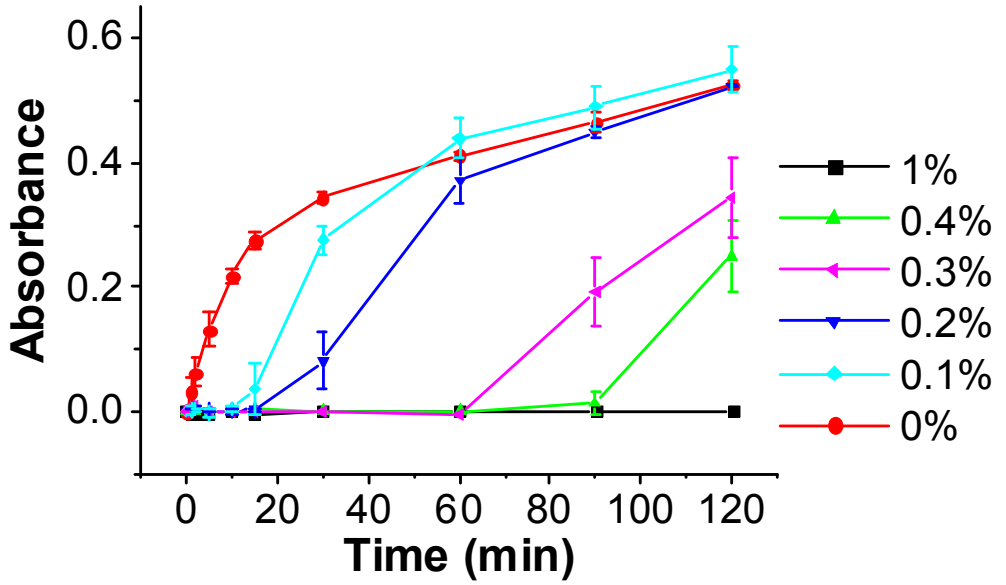

Figure 3.18: Effect of SA on DA polymerization under dark conditions. Time dependent absorption change (420 nm) of DA solutions (2 mg/mL, pH 8.5, in dark) with different SA concentration were tested. DA polymerization showed longer induction period with higher concentration of SA.

When irradiated under UV, however, the results are completely different. As shown in Figure 3.19, DA starts to polymerize immediately after UV irradiation (also see in Figure 3.17, f-h), no induction period could be clearly observed, and the polymerization speed under UV is much higher than the polymerization speed in the dark. The phenomenon could probably be attributed to the formation of reactive oxygen species (ROS) under UV irradiation.[70,242] When exposed to UV light, oxygen forms ROS quickly, thereby exhausting SA and leading to DA polymerization .

The hypothesis is also confirmed by the UV-dark OFF-ON test. As shown in Figure 3.20, when being kept in dark for 3h, DA solution (1% wt. SA with respect to the DA) exhibits no polymerization at all. While after 2 min UV at any time point, DA starts to polymerize even in dark environment. This means the SA is completely consumed during the UV irradiation step, therefore the polymerization in the dark could not be inhibited anymore.

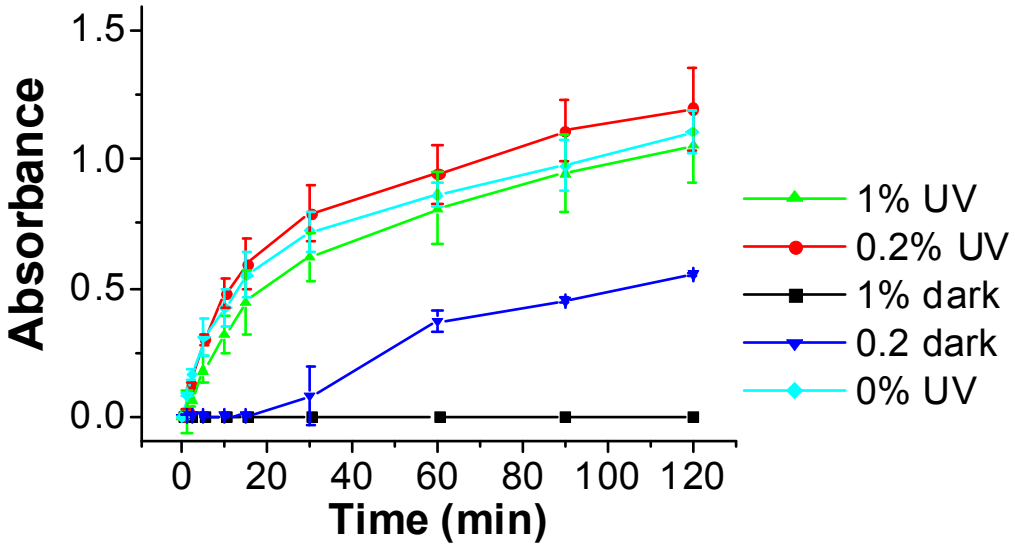

Figure 3.19: Effect of SA on DA polymerization under UV irradiation. Time dependent absorption change (420 nm) of DA solutions (2 mg/mL, pH 8.5, under UV irradiation) with different SA concentration were tested. No induction period could be observed, solution with different SA concentrations exhibit no difference in absorption change.

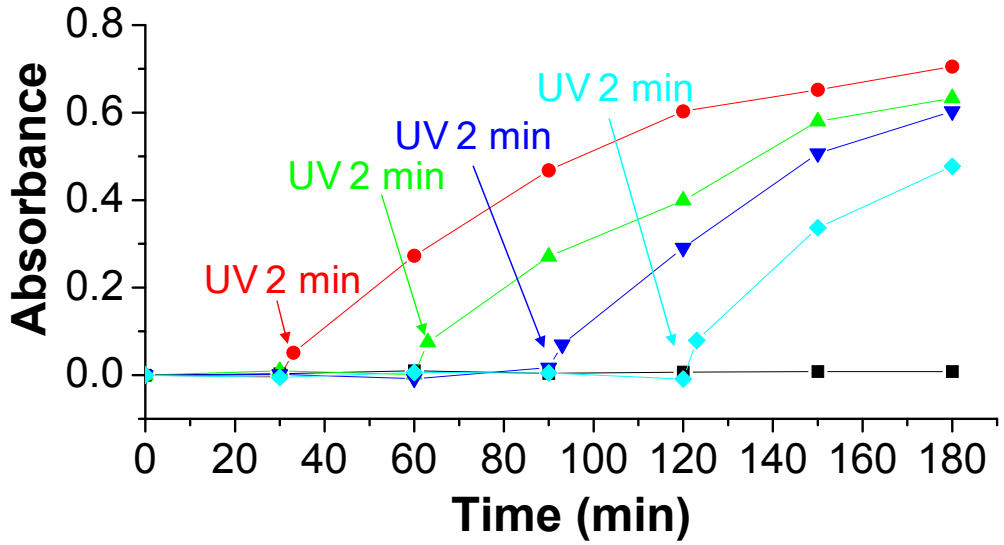

Figure 3.20: Absorbance change of the DA solution during ON-OFF experiment. For the test, DA solution (2 mg/mL, pH 8.5, containing 1% wt. SA with respect to the DA) was kept in the dark during 3h, and samples were UV irradiated for 2 min at different time points. The absorbance of the solution at 420 nm was recorded after each 30 min. From the graph it is obvious that SA cannot inhibit DA polymerization in the dark after 2 min of UV irradiation.

By increasing the concentration of SA, it is possible to achieve long-term control of DA polymerization in basic solutions. As shown in Figure 3.21, DA solution without SA starts to

polymerize immediately after the formation of the solution, while with 5% wt. SA (with regard to DA) it is possible to inhibit DA polymerization for over 24h. Nevertheless, 6 min UV irradiation is able to "initiate" the polymerization at any time points in between, therefore enabling a better control of DA polymerization.

SA is also able to inhibit DA polymerization after the onset of polymerization. As shown in Figure 3.22, by adding 5% wt. SA (with respect to the DA) into a polymerizing DA solution, the polymerization of DA could be completely stopped. However, 1% wt. of SA is not enough for complete inhibition of DA polymerization.

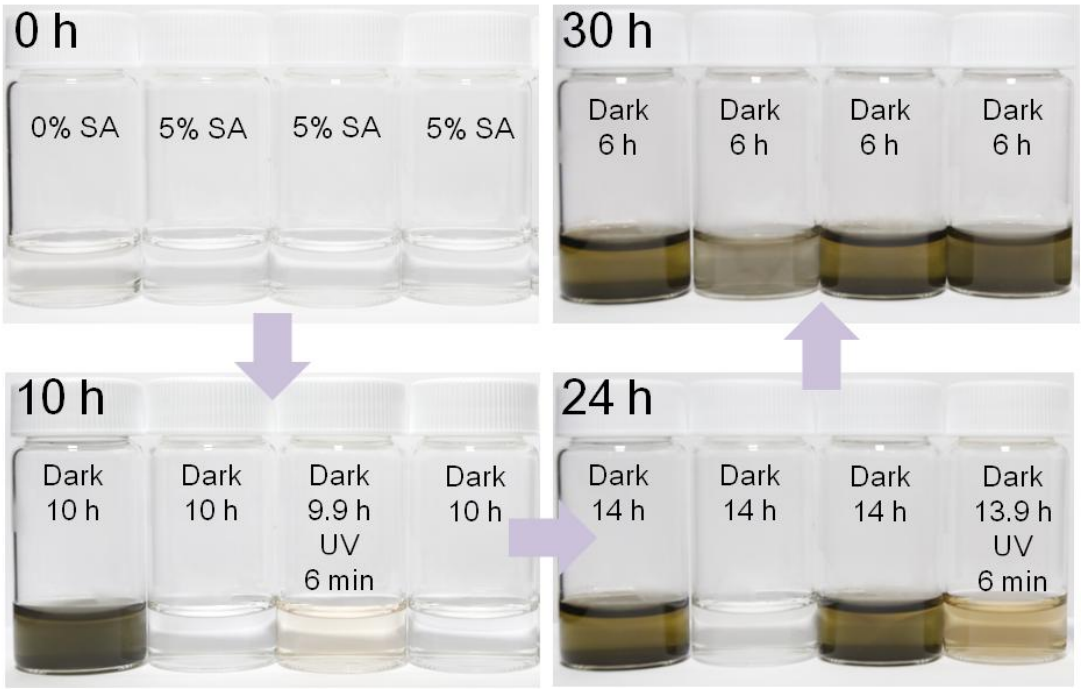

Figure 3.21: Long term test for the UV controlled DA polymerization at pH 8.5. SA (5% wt. corresponding to DA) was added into the DA solution to inhibit polymerization, and DA polymerization could be inhibited for about 30h. The polymerization could be initiated at any time point by a 6 min UV irradiation.

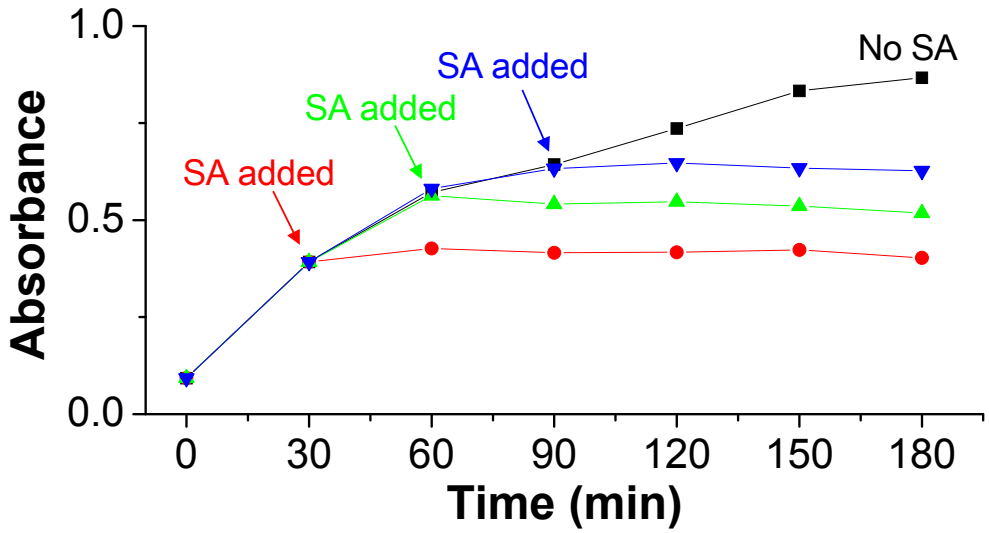

Figure 3.22: SA can "stop" DA polymerization during the propagation. Polymerization can be stopped by adding 5% wt. of SA to a 2 mg/mL of DA solution..

By combining SA and UV irradiation, it is possible to achieve full control on DA polymerization in basic solutions. As shown in Figure 3.23, by adding 1% wt. (with respect to the DA) of SA, DA polymerization was completely inhibited for 1h. By UV irradiation for 2 min, DA started to self-polymerize in the dark and the absorbance of the solution increased. After the addition of 3% wt. SA at the time point of 2h, PD propagation was stopped, the absorbance of the solution was constant for 1h. 5 min UV irradiation could restart the polymerization, as proved by the increase of absorbance at 420 nm. The "inhibition-initiation" cycle could be repeated by a sequential perform addition of SA and UV irradiation, demonstrating a good control over the DA polymerization. However, it should be point out that, as the DA polymerization goes further, the amount of SA required for inhibition also increases.

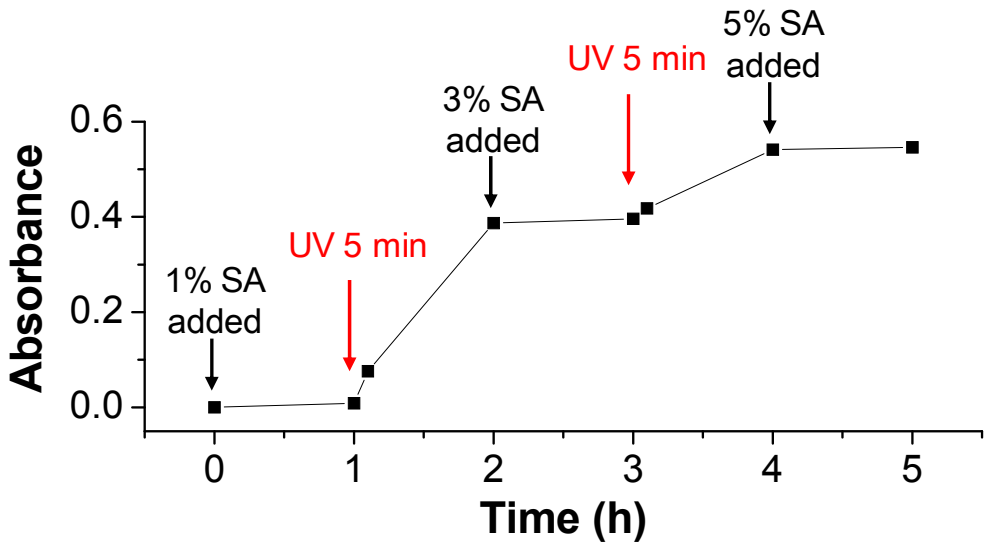

Figure 3.23: Full control of DA polymerization by combining SA and UV irradiation. 2 mg/mL DA solution with 1% wt. (with respect to DA) SA was placed in the dark for 1h, followed by 5 min UV irradiation to initiate the polymerization. After another 1h, 3% wt. (with respect to DA) SA was added into the solution to stop the polymerization. The inhibition-initiation cycle was repeated twice and the absorbance of the solution (at 420 nm) was recorded at each time point. The percentage of the SA refers to the weight of DA in the solution.

The detailed mechanism for the inhibition effect of SA is not clear yet. However, from the former reports on the antioxidation effect of SA and catechol, a possible mechanism could be proposed. SA is a highly reactive antioxidant and could react with oxygen quickly in aqueous solution, which has been used in grape wine protection.[243,244] The reaction was believed to result in dehydroascorbic acid and hydrogen peroxide (Figure 3.24a).[243,244] While in basic solutions, hydrogen peroxide would be decomposed to form water and oxygen (Figure 3.24a),[245,246] thus in the oxidation process of SA, oxygen works partly as a "catalyst". The SA oxidation reaction can occur repeatedly until SA is completely consumed, and then DA oxidation starts. Since the oxidation reaction of catechol was also reported to produce H_2O_2 (Figure 3.24b),[247] in this case the oxidation process should be similar to the oxidation process of SA. Therefore, I can propose a hypothesis for the inhibition effect of SA (Figure 3.25): in DA solution without SA, DA reacts with oxygen to produce different quinones (Figure 3.25, reaction a), followed by the polymerization step. If SA is added previously, however, the oxidation reaction is limited to the reaction between oxygen and SA (Figure 3.25, reaction b). The oxidation reaction continues until the SA is completely consumed, and then DA oxidation starts (Figure 3.25, reaction a). If SA is added during the propagation, SA

will react with oxygen (Figure 3.25, reaction b) prior to DA, and reduce the oxidized quinones back to catechols (Figure 3.25, reaction c), thus inhibiting the polymerization.

This hypothesis can explain many unexpected phenomena occurred during our experiments. For example, (1) why does the addition of H_2O_2 inhibits the DA polymerization (Figure 3.7b, Figure 3.26)? This can be explained by the fact that the addition of H_2O_2 would push the equilibrium of the DA oxidation reaction (Figure 3.25b) to the DA side, thus inhibiting the DA oxidation. However, the decomposition of H_2O_2 (increase of O_2 concentration) will finally push the equilibrium of the reaction to the DA quinone side, triggering the start of DA oxidation and polymerization. (2) Why is more SA required to inhibit DA polymerization as the propagation goes on (Figure 3.23)? In this case, SA reacts not only with oxygen in the solution, but also with the produced quinones in the solution (which were previously oxidized in the DA oxidation cycle reaction).[247] As the polymerization goes further, more and more DA molecules are oxidized. To completely inhibit the oxidation, the amount of SA should be more than the total amount of oxygen and quinone. Thus, as the polymerization goes on, more SA is required for inhibition. This hypothesis can explain the observed experimental data. However, more evidence is required to confirm this.

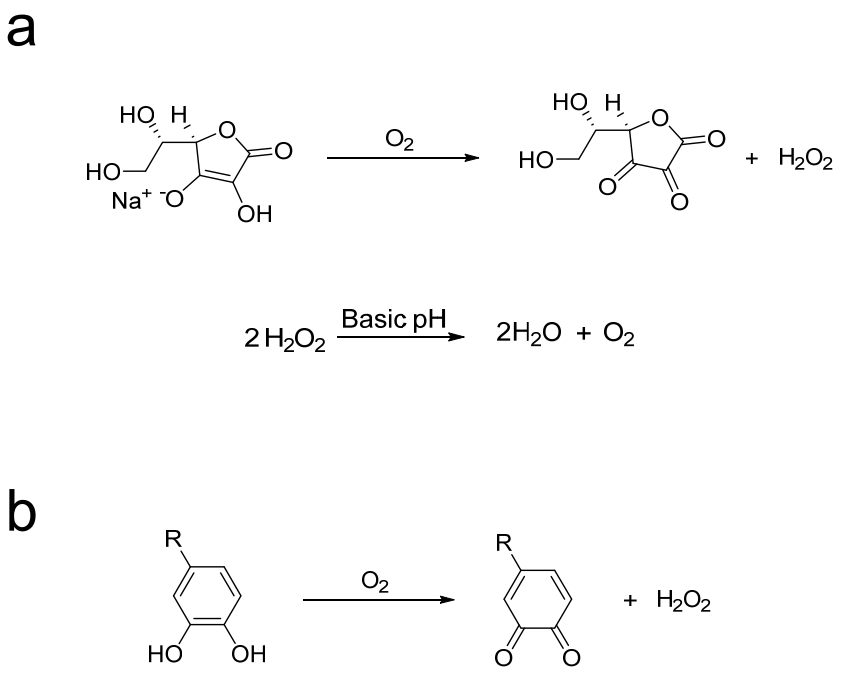

Figure 3.24: Reported oxidation reaction for SA and catechol. (a) The oxidation reaction of SA in basic solution.[243,244] (b) The oxidation reaction of catechol structure in basic solution.[247,248]

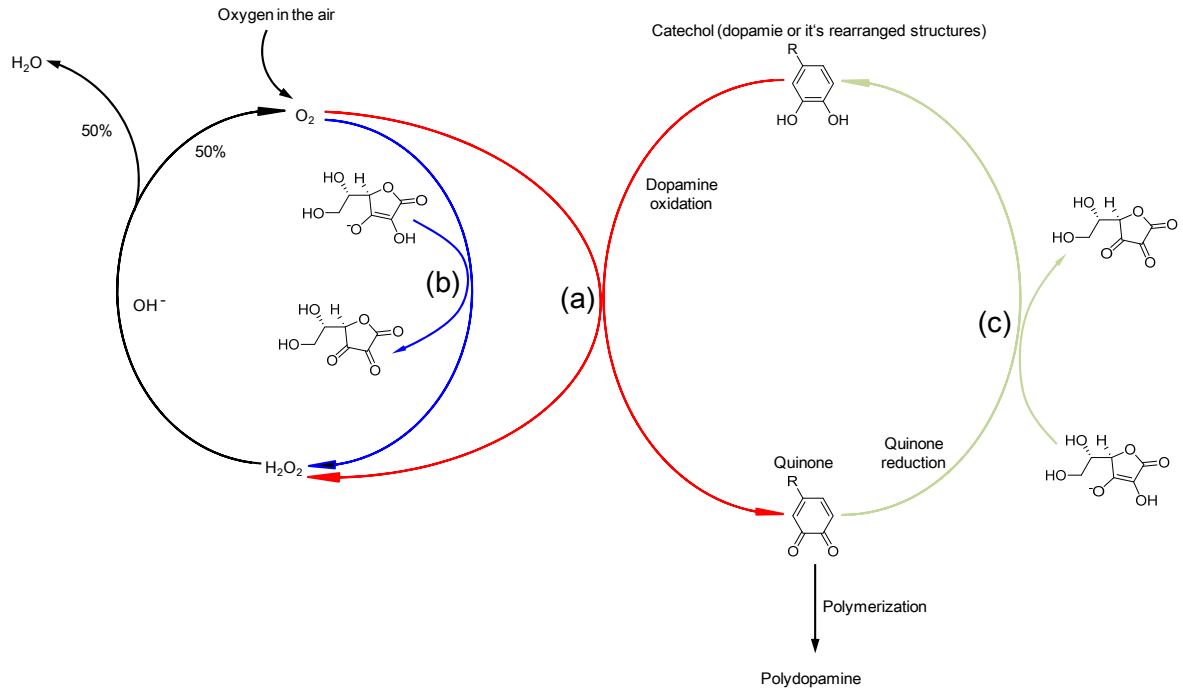

Figure 3.25: Proposed mechanism for the inhibition effect of SA on DA polymerization. (a) Oxidation of catechol structure under basic conditions. (b) Oxidation of SA under basic conditions. (c) Reaction between quinone and SA, quinone is reduced back to catechol and SA is oxidized to dehydroascorbate.

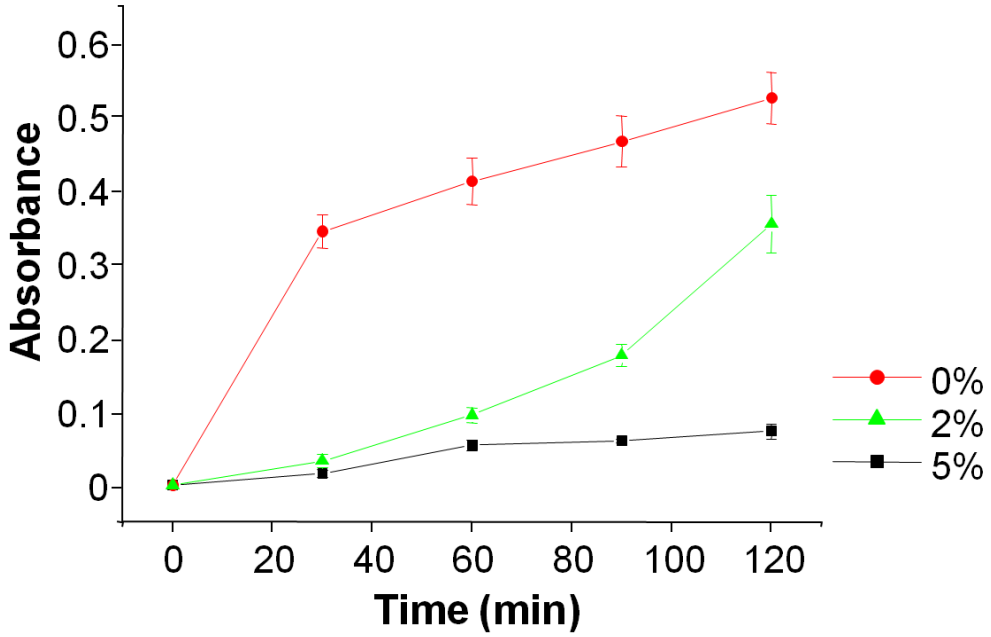

Figure 3.26: UV-Vis absorbance curves of DA solutions containing different concentrations of H_2O_2, stored in the dark. By addition of H_2O_2, DA polymerization and presumably oxidation is inhibited. The percentage in the graph refers to the weight percentage with respect to the DA concentration.

From the UV-Vis absorbance measurements it can be concluded that DA polymerization in basic solutions could be well controlled by the cooperation of SA and UV irradiation. However, whether the addition of SA would affect PD deposition is unknown. To investigate the effect of SA on the PD deposition, two PD surfaces on glass substrate were prepared. One PD surface was prepared by normal DA deposition method (10 mM Tris pH 8.5 buffer, 2 mg/mL DA, dark 24h), and the other one was prepared using the UV-SA method DA polymerization. 3% wt. of SA was added to the DA solution. This leads to the inhibition of polymerization for 6h, followed by 6 min of UV irradiation (7.5 mW/cm^2) at 260 nm to start the polymerization. The coating procedure was allowed to last 24h. Figure 3.27a shows a photograph of the two PD surfaces. No difference in color and light transmittance could be seen by naked eyes. SEM was performed on the two PD surfaces (Figure 3.27b and Figure 3.27c). The surface topography of the obtained PD layers are very similar. The thickness of the PD layers was investigated by AFM scratch test. Results indicate that in both cases the thickness of the coated PD layers was around 17 nm. In summary, the UV-SA method offered a way to control DA polymerization without affecting the thickness and topography of the resulting PD coating.

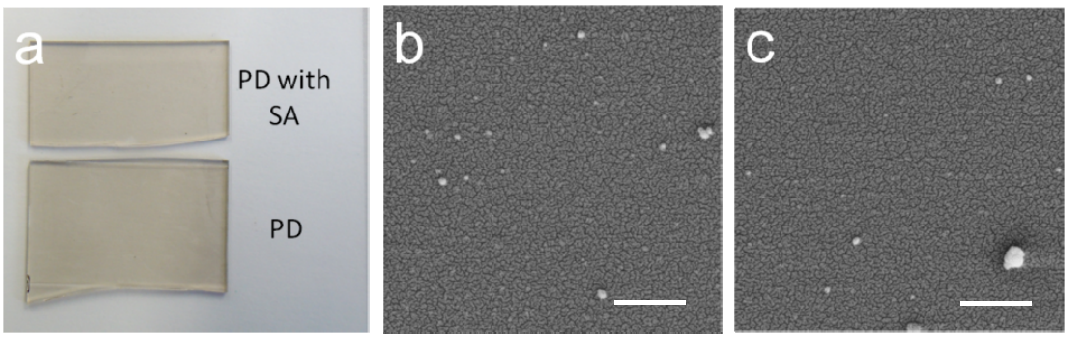

Figure 3.27: PD surfaces coated by a standard method in basic conditions and the UV-SA method. (a) Photograph of the obtained PD surfaces formed by standard DA polymerization and the UV-SA controlled DA polymerization. No visual difference can be seen. (b) SEM micrograph of the PD surface formed by the standard DA polymerization. (c) SEM image of the PD surface formed by the UV-SA controlled DA polymerization. Scale bars: 1 μm.

Since SA can efficiently inhibit DA polymerization in the dark, and exhibit almost no effect on DA polymerization under UV, it is possible to make PD patterns by using a photomask. Figure 3.28a and Figure 3.29 shows a CN^- intensity map on a PD coated glass surface. A clear pattern could be observed, confirming the successful formation of PD pattern

on the surface. By immersing a PD pattern into a $AgNO_3$ solution for 18h, silver nanoparticles were deposited on the PD surface, and the pattern could be easily observed by naked eye (Figure 3.28b) or by SEM (Figure 3.28c and 3.28d).

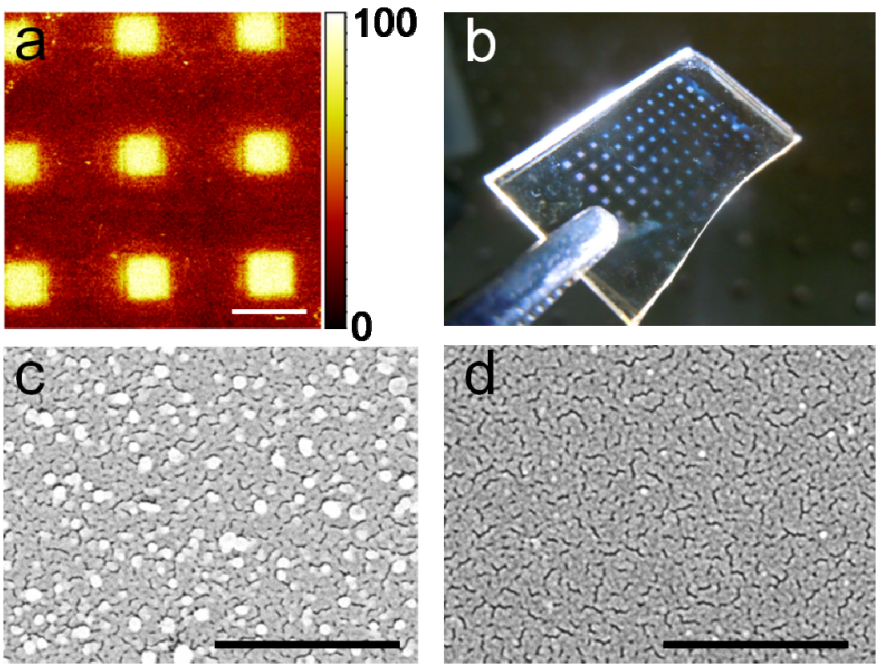

Figure 3.28: PolyDA patterns obtained by UV irradiation of a DA solution through a photomask. (a) ToF-SIMS mapping results, a CN^- intensity map. (b) Photo (from the opposite side) of a silver nanoparticle pattern obtained by immersing PD coated glass into a $AgNO_3$ solution for 24h, silver nanoparticles are deposited on the PD coated (irradiated) areas. SEM of the (c) irradiated area and (d) masked area. The scale bars in the (c) and (d) refer to 200 nm.

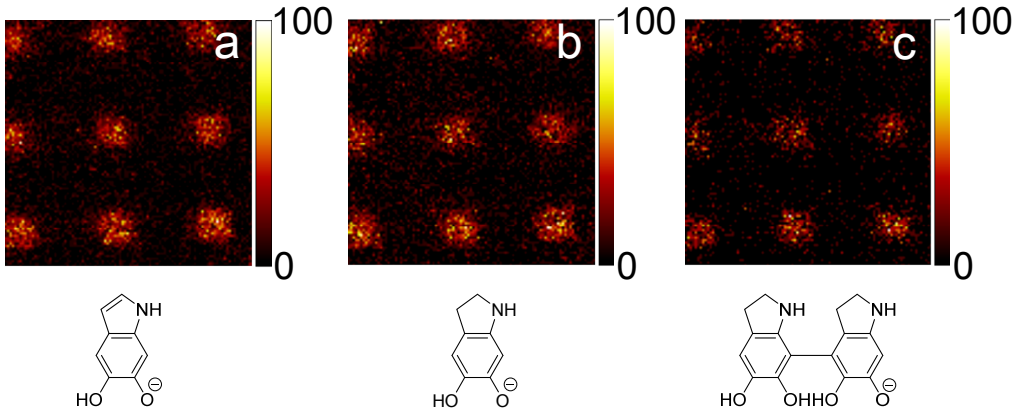

Figure 3.29: Fragments of the repeat units found in the ToF-SIMS results corresponding to Figure 3.28a. (a) m/z=148, corresponds to 3,4-dihydroxy indole. (b) m/z=150 corresponds to

another common repeat unit in PD (see structure above). (c) m/z=299, corresponds to a dimer of the fragment in (b).

3.1.5. Summary

In this section, a novel method allowing for the effective control of dopamine (DA) polymerization by UV light is described. Irradiation of a DA solution with UV light at both acidic and basic conditions showed a strong increase in the absorption of the solution at 420 nm – a characteristic peak of PD. Interestingly, the decrease of oxygen concentration in solution slowed down both the UV- and base-stimulated DA polymerization, indicating that both reactions involve an oxidation step and require oxygen. Additional experiments showed that ROS, such as hydroxyl radicals could accelerate the DA polymerization even under acidic conditions, while the addition of a ROS scavenger could inhibit both the base- and UV-induced polymerization of DA at different pH. This indicates that the UV-triggered DA polymerization is based on the ROS generated under UV irradiation. Owing to the short half-life of ROS, it was shown that the UV-induced DA polymerization could be controlled by UV light (ON/OFF possibility). By controlling the concentration of sodium ascorbate (SA) in the solution, DA polymerization in basic conditions could also be controlled, and a possible mechanism for the inhibition effect of SA is proposed. The UV-induced DA polymerization could be used to coat different materials including glass, silicon, or gold. It was also shown that the method was compatible with photopatterning and could be used to generate micropatterns of PD coating on different materials. The photopatterning method can potentially be employed on curved surfaces, porous surfaces, or particles, where the micro contact printing method is difficult to apply.

3.2 Reversible and Rewritable Surface Functionalization and Patterning via Photodynamic Disulfide Exchange

3.2.1 Background

Light-promoted precise spatial control of target molecules on surfaces is crucial in the development of novel bioanalytical, diagnostic or sensor tools. Proteins, DNA fragments, peptides and antibodies,[78–81,249,250] as well as hydrogels,[251] have been immobilized and patterned using a number of photochemical methods, such as, thiol-yne,[61] thiol-ene,[252] azide-yne (by photoreduction of copper II),[66] terazole-ene,[69] photo-triggered Diels–Alder reaction,[253] Paterno-Buchi reaction,[64] and some other chemistries capable of photo-triggered formation of reactive functional groups.[68,254–256] However, most of the existing photochemical methods lead to irreversible permanent surface functionalization, which limits possible applications in the formation of materials and surfaces with dynamic and responsive properties or reusable functionalities. Reversible surface functionalization methods can be applied to introduce, exchange or remove a functionality and, thus, generate "smart" surface and patterns. Examples of possible functionalities of such dynamic surfaces are reusability of substrates, possibility to perform "write and erase" procedures (i.e. rewritable surfaces), formation of complex, multi-component and gradient patterns, capture-and-release properties, and the possibility of *in-situ* manipulation of local environment.

Reversible surface functionalization could be achieved by using reversible chemistries. A number of reversible chemistries,[34,144–147,149–158] such as, electrically assisted ionoprinting,[34] Schiff-base reaction,[144] DNA hybridization,[151] Diels-Alder reactions,[152] host-guest interaction,[153,157] and alkoxyamine-based chemistry,[158] have been applied on surfaces for reversible functionalization or reversible functionalization/patterning applications.

However, currently most of the existing reversible surface functionalization/patterning strategies have limitations. For example, the time required for modification-recovery cycle of most strategies takes from several to dozens of hours.[144,145,150,152,153,155–158] Strategies based on thermal treatment cannot be well controlled.[152,158] Furthermore, for patterning applications, most of the reported strategies employ contact-based methods, which can be poorly controllable and not suitable for *in-situ* manipulations.[9,257]

Although photochemistry could offer a solution to most of the existing weaknesses of the reversible surface functionalization and patterning methods, the commonly used photo chemistries are based on irreversible reactions.[61,146,258,259] To our knowledge only two photo-induced reversible patterning strategies have been reported so far. Popik et al.[149] showed that reactive *o*-naphthoquinone methides (oNQMs) produced under UV light from

3-(hydroxymethyl)-2-naphthol could react with surface thiol groups to yield thioether conjugates, which could be subsequently cleaved by a secondary UV irradiation to regenerate the surface thiols.[149] In a recent publication, Anseth et al. described the use of allyl sulfides incorporated into a hydrogel to achieve reversible modification with thiol containing biomolecules.[146]

In this section I present a new reversible photopatterning strategy based on a photo-induced disulfide exchange reaction, that allows for the reversible photo-functionalization, patterning as well as exchange or removal of surface functional groups (Figure 3.30). The disulfide bond is known to undergo reversible cleavage under basic conditions via thiol-disulfide exchange reactions through intermediate thiolate anions.[260–262] However, disulfides can also undergo dynamic exchange reactions by homolytic photo-cleavage to sulfenyl radicals (Figure 3.30a). This reaction was recently adopted for the synthesis of self-healing polymers.[263,264] I hypothesized that dynamic nature of the disulfide homolysis and recombination under UV irradiation could be used to achieve reversible dynamic functionalization of disulfide surfaces (Figure 3.30b).

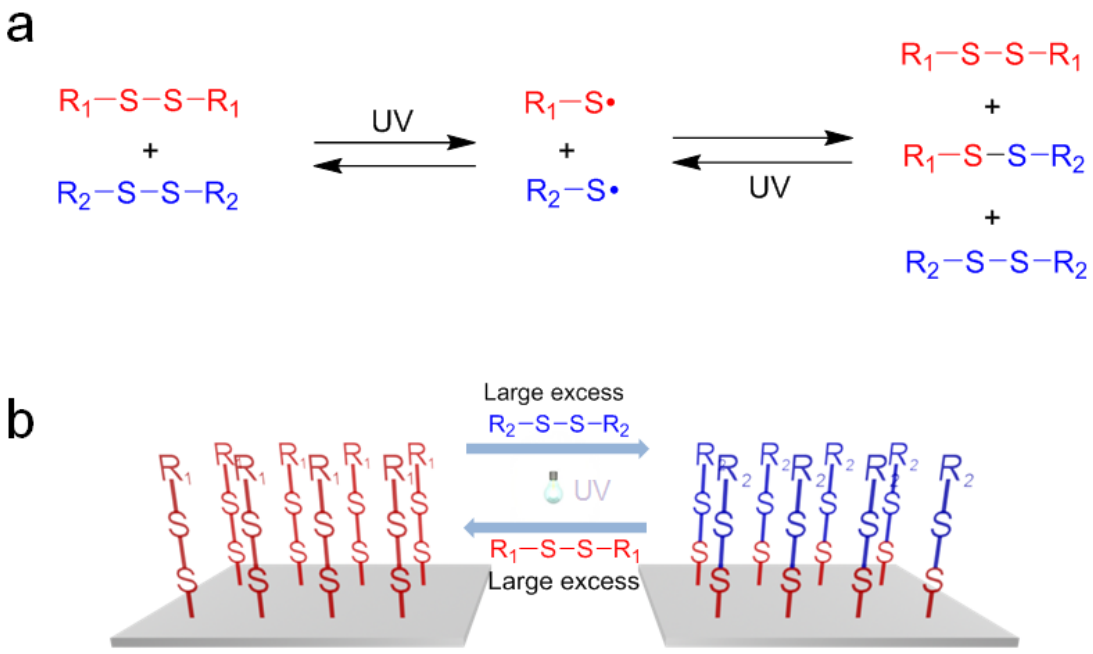

Figure 3.30: Principle of the UV induced disulfide exchange on disulfide surface. (a) Schematic representation of a photo dynamic disulfide exchange reaction (PDDE). Disulfides are converted into two sulfenyl radicals under UV irradiation, which can combine with each other to form new disulfides. The new disulfides can again be activated to sulfenyl radicals, thus making the process reversible. (b) Schematic representation of the reversible surface modification based on the PDDE.

3.2.2 Modification on disulfide surface

The disulfide surface was obtained by esterification of carboxyethyl disulfide (CED) with the hydroxy groups on a porous HEMA-EDMA surface. The obtained CED-modified disulfide surface (CED surface) is hydrophilic with a static water contact angle (WCA) of 44±2° (Figure 3.31a). After 2 min of UV irradiation (260 nm, 7.5 mW/cm^2) in the presence of dibutyl disulfide (DBD) the static WCA increases to 128° indicating the modification with the hydrophobic butyl sulfide groups. The produced BD surface can be again modified with CED by wetting the surface with a CED solution in DMF and irradiating with UV (260 nm, 7.5 mW/cm^2) for 2 min restoring the original hydrophilicity of the surface (static WCA 45°).

In order to show the reversibility of the photoinduced disulfide exchange, the reaction was repeated 20 times (10 cycles). The results shown in Figure 3.31b confirm perfect reversibility of the surface modification without significant change of wettability even after 20 consecutive UV-induced functionalizations performed on the same substrate. The SEM images of the disulfide surfaces demonstrate no morphology change during the esterification and disulfide exchange process (Figure 3.32).

The fast kinetics of photo-induced transformations is vital for reducing irradiation time and reducing UV damage to the surface, thereby resulting in patterns of better contrast and higher resolution. In order to investigate the kinetics of the PDDE, a CED surface was pre-wetted with a DMF solution of DBD (20% wt. in DMF, containing 5% wt. DMPAP as a photoinitiator), followed by UV irradiation (260 nm, 7.5 mW/cm^2) through a quartz slide for 5 s, 15 s, 30 s, 60 s, 120 s. After irradiation was finished, the quartz glass was removed and the surface was washed with acetone, dried under a stream of N_2 and static WCA was measured. Figure 3.31c shows that static WCAs increases from 43 ± 4° up to 114 ± 2° within the first 5 s followed by stabilization at 125±3° at around 15 s. The same experiment was performed using the butyl disulfide modified surface (BD surface), which was modified by the hydrophilic CED solution. The kinetics of this reaction is very similar to the modification with DBD (Figure 3.31c) with completeness of the reaction at ~15 s. The reaction kinetics was also investigated using different UV light intensity and wavelengh: (a) low intensity (~0.2 mW/cm^2) 254 and 365 nm and medium intensity (~2 mW/cm^2) 254 and 365 nm. The kinetics of disulfide exchange was the same for both wavelengths, while the reduction of light intensity resulted in a slight decrease of the rate of transformation (Figure 3.35). Even in the case of a simple handheld TLC irradiation lamp and 365 nm UV light, the surface modification was complete in 5 min

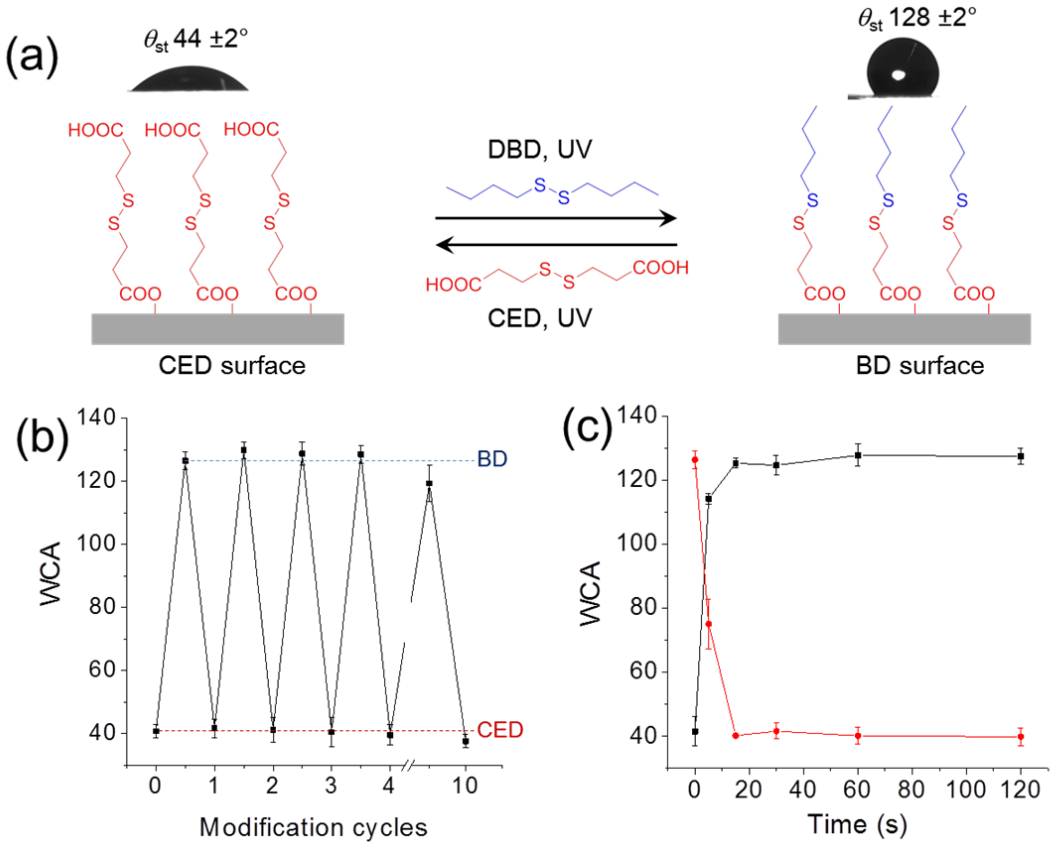

Figure 3.31: Kinetics and reversibility of the PDDE on a disulfide surface. (a) Schematic showing the change of surface hydrophilicity upon switching between CED and BD-surfaces using the PDDE. (b) Static WCA as a function of surface modification cycle number. The CED surface was modified with DBD under UV (1 min, 7.5 mW/cm^2, 260 nm), followed by the modification of the produced BD-surface with CED, etc. The DBD-CED modification cycle was repeated 10 times and the WCA of the surface was measured after each modification. (c) Graph showing the static WCA as a function of the irradiation time. ■ Modification of CED surface by DBD solution. ● Modification of BD surface by CED solution.

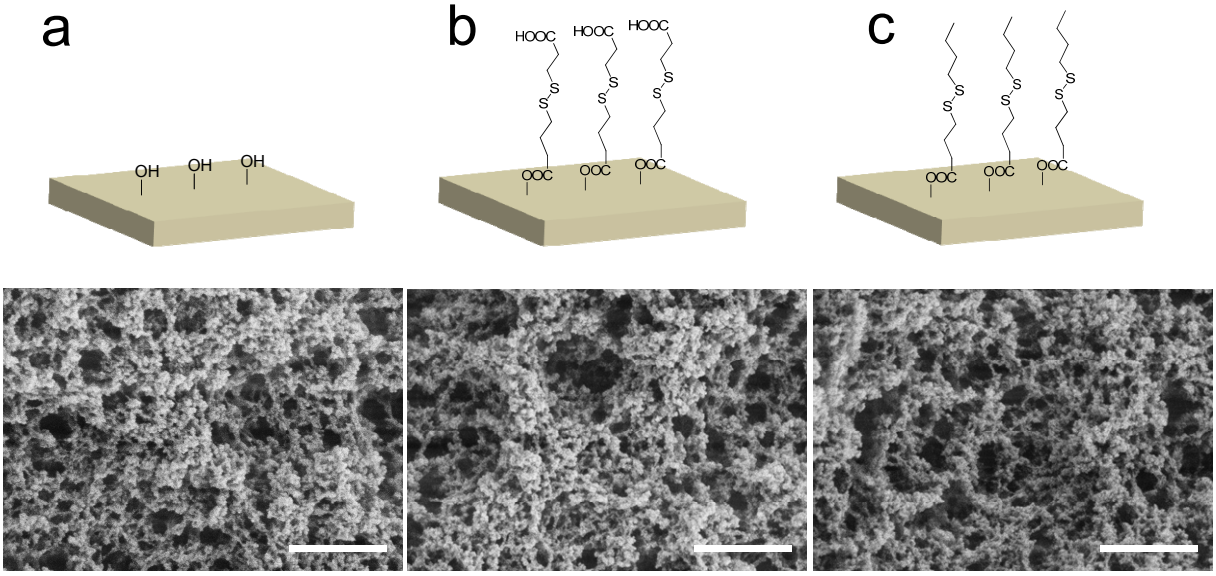

Figure 3.32: SEM images of the HEMA-EDMA surface before and after disulfide modification. No differences could be found on the morphology of the surface. (a) HEMA-EMDA surface. (b) CED surface after the esterification of HEMA-EDMA with CED. (c) BD surface after disulfide exchange on CED surface. The scale bars in the images refer to 1 μm.

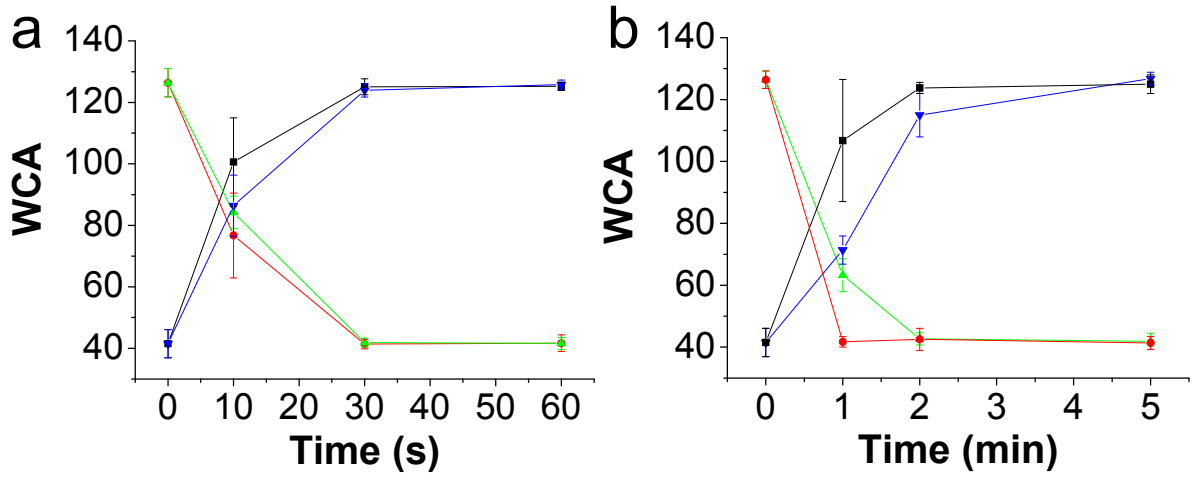

Figure 3.33: Kinetics of photodynamic disulfide exchange on the surface. (a) Disulfide exchange under medium (~2 mW/cm^2) UV intensity at the wavelength of 254 nm and 365 nm, respectively. Samples: ■ CED surface modified by DBD solution under 254 nm UV light. ● BD surface modified by CED solution under 254 nm UV light. ▼ CED surface modified by DBD solution under 365 nm UV light. ▲ BD surface modified by CED solution under 365 nm UV light. (b) Disulfide exchange under weak (~0.2 mW/cm^2) UV intensity at the wavelength of 254 nm and 365 nm, respectively. ■ CED surface modified by DBD solution

under 254 nm UV light. ● BD surface modified by CED solution under 254 nm UV light. ▼ CED surface modified by DBD solution under 365 nm UV light. ▲ BD surface modified by CED solution under 365 nm UV light.

3.2.3 Patterning performance on disulfide surface through UV induced disulfide exchange

The reversible nature of the PDDE allows for two possible surface functionalization and patterning strategies, where a functional group can be either (a) introduced onto a disulfide surface, or (b) deleted by replacing a functional group with a background functionality. In order to show these possibilities, I prepared a CED disulfide surface on HEMA-EDMA porous substrate by esterification. Figure 3.34a shows that the CED functionality can be conveniently replaced by a new fluorescent group to generate fluorescent FITC-disulfide surface (Figure 3.34b and Figure 3.34c). In the next step, the fluorescent FITC groups can be replaced with new non-fluorescent functional groups. I used a quartz photomask to generate a micropattern of fluorescent FITC-disulfide areas (non-irradiated areas) and the newly introduced non-fluorescent butyl disulfide areas where the surface was irradiated with UV light (Figure 3.34d). All PDDE steps were finished in less than 5 min of UV irradiation. Patterns with variety of different shapes could easily be obtained by using different photomasks (Figure 3.34e). In this case, a DB-surface was used to directly pattern FITC-disulfide using a photomask. The smallest feature size of the produced pattern was 10 μm (Figure 3.34f), which was limited by the porous nature of substrate and disulfide diffusion. Increasing the viscosity of the solution and reducing the roughness of the surface can potentially increase the resolution of the patterning.

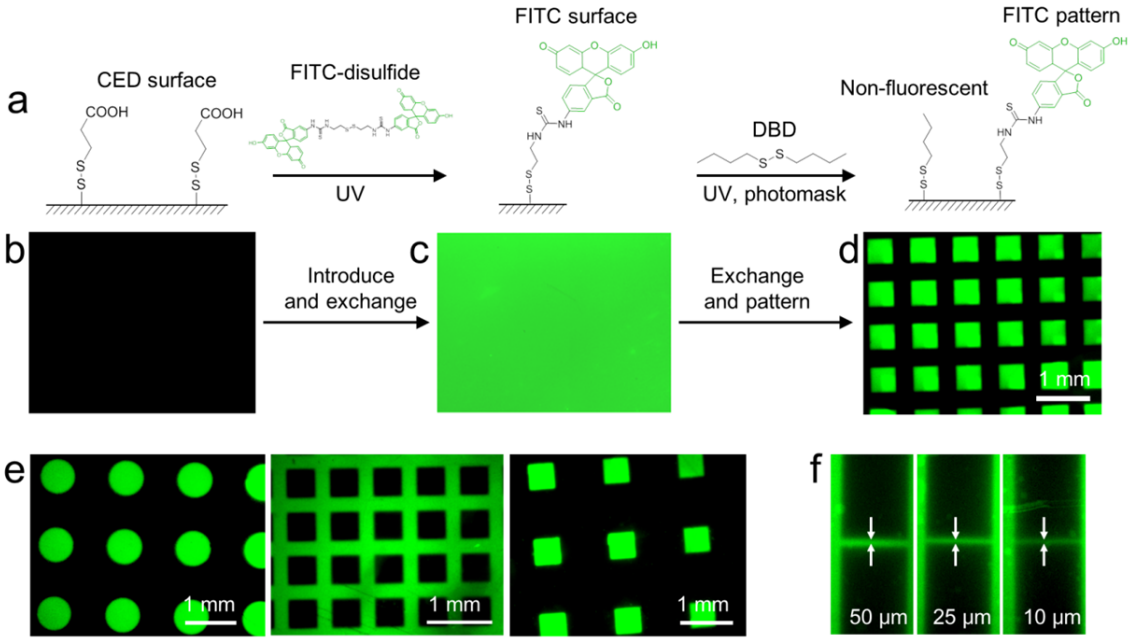

Figure 3.34: (a) Schematic of the surface functionalization using the PDDE. First, fluorescent FITC-labeled disulfide was introduced by replacing the CED groups with the FITC-disulfide to generate a fluorescent FITC-surface. In the second step, non-fluorescent dibutyl disulfide was patterned through a photomask on the surface by replacing the FITC-labeled disulfides. The disulfide surface was covered with a 10 mg/mL FITC-disulfide DMSO solution and irradiated with UV for 2 min. (b, c and d) Fluorescence microscope images of the CED, FITC-surface and the DB-FITC patterned surfaces, respectively. (e)Patterns of FITC-labeled disulfide with different geometries. FITC-disulfide was introduced by replacing butyl disulfide modified surface (DB-surface). (f) FITC-CED patterns showing the possibility to pattern features as small as 10 µm using the PDDE method.

The PDDE was confirmed by ToF-SIMS (Figure 3.35). ToF-SIMS examination of a BD-CED pattern shows a homogenous distribution of sulfur (S^-, Figure 3.35b) and disulfide (S_2^-, Figure 3.36a) ions on the surface, while the butyl sulfide fragment is only found in the areas irradiated with UV light in the presence of DBD (Figure 3.35b and 3.36b). Other corresponding ions were also detected by ToF-SIMS (Figure 3.36c and Figure 3.36d).

The chemical tolerance of surface modification and patterning methods is critical for direct patterning of non-protected biomolecules and other chemicals in sensor or bioanalytical applications. The tolerance of the surface PDDE reaction to carboxy, hydroxy, and amino groups has been evaluated. ToF-SIMS results, shown in Figure 3.35, confirm the formation of both hydroxyl- and amino- patterns when 2-hydroxyethyl disulfide (HED) or 2-aminoethyl disulfide (AED) were used in the PDDE, respectively.

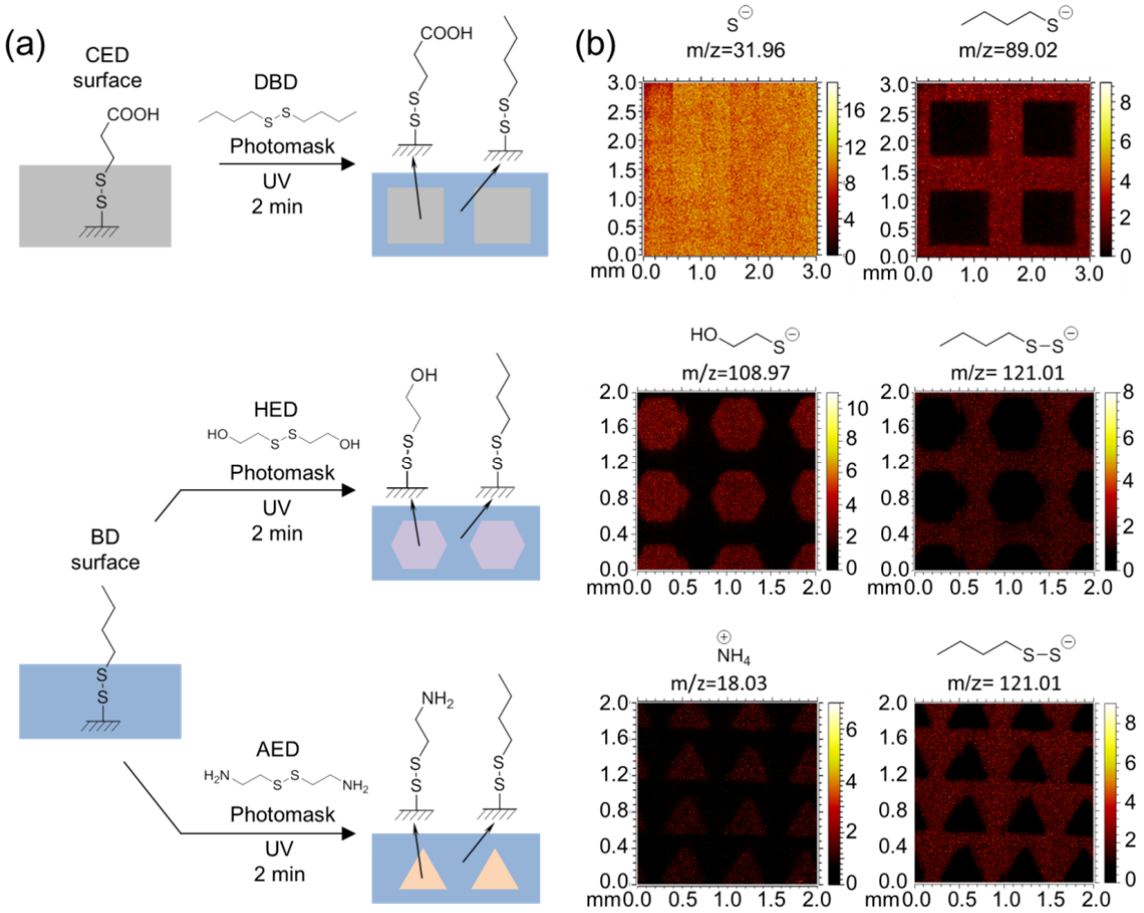

Figure 3.35: (a) Schematic representation of the surface patterning using the PDDE. (b) ToF-SIMS maps corresponding to the surface patterns from (a).

The performance of reversible patterning of disulfide surface could easily be confirmed by the reversible formation of superhydrophobic-superhydrophilic patterns. By modifying macroporous disulfide surface with didodecane disulfide (with photomask), a superhydrophobic-superhydrophilic pattern could be obtained. The pattern could be erased by modifying the surface using CED solution (Figure 3.37).

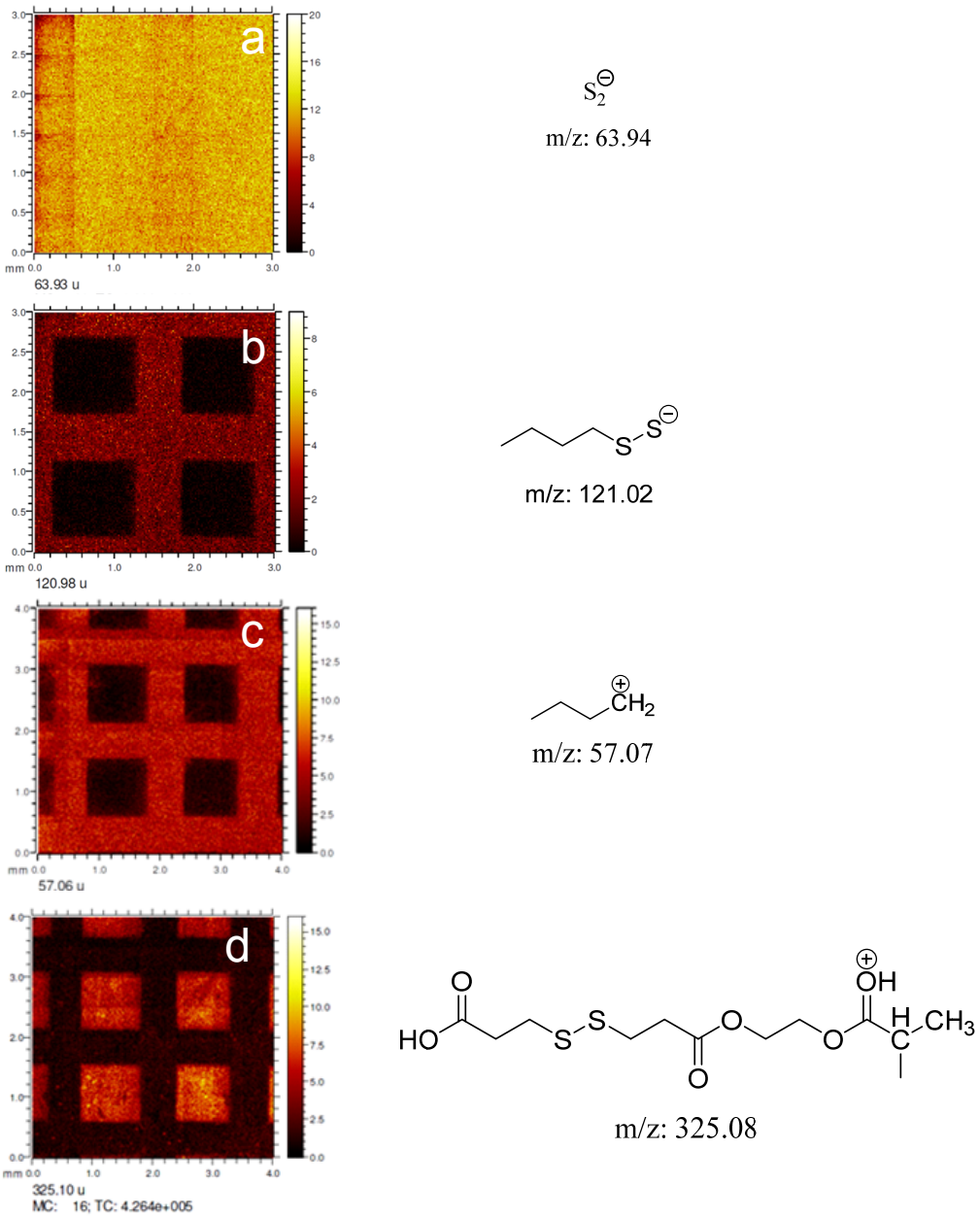

Figure 3.36: ToF-SIMS mapping results on a patterned BD-CED surface. The pattern was formed by UV irradiation on CED surface in DBD solution with a photomask: (a) and (b) are in negative mode, (c)-(e) are in positive mode. The negative and positive mode tests were done in different areas. (a) Mapping result of the fragment with m/z=63.93, which refers to the disulfide anion. No pattern could be observed since the sulfur is homogeneous distributed on the surface. (b) Mapping result of the fragment with m/z=120.98, which refers to the fragment of butyl disulfide anion. A clear pattern can be observed on the irradiated area. (c) Mapping result of the fragment with m/z=57.06, which refers to the butyl cation from the butyl sulfide chain. Only the irradiated area showed signal of this fragment. (d) Mapping result of the fragment with m/z=325.1, which probably refers to a CED-HEMA side chain derivative. Only non-irradiated area showed signal of this peak.

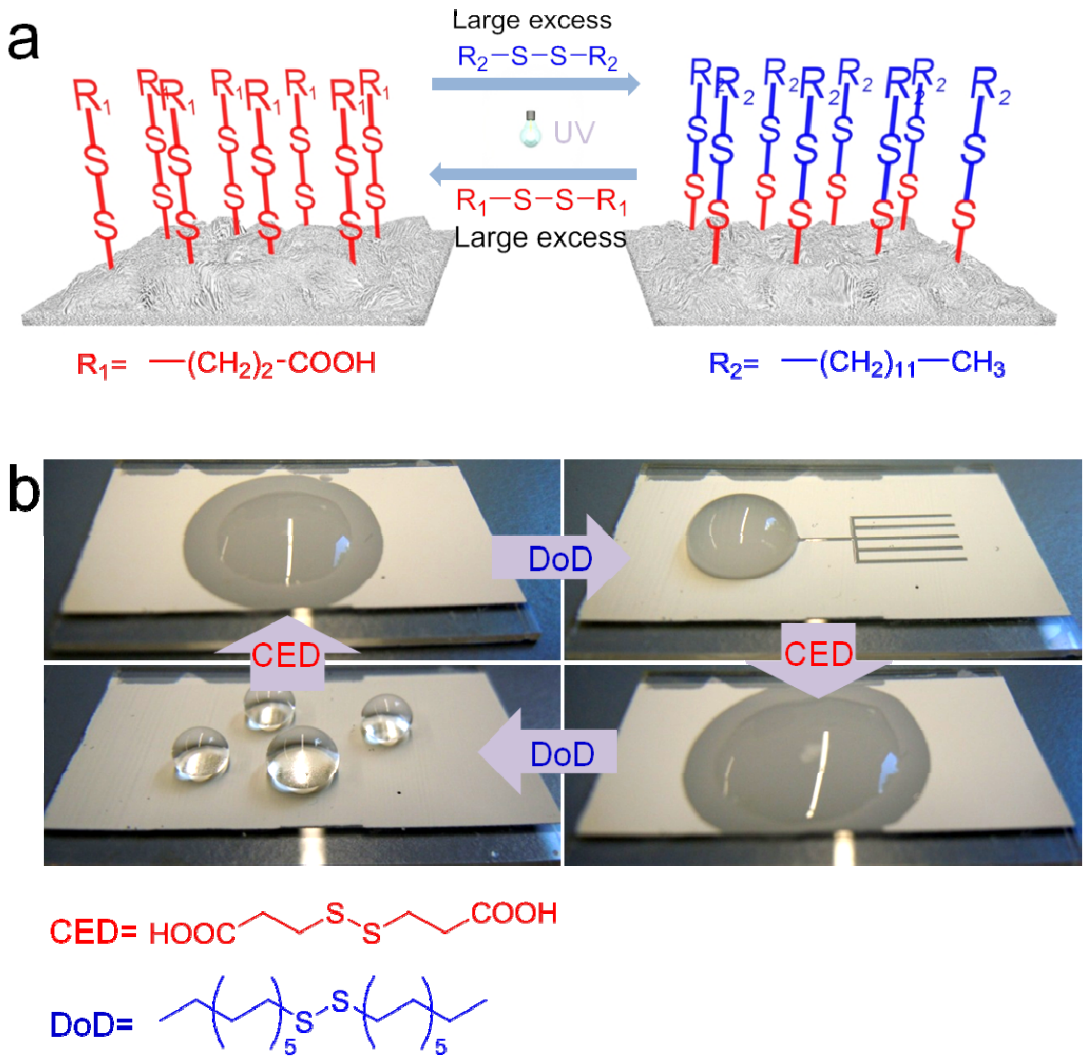

Figure 3.37: Rewritable superhydrophobic-superhydrophilic patterns formed by UV-induced exchange of didodecyl disulfide (DoD) and CED on a macroporous surface. (a) Schematic illustration of the principle of the modification. (b) Photo of the resulted surfaces. CED surface is a highly hydrophilic surface. Modification of the CED surface with DoD solution takes place under UV irradiation for 5 min with a photomask, resulting in a superhydrophobic-superhydrophilic pattern. After flood UV irradiated 5 min in CED solution, the surface becomes superhydrophilic again. After 5 min of UV irradiatedion in the DoD solution, the surface becomes superhydrophobic.

3.2.5 Summary

In summary, in this section a strategy to produce reversible surfaces and rewritable patterns was demonstrated. By introducing disulfide bond onto HEMA-EDMA surface, a disulfide surface capable of reversible functionalization was obtained. The disulfide surface can be reversible modified by using different disulfide solutions. Rewritable patterns with different functionalities could be obtained by applying a photomask. The method could be potentially used to control the on-off states of microchannels in microfluidic devices. Other possible applications may include *in-situ* control of the environment of cell incubation, reusable surfaces and patterns, and surfaces for controlled release of thiols.

3.3 Paint-like Superhydrophobic Coating based on cyanoacrylates

3.3.1. Background

Superhydrophobic surfaces, i.e. surfaces with both advancing and receding water contact angles (WCAs) above 150º, have attracted much attention during the last decade mainly because of their extreme water repellent and self-cleaning properties.[159,162,164–169] Superhydrophobic surfaces can potentially find numerous applications in a variety of industrial and research fields ranging from coatings for solar cells and biotechnological reactors to coatings for microfluidic devices and microarrays. During the past decade, a number of methods for the fabrication of superhydrophobic surfaces have been reported.[171–184] However, despite a lot of research, most of the methods still require multi-step procedures,[181] harsh conditions,[182] UV-irradiation or oxygen-free conditions.[183,184] Clearly, paint-like methods, i.e. methods equally applicable to different substrates and non-planar surfaces under ambient and oxygen rich conditions, are desirable in the field of superhydrophobic coatings.

Previously, a method for the preparation of porous superhydrophobic surfaces by photopolymerization induced phase separation was reported.[184] In this method, a mixture of alkyl methacrylates, porogen and initiator was irradiated by UV light, which led to the formation of a highly porous polymer surface with superhydrophobic properties. Although the method is very versatile, it still requires oxygen-free environment, thus the surface should be covered by a glass plate to form a closed system during the polymerization. As a result, the method cannot be applied to nonflat surfaces and under air environment.

It was hypothesized that by substituting alkyl methacrylates used in the previous method with alkyl cyanoacrylates, the method for the preparation of superhydrophobic coatings could be improved. Due to the anionic mechanism of the polymerization of cyanoacrylates, the polymerization could be performed without UV-irradiation. Because of the very high activity of cyanoacrylates, no oxygen-free atmosphere should be necessary and, therefore, the method could be applicable to 3D substrates. In addition, due to the good adhesion of polycyanoacrylates to different substrates, no special surface pretreatment should be required. Alkyl cyanoacrylates are well known for their use as a “super-glue” and as a surgery adhesive.[265] Their polymers were found to be biocompatible and biodegradable, making them suitable for applications in biology and medicine.[266] Cyanoacrylates are also known to be more reactive than corresponding acrylates and methacrylates and polymerize via anionic polymerization instantaneously in the presence of traces of water, usually forming a strong

bond to the substrate.

In this section, a novel paint-like method for making superhydrophobic polymer coatings on different substrates is developed. The method is based on creating a film of the 2-octyl cyanoacrylate on a substrate followed by brief immersion of the film into aqueous ethanol. This treatment initiates anionic polymerization of the cyanoacrylate and simultaneously triggers the phase separation leading to the formation of a highly porous superhydrophobic poly(octyl cyanoacrylate) film strongly adhered to the substrate. Contrary to the free-radical polymerization,[267] anionic polymerization of 2-octyl cyanoacrylates is not inhibited by oxygen, thereby allowing for the fabrication of superhydrophobic coatings on both planar and three-dimensional open substrates without protection from oxygen.

To make a rough surface, I empolyed a painting-immersing method (Figure 3.38). The procedure is described as follows: a monomer drop was added onto the substrate and spread, either by spin coater, glass plate or a finger. After spreading, the substrate was immersed into a mixture of water and ethanol (with different water/ethanol volume ratios: 1/100 for ethyl cyanoacrylate; 8/100 for butyl cyanoacrylate, and various ratios for 2-octyl cyanoacrylate). The immersion time was varied between 5 and 40 s. The substrate was then removed from the solvent and dried in air, which gave a thin highly porous polymer film attached to the substrate. By the one-step process described above, a porous coating could be formed in a minute.

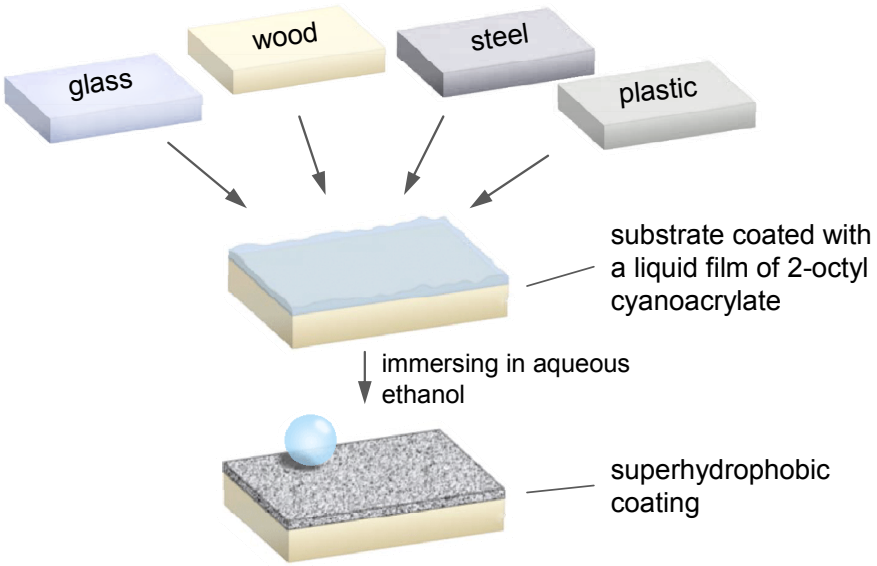

Figure 3.38: Schematic representation of the method of making superhydrophobic porous poly(alkyl cyanoacrylate) coating on different substrates.

3.3.2. Porous surfaces prepared by using different cyanoacrylates

Since superhydrophobicity is a result of the combination of surface roughness and hydrophobicity of the material itself, I decided to test how the length of the alkyl tail in the cyanoacrylate affects the morphology as well as the resulting superhydrophobicity. I produced three porous polymer surfaces using the above procedure from ethyl, butyl or 2-octyl cyanoacrylates. Only poly(2-octyl cyanoacrylate) film showed superhydrophobicity (Table 3.1), while butyl and ethyl cyanoacrylate led to hydrophobic surfaces with static, advancing and receding WCAs of 152±3º, 163±3º, 146±4º, and 126±1º, 130±2º, 0º, respectively.

Table 3.1: Static, advancing and receding WCAs of the obtained porous poly(alkyl cyanoacrylate) surfaces.

Alkyl group	Static WCA	Advancing WCA	Receding WCA
Ethyl	126±1º	130±2º	0
Butyl	152±3º	163±3º	146±4º
Octyl	159±3º	164±2º	153±2º

Figure 3.39 shows scanning electron microscopy (SEM) images of the produced poly(alkyl cyanoacrylate) coatings. The polymerization of a liquid layer of the monomer spread on the surface is triggered by the water contained in the ethanol solution. However, since only the monomer but not the polymer is soluble in ethanol, the polymerization is accompanied by simultaneous phase separation resulting in the formation of a highly porous polymer network distinguishable in the SEM images. Poly(butyl cyanoacrylate) and poly(2-octyl cyanoacrylate) based surfaces exhibited similar morphology, however, poly(ethyl cyanoacrylate) surface showed much smaller globule and pore sizes – in the order of 110±30 nm. This was probably caused by the higher activity of the ethyl cyanoacrylate than that of the other two monomers, which resulted in more nucleation sites at the onset of polymerization. Another possible explanation is that ethanol-water mixture is a better solvent for the initially formed poly(ethyl cyanoacrylate) chains, which could lead to a later onset of phase separation and, thus, smaller pores and globules.

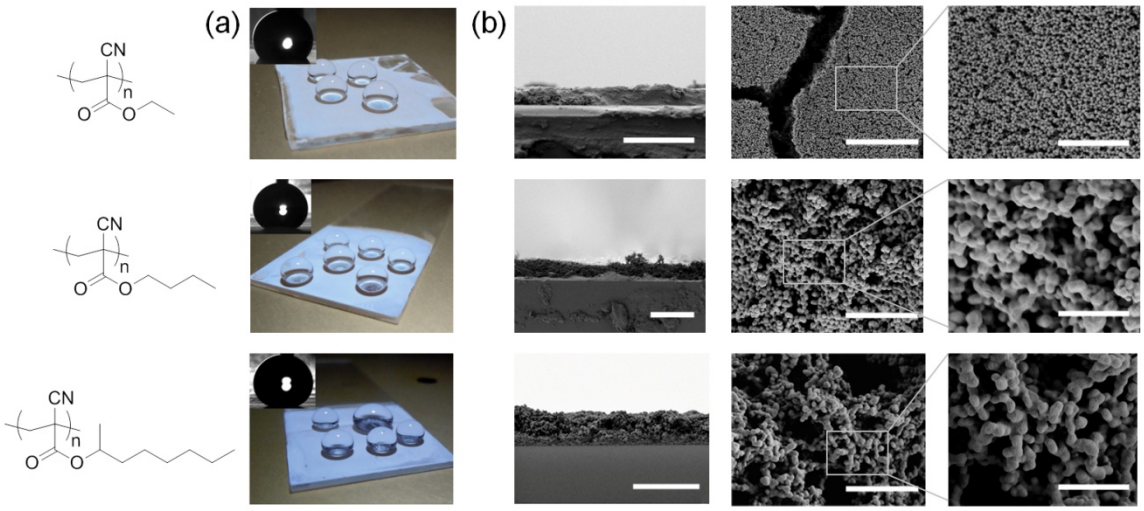

Figure 3.39: (a) Photographs of the porous polymer films made by anionic polymerization of ethyl, butyl and 2-octyl cyanoacrylates. Water/ethanol volume ratio for each sample: ethyl cyanoacrylate (1:100), butyl cyanoacrylate (8:100), 2-octyl cyanoacrylate (water:ethanol=20:100). (b) SEM images of the porous polymer films (cross-section and top view). Scale bars: 20 μm (top left), 30 μm (left column, middle and bottom), 5 μm (middle column), 2 μm (right column).

3.3.3. Effect of the water concentration in ethanol on the morphology of porous surfaces.

As morphology of the porous structure may depend on the amount of initiator[268] as well as on the composition of the porogen,[184,269,270] I decided to analyze how the ethanol/water ratio influences the morphology and hence superhydrophobicity of the produced porous poly(2-octyl cyanoacrylate). Six water-ethanol mixtures were tested and the results, presented in Figure 3.40, confirmed that both the superhydrophobicity and morphology of the porous polymer structures significantly depended on the amount of water present in the mixture. As shown in Figure 3.40a, the receding WCA of the samples increased from 77º to 153º as the amount of water increased from 2% to 16.7%. The static and advancing WCAs changed only slightly. When water concentration reached about 16.7% (10 ml in 50 ml ethanol), the surface exhibited the most superhydrophobic behavior, with the static, advancing and receding WCAs of 159±3º, 164±2º, 153±2º, respectively. The reason for the difference in hydrophobicity becomes clear when morphologies of the corresponding porous structures are compared (Figure 3.40b, 3.40c). As can be seen from the Figure, the size of pores and polymer globules increased gradually upon the increase in water concentration, thereby resulting in larger multiscale roughness of the surfaces and more pronounced superhydrophobicity.[184,271]

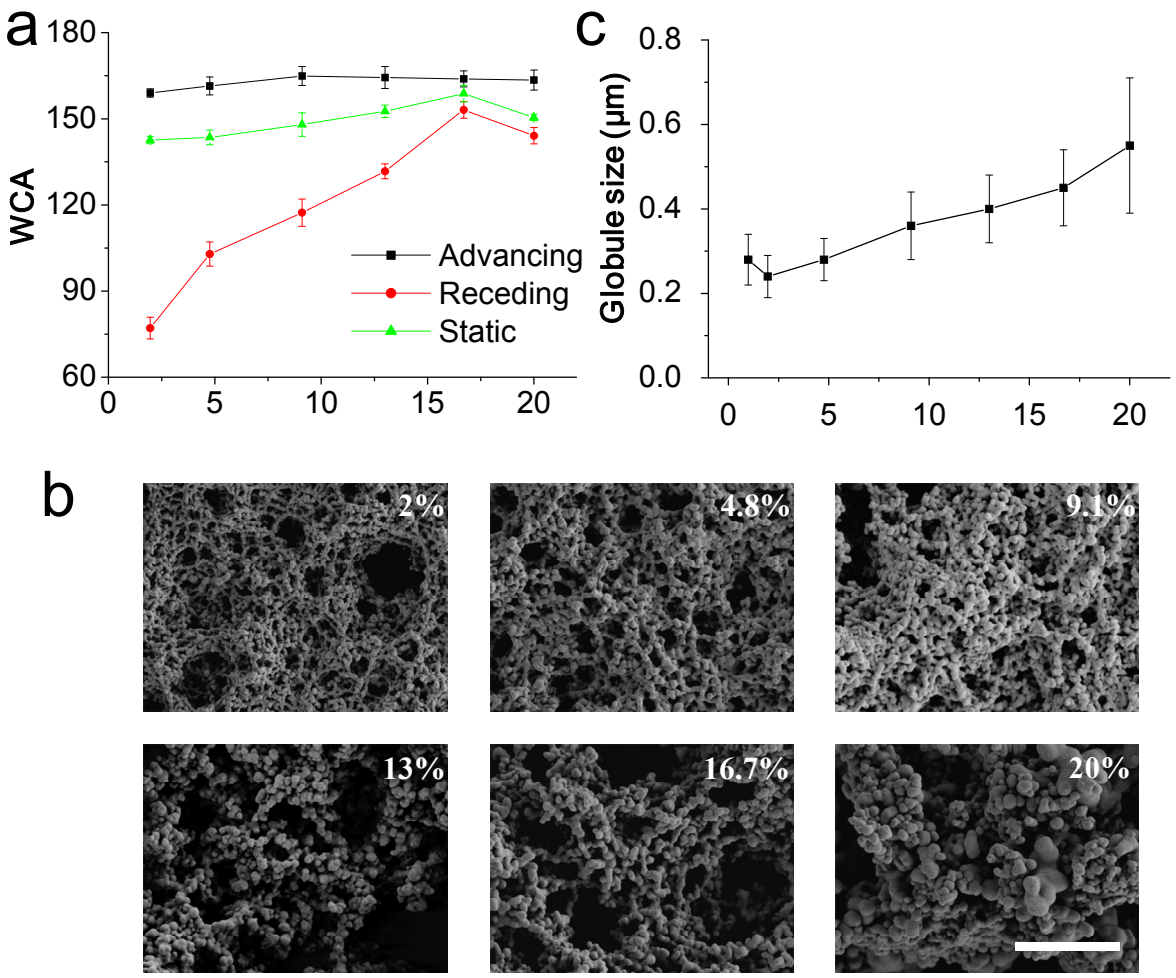

Figure 3.40: (a) Relation between WCAs and the concentration of water in the water/ethanol mixture used to produce porous poly (2-octyl cyanoacrylate) surfaces. (b) Mophologies of the samples produced using water/ethanol mixtures with different water content. Scale bar 5 µm. (c) Relation between average polymer globule size and the water content.

3.3.4. Long term stability of the porous polycyanoacrylate surface

Long term stability of the superhydrophobic property is very important for practical applications of such coatings. Stability of the superhydrophobic poly(2-octyl cyanoacrylate) surface both in indoor and outdoor environments for several weeks was tested. The results showed that WCAs decreased only by ~2º in the case of the 4 weeks indoor test (Figure 3.41a). Even after 5 month, the test surface still exhibited superhydrophobicity, with static, advancing and receding WCA of 154±3º, 162±2º, 152±2º, respectively. Storing a sample outdoor for 6 weeks resulted in a decrease in static advancing and receding WCAs by 6º, 4º and 5º, respectively, thereby showing in part faster deterioration of the superhydrophobic

properties of the produced poly(2-octyl cyanoacrylate) coating in the outdoor environment (Figure 3.41b).

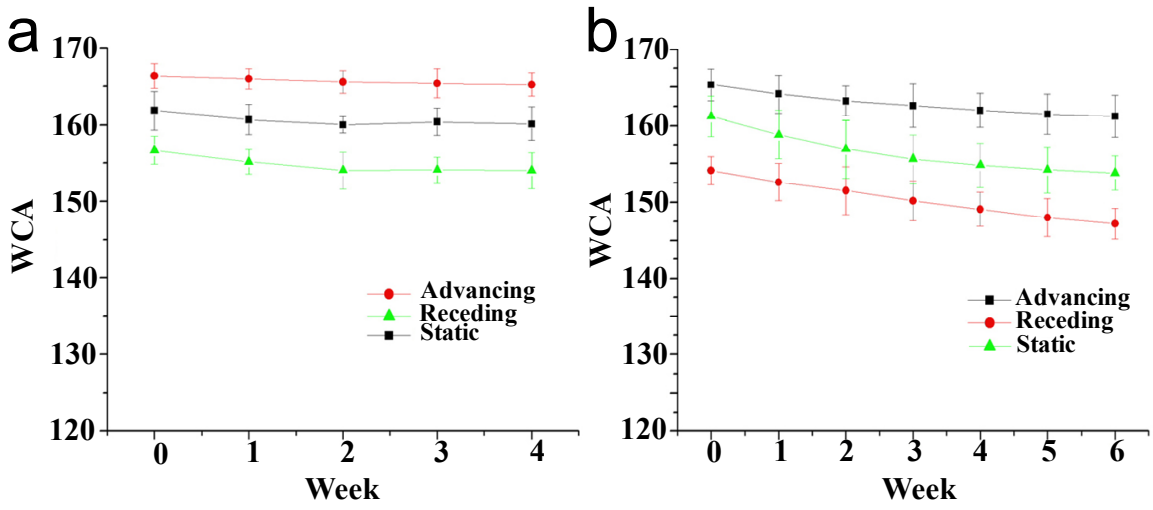

Figure 3.41: Stability of the produced superhydrophobic surfaces. (a)WCA (static, advancing and receding) of a poly(2-octyl cyanoacrylate) superhydrophobic film over 4 weeks (indoor). (b) WCA of a poly(2-octyl cyanoacrylate) superhydrophobic film over 6 weeks (outdoor)

3.3.5. Application of the coating method on different substrates

The ability to create a strongly adherent superhydrophobic coating on different materials is important for many applications. However, most of reported methods for making superhydrophobic coatings are still limited to only specific materials.[172,272,273] An advantage of our method, known from the use of "super-glue", is that polymerized alkyl cyanoacrylates usually form a very strong bond with the substrate. Figure 3.42 shows examples of prepared superhydrophobic porous poly(2-octyl cyanoacrylate) coatings on different substrates. The polymer film adhered well to such materials as acrylic coated cloth tape, paper, cotton cloth, glass and wood. Due to the biocompatibility of the polymer and gentleness of the procedure, a superhydrophobic poly(2-octyl cyanoacrylate) film could be even formed on skin.

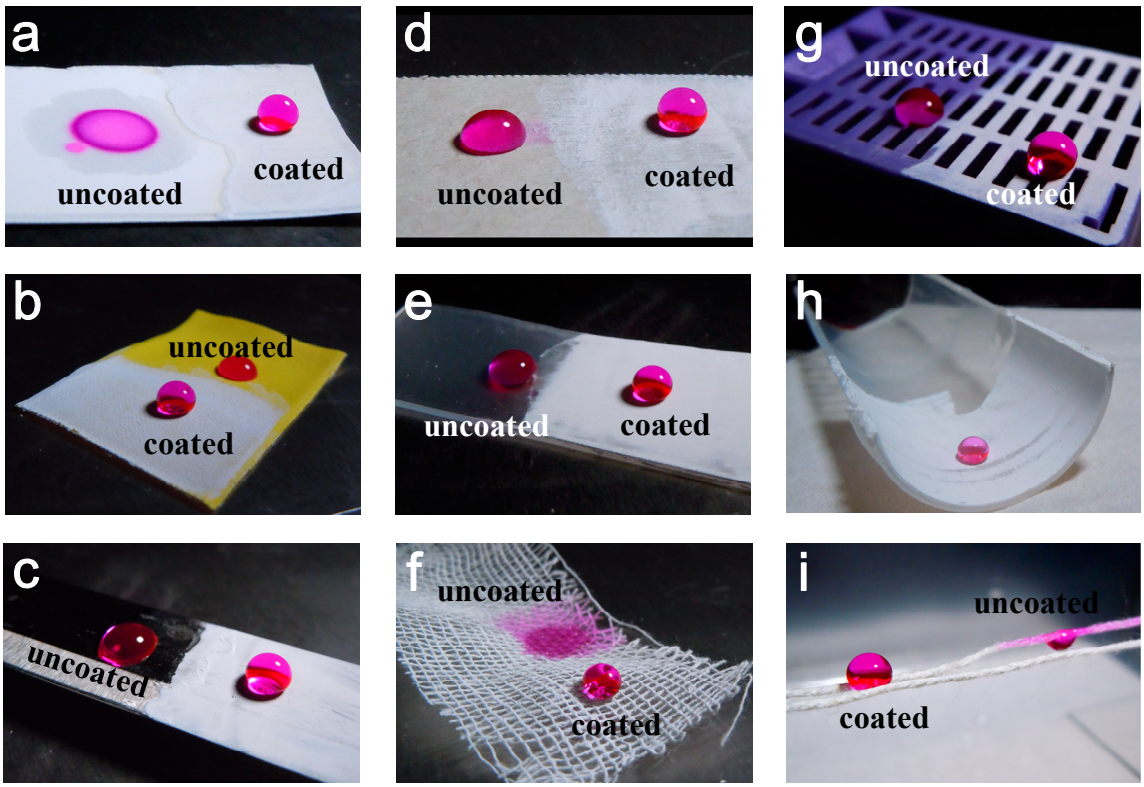

Figure 3.42: Superhydrophobic poly(2-octyl cyanoacrylate) coatings on different flat and nonflat substrates. Pictures are showing water droplets dyed with Rhodamine. (a) TLC plate, (b) acrylic coated cloth tape, (c) steel, (d) paper, (e) polypropylene, (f) cotton gauze, (g) mesh-like plastic surface, (h) curved tube-like surface, (i) cotton fibers.

Creating superhydrophobic coatings on 3D substrates is usually challenging. I show that our method is applicable to nonflat surfaces (Figure 3.42). Static, advancing and receding WCAs on different substrates after coating are summarized in Table 3.2. The coated surfaces are stable to some organic solvents such as methanol, ethanol and n-hexane, however, can be damaged in diethyl ether, acetone, dimethyl sulfoxide, tetrahydrofuran, chloroform and dimethyl-formamide.

Table 3.2: WCA of porous poly(2-octyl cyanoacrylate) surface on different materials.

	Static WCA	Advacing WCA	Receding WCA
acrylic tape	161º	162º	157º
TLC plate (silica)	157º	163º	149º
polypropylene	162º	164º	152º
cotton gauze	162º	165º	145º
steel	159º	164º	151º
paper	155º	163º	141º
wood	157º	165º	143º

3.3.6 Summary

In summary, a novel, fast and convenient "paint-like" method for coating surfaces with a superhydrophobic porous polymer film is demonstrated. By using commercially available and biocompatible 2-octyl cyanoacrylate as a monomer and water/ethanol mixture as both the porogen and initiator, a variety of different substrates could be made superhydrophobic within seconds. The method does not require complex equipment, air-free atmosphere, harsh conditions and can be applied to surfaces of complex non-flat geometries. The method shows good reproducibility and the obtained superhydrophobic surface is stable for at least several weeks in the outdoor environment. I expect that this low-cost, fast and convenient method will find numerous applications in a variety of research and industrial areas.

4. Conclusions and outlook

This PhD work describes three projects aimed at the improvement of existing or development and investigation of new ways to control surface chemical functionality, surface topography or hydrophobicity spatially and/or temporally. The first part focuses on the UV control of dopamine (DA) polymerization and polydopamine deposition. The second part deals with reversible surface functionalization and patterning based on photodynamic disulfide exchange, and finally, a facile method to generate superhydrophobic surfaces on different substrates is presented.

In the first part, it was hypothesized that DA polymerization could be triggered by reactive oxygen species (ROS) formed under UV irradiation, thus enabling UV control of DA polymerization. It was found that UV irradiation could significantly accelerate DA polymerization, and could trigger DA polymerization under acidic and neutral pH where DA polymerization without UV is inhibited. By cooperation with an antioxidant, sodium ascorbate, well controlled DA polymerization in basic solutions was also demonstrated. UV controlled DA polymerization was applied for surface coating, and polyDA patterns were obtained both on smooth and rough surfaces.

In the second part, disulfide functionality was introduced onto porous HEMA-EDMA surface. The obtained disulfide surface could react with other disulfides through a disulfide exchange reaction under UV irradiation. It was shown that the exchange reaction was very fast and reversible. Different disulfide surface could be obtained by the modification of the surface with a new disulfide. It was also shown that the process was perfectly reversible. Rewritable patterns were successfully obtained by applying a photomask during modification. Peptides and proteins could be patterned on the disulfide surface, and rewritable superhydrophobic/superhydrophilic patterns were demonstrated.

Finally, I employed the anionic polymerization of cyanoacrylates and polymerization induced phase separation to form porous superhydrophobic coatings. Cyanoacrylates are known to easily undergo anionic polymerization, which cannot be stopped by radical inhibitors such as oxygen. The approach to form porous surface is based on creating a liquid film of an alkyl cyanoacrylate on a substrate followed by treating the film with aqueous ethanol. This treatment initiates polymerization of the cyanoacrylate and simultaneously triggers phase separation leading to the formation of a highly porous poly(alkyl cyanoacrylate) film strongly adhered to the substrate. Stable superhydrophobic surfaces were

obtained by this method and the method was successfully applied on different materials with different shapes.

Despite the progress, there are also challenges in each project, which need to be resolved in the future. For UV triggered DA polymerization project, the polymerization speed needs to be improved, the mechanism of UV initiation and SA inhibition should be better understood, and more applications should be tested. For the disulfide surface project, the stability of the surface should be investigated, more application of the method should be present. For polycyanoacrylate surface project, currently the mechanical strength of the obtained superhydrophobic polymer layer is quite low because of its porous structure. Possible solutions include the use of a cyanoacrylate crosslinker and optimization of the porous structure.

The methods developed in this thesis can be potentially applied in the field of surface modification for different purposes. For example, UV controlled DA polymerization can be applied in industrial fabrication of polydopamine coatings under more controlled conditions; it can also be employed in research to control the kinetics of DA polymerization to understand the detailed mechanism of DA polymerization. The disulfide-based photo-reversible surface modification can be employed to form reusable surface and patterns for different applications such as reversible ink printing device. It can also be used for closing or opening microfluidic channels *in-situ* or to manipulate the cell environment *in-situ*. Polycyanoacrylate based superhydrophobic surfaces can be used to make superhydrophobic surface on different materials to simply transform them to superhydrophobic, it can be a potential method for superhydrophobic coatings in our daily life.

5. References

(1) Arnold, R. M.; Patton, D. L.; Popik, V. V; Locklin, J. *Acc. Chem. Res.* **2014**, *47*, 2999.

(2) Govindarajan, T.; Shandas, R. *Polymers* **2014**, *6*, 2309.

(3) Ata, M. S.; Liu, Y.; Zhitomirsky, I. *RSC Adv.* **2014**, *4*, 22716.

(4) Meyers, S. R.; Grinsta, M. W. *Chem. Rev.* **2012**, 1615.

(5) Kingshott, P.; Andersson, G.; McArthur, S. L.; Griesser, H. J. *Curr. Opin. Chem. Biol.* **2011**, *15*, 667.

(6) Ye, Q.; Zhou, F.; Liu, W. *Chem. Soc. Rev.* **2011**, *40*, 4244.

(7) Rana, D.; Matsuura, T. *Chem. Rev.* **2010**, *110*, 2448.

(8) Bélanger, D.; Pinson, J. *Chem. Soc. Rev.* **2011**, *40*, 3995.

(9) Ercole, F.; Davis, T. P.; Evans, R. a. *Polym. Chem.* **2010**, *1*, 37.

(10) Prakash, S.; Karacor, M. B.; Banerjee, S. *Surf. Sci. Rep.* **2009**, *64*, 233.

(11) Darmanin, T.; Taffin de Givenchy, E.; Amigoni, S.; Guittard, F. *Adv. Mater.* **2013**, *25*, 1378.

(12) Ionov, L.; Synytska, A. *Phys. Chem. Chem. Phys.* **2012**, *14*, 10497.

(13) Verho, T.; Bower, C.; Andrew, P.; Franssila, S.; Ikkala, O.; Ras, R. H. a. *Adv. Mater.* **2011**, *23*, 673.

(14) Zhang, L.; Zhao, N.; Xu, J. *J. Adhes. Sci. Technol.* **2014**, *28*, 769.

(15) Drelich, J.; Chibowski, E.; Meng, D. D.; Terpilowski, K. *Soft Matter* **2011**, *7*, 9804.

(16) Tettey, K. E.; Dafinone, M. I.; Lee, D. *Mater. Express* **2011**, *1*, 89.

(17) Manna, U.; Broderick, A. H.; Lynn, D. M. *Adv. Mater.* **2012**, *24*, 4291.

(18) Haensch, C.; Hoeppener, S.; Schubert, U. S. *Chem. Soc. Rev.* **2010**, *39*, 2323.

(19) Wasserberg, D.; Nicosia, C.; Tromp, E. E.; Subramaniam, V.; Huskens, J.; Jonkheijm, P. *J. Am. Chem. Soc.* **2013**, *135*, 3104.

(20) Glinel, K.; Thebault, P.; Humblot, V.; Pradier, C. M.; Jouenne, T. *Acta Biomater.* **2012**, *8*, 1670.

(21) Bright, F. V; Pagliaro, M. *Acc. Chem. Res.* **2014**, *47*, 678.

(22) Lee, H.; Lee, B. P.; Messersmith, P. B. *Nature* **2007**, *448*, 338.

(23) Wong, T.-S.; Kang, S. H.; Tang, S. K. Y.; Smythe, E. J.; Hatton, B. D.; Grinthal, A.; Aizenberg, J. *Nature* **2011**, *477*, 443.

(24) Sureshkumar, M.; Siswanto, D. Y.; Chen, Y.-C.; Lee, C.-K.; Wang, M.-J. *J. Polym. Sci. Part B Polym. Phys.* **2013**, *51*, 303.

(25) Li, Z. F.; Ruckenstein, E. *Synth. Met.* **2002**, *129*, 73.

(26) Kotsuchibashi, Y.; Wang, Y.; Kim, Y.-J.; Ebara, M.; Aoyagi, T.; Narain, R. *ACS Appl. Mater. Interfaces* **2013**, *5*, 10004.

(27) He, L.; Fullenkamp, D. E.; Rivera, J. G.; Messersmith, P. B. *Chem. Commun.* **2011**, *47*, 7497.

(28) Chen, L.; Wang, W.; Su, B.; Wen, Y.; Li, C.; Zhou, Y.; Li, M.; Al, C. E. T. *ACS Nano* **2014**, *8*, 744.

(29) Lim, H. S.; Han, J. T.; Kwak, D.; Jin, M.; Cho, K. *J. Am. Chem. Soc.* **2006**, *128*, 14458.

(30) Tian, D.; Song, Y.; Jiang, L. *Chem. Soc. Rev.* **2013**, *42*, 5184.

(31) Nie, Z.; Kumacheva, E. *Nat. Mater.* **2008**, *7*, 277.

(32) Zhou, X.; Boey, F.; Huo, F.; Huang, L.; Zhang, H. *Small* **2011**, *7*, 2273.

(33) Geissler, M.; Xia, Y. *Adv. Mater.* **2004**, *16*, 1249.

(34) Palleau, E.; Morales, D.; Dickey, M. D.; Velev, O. D. *Nat. Commun.* **2013**, *4*, 2257.

(35) Yang, S.; Lei, Y. *Nanoscale* **2011**, *3*, 2768.

(36) Lei, Y.; Yang, S.; Wu, M.; Wilde, G. *Chem. Soc. Rev.* **2011**, *40*, 1247.

(37) Hook, a L.; Voelcker, N. H.; Thissen, H. *Acta Biomater.* **2009**, *5*, 2350.

(38) Juang, J.-Y.; Bogy, D. B. *Microsyst. Technol.* **2005**, *11*, 950.

(39) Di, C.; Davide, F. A. M.; Amaldo, D.; Sberveglieri, G.; Nelli, P.; Faglia, G.; Perego, C. *Sensors Actuators B Chem.* **1995**, *25*, 801.

(40) Hau, W. L. W.; Trau, D. W.; Sucher, N. J.; Wong, M.; Zohar, Y. *J. Micromechanics Microengineering* **2003**, *13*, 272.

(41) You, I.; Yun, N.; Lee, H. *Chemphyschem* **2013**, *14*, 471.

(42) Zahner, D.; Abagat, J.; Svec, F.; Fréchet, J. M. J.; Levkin, P. a. *Adv. Mater.* **2011**, *23*, 3030.

(43) Chien, H.-W.; Tsai, W.-B. *Acta Biomater.* **2012**, *8*, 3678.

(44) Sun, K.; Xie, Y.; Ye, D.; Zhao, Y.; Cui, Y.; Long, F.; Zhang, W.; Jiang, X. *Langmuir* **2012**, *28*, 2131.

(45) Luo, D.; Sun, X. W.; Dai, H. T.; Liu, Y. J.; Yang, H. Z.; Ji, W. *Appl. Phys. Lett.* **2009**, *95*, 151115.

(46) Chan, C.-M.; Ko, T.-M.; Hiraoka, H. *Surf. Sci. Rep.* **1996**, *24*, 1.

(47) Ruckenstein, E.; Li, Z. F. *Adv. Colloid Interface Sci.* **2005**, *113*, 43.

(48) Lin, J.; Siddiqui, J. A.; Ottenbrite, R. M. *Polym. Adv. Technol.* **2001**, *292*, 285.

(49) Feng, W.; Li, L.; Ueda, E.; Li, J.; Heißler, S.; Welle, A.; Trapp, O.; Levkin, P. a. *Adv. Mater. Interfaces* **2014**, *1*, 1400269.

(50) Rostovtsev, V. V; Green, L. G.; Fokin, V. V; Sharpless, K. B. *Angew. Chemie Int. Ed.* **2002**, *41*, 2596.

(51) Deng, X.; Mammen, L.; Vollmer, D. *Science* **2012**, *502*, 67.

(52) Lyu, S. C.; Zhang, Y.; Lee, C. J. *Chem. Mater.* **2003**, *15*, 3294.

(53) Chen, W.; Mccarthy, T. J. *Macromolecules* **1997**, *30*, 78.

(54) Tsubota, T.; Tanii, S.; Ishida, T.; Nagata, M.; Matsumoto, Y. *Diam. Relat. Mater.* **2005**, *14*, 608.

(55) Roy, D.; Knapp, J. S.; Guthrie, J. T.; Perrier, S. *Biomacromolecules* **2008**, *9*, 91.

(56) Matyjaszewski, K.; Dong, H.; Jakubowski, W.; Pietrasik, J.; Kusumo, A. *Langmuir* **2007**, *23*, 4528.

(57) Mosiewicz, K. A.; Kolb, L.; van der Vlies, A. J.; Martino, M. M.; Lienemann, P. S.; Hubbell, J. A.; Ehrbar, M.; Lutolf, M. P. *Nat. Mater.* **2013**, *12*, 1072.

(58) Li, J.; Li, L.; Du, X.; Feng, W.; Welle, A.; Trapp, O. *Nano Lett.* **2015**, *15*, 675.

(59) Petersen, S. B.; Kold di Gennaro, A.; Neves-Petersen, M. T.; Skovsen, E.; Parracino, A. *Appl. Opt.* **2010**, *49*, 5344.

(60) Li, L.; Li, J.; Du, X.; Welle, A.; Grunze, M.; Trapp, O.; Levkin, P. A. *Angew. Chem. Int. Ed.* **2014**, *53*, 3835.

(61) DeForest, C. A.; Polizzotti, B. D.; Anseth, K. S. *Nat. Mater.* **2009**, *8*, 659.

(62) Lowe, A. B.; Hoyle, C. E.; Bowman, C. N. *J. Mater. Chem.* **2010**, *20*, 4745.

(63) Hong, C.; You, Y.; Pan, C. *Chem. Mater.* **2005**, *17*, 2247.

(64) Junkers, T. *Eur. Polym. J.* **2015**, *62*, 273.

(65) Gruendling, T.; Oehlenschlaeger, K. K.; Frick, E.; Glassner, M.; Schmid, C.; Barner-Kowollik, C. *Macromol. Rapid Commun.* **2011**, *32*, 807.

(66) Chen, R. T.; Marchesan, S.; Evans, R. A.; Styan, K. E.; Such, G. K.; Postma, A.; Mclean, K. M.; Muir, B. W.; Caruso, F. *Biomacromolecules* **2012**, *13*, 889.

(67) Pauloehrl, T.; Delaittre, G.; Bruns, M.; Meißler, M.; Börner, H. G.; Bastmeyer, M.; Barner-Kowollik, C. *Angew. Chemie Int. Ed.* **2012**, *51*, 9181.

(68) Orski, S. V.; Poloukhtine, A. A.; Arumugam, S.; Mao, L.; Popik, V. V.; Locklin, J. *J. Am. Chem. Soc.* **2010**, *132*, 11024.

(69) Song, W.; Wang, Y.; Qu, J.; Madden, M. M.; Lin, Q. *Angew. Chemie Int. Ed.* **2008**, *47*, 2832.

(70) Hideg, E.; Barta, C.; Kálai, T.; Vass, I.; Hideg, K.; Asada, K. *Plant Cell Physiol.* **2002**, *43*, 1154.

(71) Yu, C.; Parikh, a. N.; Groves, J. T. *Adv. Mater.* **2005**, *17*, 1477.

(72) Koo, G.-H.; Jang, J. *Fibers Polym.* **2009**, *9*, 674.

(73) Rostovtsev, V. V; Green, L. G.; Fokin, V. V; Sharpless, K. B. *Soft Matter* **2007**, *3*, 168.

(74) Berkowski, K. L.; Plunkett, K. N.; Yu, Q.; Moore, J. S. *J. Chem. Educ.* **2005**, *82*, 1365.

(75) Lai, Y.; Pan, F.; Xu, C.; Fuchs, H.; Chi, L. *Adv. Mater.* **2013**, *25*, 1682.

(76) Salaita, K.; Wang, Y.; Mirkin, C. a. *Nat. Nanotechnol.* **2007**, *2*, 145.

(77) Tortorich, R.; Choi, J. W. *Nanomaterials* **2013**, *3*, 453.

(78) Blawas, A. S.; Reichert, W. M. *Biomaterials* **1998**, *19*, 595.

(79) Ganesan, R.; Yoo, S. Y.; Choi, J. H.; Lee, S. Y.; Kim, J. B. *J. Mater. Chem.* **2008**, *18*, 703.

(80) Kim, Y. K.; Ryoo, S. R.; Kwack, S. J.; Min, D. H. *Angew. Chemie Int. Ed.* **2009**, *48*, 3507.

(81) Jang, K.; Sato, K.; Mawatari, K.; Konno, T.; Ishihara, K.; Kitamori, T. *Biomaterials* **2009**, *30*, 1413.

(82) Zhu, R.; Ebner, A.; Kastner, M.; Preiner, J.; Howorka, S.; Hinterdorfer, P. *Chemphyschem* **2009**, *10*, 1478.

(83) Bandara, N.; Zeng, H.; Wu, J. *J. Adhes. Sci. Technol.* **2013**, *27*, 2139.

(84) Lee, B. P.; Messersmith, P. B.; Israelachvili, J. N.; Waite, J. H. *Annu. Rev. Mater. Res.* **2011**, *41*, 99.

(85) Lee, H.; Dellatore, S. M.; Miller, W. M.; Messersmith, P. B. *Science* **2007**, *318*, 426.

(86) Sileika, T. S.; Kim, H. Do; Maniak, P.; Messersmith, P. B. *ACS Appl. Mater. Interfaces* **2011**, *3*, 4602.

(87) Kang, S. M.; Hwang, N. S.; Yeom, J.; Park, S. Y.; Messersmith, P. B.; Choi, I. S.; Langer, R.; Anderson, D. G.; Lee, H. *Adv. Funct. Mater.* **2012**, *22*, 2949.

(88) Zhang, L.; Wu, J.; Wang, Y.; Long, Y.; Zhao, N.; Xu, J. *J. Am. Chem. Soc.* **2012**, *134*, 9879.

(89) Dreyer, D. R.; Miller, D. J.; Freeman, B. D.; Paul, D. R.; Bielawski, C. W. *Chem. Sci.* **2013**, *4*, 3796.

(90) Müller, M.; Kessler, B. *Langmuir* **2011**, *27*, 12499.

(91) Swift, J. a. *Int. J. Cosmet. Sci.* **2009**, *31*, 143.

(92) Dreyer, D. R.; Miller, D. J.; Freeman, B. D.; Paul, D. R.; Bielawski, C. W. *Langmuir* **2012**, *28*, 6428.

(93) Liebscher, J.; Mrówczyński, R.; Scheidt, H. a; Filip, C.; Hădade, N. D.; Turcu, R.; Bende, A.; Beck, S. *Langmuir* **2013**, *29*, 10539.

(94) Della Vecchia, N. F.; Avolio, R.; Alfè, M.; Errico, M. E.; Napolitano, A.; d'Ischia, M. *Adv. Funct. Mater.* **2013**, *23*, 1331.

(95) Kim, H. W.; McCloskey, B. D.; Choi, T. H.; Lee, C.; Kim, M.-J.; Freeman, B. D.; Park, H. B. *ACS Appl. Mater. Interfaces* **2013**, *5*, 233.

(96) Ouyang, R.; Lei, J.; Ju, H. *Chem. Commun.* **2008**, 5761.

(97) Wei, Q.; Zhang, F.; Li, J.; Li, B.; Zhao, C. *Polym. Chem.* **2010**, *1*, 1430.

(98) Lee, H.; Scherer, N. F.; Messersmith, P. B. *Proc. Natl. Acad. Sci.* **2006**, *103*, 12999.

(99) Catron, N. D.; Lee, H.; Messersmith, P. B. *Biointerphases* **2006**, *1*, 134.

(100) Flanigan, C. M.; Crosby, A. J.; Shull, K. R. *Macromolecules* **1999**, *32*, 7251.

(101) Flanigan, C. M.; Shull, K. R. *Langmuir* **1999**, *15*, 4966.

(102) Moser, J.; Punchihewa, S.; Infelta, P. P.; Gratzel, M. *Langmuir* **1991**, 3012.

(103) Chen, L. X.; Liu, T.; Thurnauer, M. C.; Csencsits, R.; Rajh, T. *J. Phys. Chem. B* **2002**, *106*, 8539.

(104) Rajh, T.; Chen, L. X.; Lukas, K.; Liu, T.; Thurnauer, M. C.; Tiede, D. M. *J. Phys. Chem. B* **2002**, *106*, 10543.

(105) Dalsin, J. L.; Lin, L.; Tosatti, S.; Vo, J.; Textor, M.; Messersmith, P. B. *Langmuir* **2005**, *21*, 640.

(106) Rodrigueaz, R.; Blesa, M. A.; Regazzoni, A. E. *J. Colloid Interface Sci.* **1996**, *177*, 122.

(107) Chen, Q.; Jia, Y.; Liu, S.; Mogilevsky, G.; Kleinhammes, A.; Wu, Y.; Hill, C.; Carolina, N. *J. Phys. Chem. C* **2008**, *112*, 17331.

(108) Ball, V.; Frari, D.; Michel, M.; Buehler, M. J.; Toniazzo, V.; Singh, M. K.; Gracio, J.; Ruch, D. *Bionanoscience* **2011**, *2*, 16.

(109) Ball, V.; Del Frari, D.; Toniazzo, V.; Ruch, D. *J. Colloid Interface Sci.* **2012**, *386*, 366.

(110) Bernsmann, F.; Ball, V.; Addiego, F.; Ponche, A.; Michel, M.; Gracio, J. J. D. A.; Toniazzo, V.; Ruch, D. *Langmuir* **2011**, 2819.

(111) Jiang, J.; Zhu, L.; Zhu, L.; Zhu, B.; Xu, Y. *Langmuir* **2011**, *27*, 14180.

(112) Bernsmann, F.; Ponche, A.; Ringwald, C.; Hemmerle, J.; Raya, J.; Bechinger, B.; Voegel, J.; Schaaf, P.; Ball, V. *J. Phys. Chem. C* **2009**, 8234.

(113) Ball, V.; Gracio, J.; Vila, M.; Singh, M. K.; Metz-Boutigue, M. H.; Michel, M.; Bour, J.; Toniazzo, V.; Ruch, D.; Buehler, M. J. *Langmuir* **2013**, *29*, 12754.

(114) Yan, J.; Yang, L.; Lin, M. F.; Ma, J.; Lu, X.; Lee, P. S. *Small* **2013**, *9*, 596.

(115) Choi, Y. J.; Jin, H. M.; Kim, B. H.; Kim, J. Y.; Kim, S. O. *Appl. Mech. Mater.* **2012**, *229-231*, 2749.

(116) Sureshkumar, M.; Siswanto, D. Y.; Lee, C. K. *J. Mater. Chem.* **2010**, *20*, 6948.

(117) Xu, H.; Shi, X.; Ma, H.; Lv, Y.; Zhang, L.; Mao, Z. *Appl. Surf. Sci.* **2011**, *257*, 6799.

(118) Sureshkumar, M.; Lee, P. N.; Lee, C. K. *J. Mater. Chem.* **2011**, *21*, 12316.

(119) Black, K. C. L.; Sileika, T. S.; Yi, J.; Zhang, R.; Rivera, J. G.; Messersmith, P. B. *Small* **2013**, 169.

(120) Shalev, T.; Gopin, A.; Bauer, M.; Stark, R. W.; Rahimipour, S. *J. Mater. Chem.* **2012**, *22*, 2026.

(121) Kuang, J.; Messersmith, P. B. *Langmuir* **2012**, *28*, 7258.

(122) Ko, E.; Yang, K.; Shin, J.; Cho, S. *Biomacromolecules* **2013**, *14*, 3202.

(123) Rivera, J. G.; Messersmith, P. B. *J. Sep. Sci.* **2012**, *35*, 1514.

(124) Liu, Q.; Huang, B.; Huang, A. *J. Mater. Chem. A* **2013**, *1*, 11970.

(125) Yang, K.; Lee, J. S.; Kim, J.; Lee, Y. Bin; Shin, H.; Um, S. H.; Kim, J. B.; Park, K. I.; Lee, H.; Cho, S. W. *Biomaterials* **2012**, *33*, 6952.

(126) Yuan, C.; Liu, Q.; Chen, H.; Huang, A. *RSC Adv.* **2014**, *4*, 41982.

(127) Rodriguez-Emmenegger, C.; Preuss, C. M.; Yameen, B.; Pop-Georgievski, O.; Bachmann, M.; Mueller, J. O.; Bruns, M.; Goldmann, A. S.; Bastmeyer, M.; Barner-Kowollik, C. *Adv. Mater.* **2013**, *25*, 6123.

(128) Sun, K.; Song, L.; Xie, Y.; Liu, D.; Wang, D.; Wang, Z.; Ma, W.; Zhu, J.; Jiang, X. *Langmuir* **2011**, *27*, 5709.

(129) Kang, K.; Lee, S.; Kim, R.; Choi, I. S.; Nam, Y. *Angew. Chemie Int. Ed.* **2012**, *51*, 13101.

(130) You, I.; Kang, S. M.; Lee, S.; Cho, Y. O.; Kim, J. B.; Lee, S. B.; Nam, Y. S.; Lee, H. *Angew. Chemie Int. Ed.* **2012**, *51*, 6126.

(131) Ni, K.; Lu, H.; Wang, C.; Black, K. C. L.; Wei, D.; Ren, Y.; Messersmith, P. B. *Biotechnol. Bioeng.* **2012**, *109*, 2970.

(132) Ryou, M. H.; Kim, J.; Lee, I.; Kim, S.; Jeong, Y. K.; Hong, S.; Ryu, J. H.; Kim, T. S.; Park, J.-K.; Lee, H.; Choi, J. W. *Adv. Mater.* **2013**, *25*, 1571.

(133) Preuss, C. M.; Tischer, T.; Rodriguez-Emmenegger, C.; Zieger, M. M.; Bruns, M.; Goldmann, A. S.; Barner-Kowollik, C. *J. Mater. Chem. B* **2014**, *2*, 36.

(134) Preuss, C. M.; Zieger, M. M.; Rodriguez-Emmenegger, C.; Zydziak, N.; Trouillet, V.; Goldmann, A. S.; Barner-Kowollik, C. *ACS Macro Lett.* **2014**, *3*, 1169.

(135) Ham, H. O.; Liu, Z.; Lau, K. H. A.; Lee, H.; Messersmith, P. B. *Angew. Chem. Int. Ed.* **2011**, *50*, 732.

(136) Tian, Y.; Cao, Y.; Wang, Y.; Yang, W.; Feng, J. *Adv. Mater.* **2013**, *25*, 2980.

(137) Li, R.; Parvez, K.; Hinkel, F.; Feng, X.; Müllen, K. *Angew. Chem. Int. Ed.* **2013**, *52*, 5535.

(138) Mason, H. S.; Allen, B.; Ingram, D. J. E. *Arch. Biochem. Biophys.* **1960**, *86*, 225.

(139) Ju, K. Y.; Lee, Y.; Lee, S.; Park, S. B.; Lee, J. K. *Biomacromolecules* **2011**, *12*, 625.

(140) Ai, K.; Liu, Y.; Ruan, C.; Lu, L.; Lu, G. M. *Adv. Mater.* **2013**, *25*, 998.

(141) Farnad, N.; Farhadi, K.; Voelcker, N. H. *Water, Air, Soil Pollut.* **2012**, *223*, 3535.

(142) Ma, Z.; Jia, X.; Hu, J.; Zhang, G.; Zhou, F.; Liu, Z.; Wang, H. *Langmuir* **2013**, *29*, 5631.

(143) Cui, J.; Yan, Y.; Such, G. K.; Liang, K.; Ochs, C. J.; Postma, A.; Caruso, F. *Biomacromolecules* **2012**, *13*, 2225.

(144) Rozkiewicz, D. I.; Ravoo, B. J.; Reinhoudt, D. N. *Langmuir* **2005**, *21*, 6337.

(145) Schofield, W. C. E.; McGettrick, J.; Bradley, T. J.; Badyal, J. P. S.; Przyborski, S. *J. Am. Chem. Soc.* **2006**, *128*, 2280.

(146) Gandavarapu, N. R.; Azagarsamy, M. A.; Anseth, K. S. *Adv. Mater.* **2014**, *26*, 2521.

(147) Tauk, L.; Schröder, A. P.; Decher, G.; Giuseppone, N. *Nat. Chem.* **2009**, *1*, 649.

(148) Fakhari, F.; Rokita, S. E. *Nat. Commun.* **2014**, *5*, 5591.

(149) Arumugam, S.; Popik, V. V. *J. Am. Chem. Soc.* **2012**, *134*, 8408.

(150) Harris, L. G.; Schofield, W. C. E.; Doores, K. J.; Davis, B. G.; Badyal, J. P. S. *J. Am. Chem. Soc.* **2009**, *131*, 7755.

(151) Muthukrishnan, G.; Roberts, C. A.; Chen, Y.; Zahn, J. D.; Hancock, W. O.; Park, U. V; Pennsyl, V. *Nano Lett.* **2004**, *4*, 2127.

(152) Gevrek, T. N.; Ozdeslik, R. N.; Sahin, G. S.; Yesilbag, G.; Mutlu, S.; Sanyal, A. *Macromol. Chem. Phys.* **2012**, *213*, 166.

(153) Yang, L.; Gomez-casado, A.; Young, J. F.; Nguyen, H. D.; Cabanas-dane, J.; Huskens, J.; Brunsveld, L.; Jonkheijm, P. *J. Am. Chem. Soc.* **2012**, *134*, 19199.

(154) Sato, T.; Amamoto, Y.; Ohishi, T.; Higaki, Y.; Takahara, A.; Otsuka, H. *Polymer* **2014**, *55*, 4586.

(155) Jin, J.; Liu, J.; Lian, X.; Sun, P.; Zhao, H. *RSC Adv.* **2013**, *3*, 7023.

(156) Roucoules, V.; Schofield, W. C. E.; Badyal, J. P. S. *J. Mater. Chem.* **2011**, *21*, 16153.

(157) Zhang, Y.; Ren, L.; Tu, Q.; Wang, X.; Liu, R.; Li, L.; Wang, J.; Liu, W.; Xu, J.; Wang, J. *Anal. Chem.* **2011**, *83*, 9651.

(158) Sato, T.; Amamoto, Y.; Yamaguchi, H.; Ohishi, T.; Takahara, A.; Otsuka, H. *Polym. Chem.* **2012**, *3*, 3077.

(159) Li, X. M.; Reinhoudt, D.; Crego-Calama, M. *Chem. Soc. Rev.* **2007**, *36*, 1350.

(160) Yan, Y. Y.; Gao, N.; Barthlott, W. *Adv. Colloid Interface Sci.* **2011**, *169*, 80.

(161) Ma, M.; Hill, R. M. *Curr. Opin. Colloid Interface Sci.* **2006**, *11*, 193.

(162) Sun, T.; Feng, L.; Gao, X.; Jiang, L. *Acc. Chem. Res.* **2005**, *38*, 644.

(163) Ma, M.; Hill, R. M.; Rutledge, G. C. *J. Adhes. Sci. Technol.* **2008**, *22*, 1799.

(164) Roach, P.; Shirtcliffe, N. J.; Newton, M. I. *Soft Matter* **2008**, *4*, 224.

(165) Feng, L.; Li, S.; Li, Y.; Li, H.; Zhang, L.; Zhai, J.; Song, Y.; Liu, B.; Jiang, L.; Zhu, D. *Adv. Mater.* **2002**, *14*, 1857.

(166) Feng, X. J.; Jiang, L. *Adv. Mater.* **2006**, *18*, 3063.

(167) Koch, K.; Barthlott, W. *Philos. Trans. A. Math. Phys. Eng. Sci.* **2009**, *367*, 1487.

(168) Gao, X.; Jiang, L. *Nature* **2004**, *432*, 36.

(169) Callies, M.; Quéré, D. *Soft Matter* **2005**, *1*, 55.

(170) Ma, M.; Hill, R. M.; Rutledge, G. C. *Nat. Mater.* **2003**, *2*, 457.

(171) Li, Y.; Li, L.; Sun, J. *Angew. Chemie Int. Ed.* **2010**, *49*, 6129.

(172) Ogihara, H.; Xie, J.; Okagaki, J.; Saji, T. *Langmuir* **2012**, *28*, 4605.

(173) Shirtcliffe, N. J.; McHale, G.; Newton, M. I.; Chabrol, G.; Perry, C. C. *Adv. Mater.* **2004**, *16*, 1929.

(174) Guo, Z.-G.; Fang, J.; Hao, J.; Liang, Y.; Liu, W. *Chemphyschem* **2006**, *7*, 1674.

(175) Hwang, H. S.; Lee, S. B.; Park, I. *Mater. Lett.* **2010**, *64*, 2159.

(176) Kinoshita, H.; Ogasahara, A.; Fukuda, Y.; Ohmae, N. *Carbon* **2010**, *48*, 4403.

(177) Lau, K. K. S.; Bico, J.; Teo, K. B. K.; Chhowalla, M.; Amaratunga, G. a. J.; Milne, W. I.; McKinley, G. H.; Gleason, K. K. *Nano Lett.* **2003**, *3*, 1701.

(178) Latthe, S. S.; Imai, H.; Ganesan, V.; Rao, a. V. *Appl. Surf. Sci.* **2009**, *256*, 217.

(179) Barthlott, W.; Allee, M.; Bonn, D.; Neinhuis, C.; Walzel, P. *Langmuir* **2005**, *21*, 956.

(180) Zhang, Y. L.; Wang, J. N.; He, Y.; He, Y.; Xu, B. B.; Wei, S.; Xiao, F. S. *Langmuir* **2011**, *27*, 12585.

(181) Pennisi, C. P.; Zachar, V.; Gurevich, L.; Member, A. P.; Struijk, J. J. *Conf. Proc. IEEE Eng. Med. Bio. Soc.* **2010**, *2010*, 3804.

(182) Zhang, L.; Zhao, N.; Li, X.; Long, Y.; Zhang, X.; Xu, J. *Soft Matter* **2011**, *7*, 4050.

(183) Kato, S.; Sato, A. *J. Mater. Chem.* **2012**, *22*, 8613.

(184) Levkin, P. A; Svec, F.; Frechet, J. M. J. *Adv. Funct. Mater.* **2009**, *19*, 1993.

(185) Du, X.; Li, J. S.; Li, L. X.; Levkin, P. a. *J. Mater. Chem. A* **2013**, *1*, 1026.

(186) Ensikat, H. J.; Ditsche-Kuru, P.; Neinhuis, C.; Barthlott, W. *Beilstein J. Nanotechnol.* **2011**, *2*, 152.

(187) Kirihara, M.; Asai, Y.; Ogawa, S.; Noguchi, T.; Hatano, A.; Hirai, Y. *Synthesis* **2007**, *2007*, 3286.

(188) Hunger, M.; Weitkamp, J. *Angew. Chemie Int. Ed.* **2001**, *40*, 2954.

(189) Klamt, A.; Ag, B.; V, D. Le. *J. Phys. Chem.* **1996**, *100*, 3349.

(190) Biver, T. *Appl. Spectrosc. Rev.* **2012**, *47*, 272.

(191) Young, T. *Philos. Trans. R. Soc. London* **1805**, *95*, 65.

(192) Tian, Y.; Su, B.; Jiang, L. *Adv. Mater.* **2014**, *26*, 6872.

(193) Berg, J. M.; Eriksson, L. G. T.; Claesson, P. M.; Borve, K. G. N. *Langmuir* **1994**, *10*, 1225.

(194) Vogler, E. A. *Adv. Colloid Interface Sci.* **1998**, *74*, 69.

(195) Mittal, K. *J. Adhes. Sci. Technol.* **2008**, *22*, 231.

(196) Wenzel, R. N. *Ind. Eng. Chem.* **1936**, *28*, 988.

(197) Cassie, A. B. D.; Baxter, S. *Trans. Faraday Soc.* **1944**, *40*, 546.

(198) Suga, M.; Asahina, S.; Sakuda, Y.; Kazumori, H.; Nishiyama, H.; Nokuo, T.; Alfredsson, V.; Kjellman, T.; Stevens, S. M.; Cho, H. S.; Cho, M.; Han, L.; Che, S.; Anderson, M. W.; Schüth, F.; Deng, H.; Yaghi, O. M.; Liu, Z.; Jeong, H. Y.; Stein, A.; Sakamoto, K.; Ryoo, R.; Terasaki, O. *Prog. Solid State Chem.* **2014**, *42*, 1.

(199) Search, H.; Journals, C.; Contact, A.; Iopscience, M.; Address, I. P. *Br. J. Appl. Phys.* **1955**, *6*, 391.

(200) Benninghoven, A. *Angew. Chemie Int. Ed.* **1994**, *33*, 1023.

(201) Malmberg, P.; Nygren, H. *Proteomics* **2008**, *8*, 3755.

(202) Custance, O.; Perez, R.; Morita, S. *Nat. Nanotechnol.* **2009**, *4*, 803.

(203) Binnig, G.; Quate, C. F.; Gerber, C. *Phys. Rev. Lett.* **1986**, *56*, 930.

(204) Cappella, B.; Dietler, G. *Surf. Sci. Rep.* **1999**, *34*, 1.

(205) Seah, M. P. *Vacuum* **1984**, *34*, 463.

(206) Seah, M. P. *Surf. Interface Anal.* **1980**, *2*, 222.

(207) Mckelvy, M. L.; Britt, T. R.; Davis, B. L.; Gillie, J. K.; Graves, F. B.; Lentz, L. A. *Anal. Chem.* **1998**, *2700*, 119R.

(208) Owen-Reece, H.; Smith, M.; Elwell, C. E.; Goldstone, J. C. *Br. J. Anaesth.* **1999**, *82*, 418.

(209) Naumann, D. *Appl. Spectrosc. Rev.* **2001**, *36*, 239.

(210) Adar, F.; Geiger, R.; Noonan, J. *Appl. Spectrosc. Rev.* **1997**, *32*, 45.

(211) Petry, R.; Schmitt, M.; Popp, J. *Chemphyschem* **2003**, *4*, 14.

(212) Feng, W.; Li, L.; Ueda, E.; Li, J.; Heißler, S.; Welle, A.; Trapp, O.; Levkin, P. a. *Adv. Mater. Interfaces* **2014**, *1*, 1400269.

(213) Ade, H. *Eur. Phys. J. Spec. Top.* **2012**, *208*, 305.

(214) Chason, E.; Mayer, T. M. *Crit. Rev. Solid State Mater. Sci.* **1997**, *22*, 1.

(215) Yasaka, M. *Rigaku J.* **2010**, *26*, 1.

(216) Parratt, L. G. *Phys. Rev.* **1954**, *95*, 359.

(217) Elwing, H. *Biomaterials* **1998**, *19*, 397.

(218) Tolmachev, V. A. *J. Optial Technol.* **1999**, *66*, 596.

(219) Pop-Georgievski, O.; Popelka, Š.; Houska, M.; Chvostová, D.; Proks, V.; Rypáček, F. *Biomacromolecules* **2011**, *12*, 3232.

(220) Synowicki, R. A. *Thin Solid Films* **1998**, *313-314*, 394.

(221) Kurella, A.; Dahotre, N. B. *J. Biomater. Appl.* **2005**, *20*, 5.

(222) Lichter, J. a.; Van Vliet, K. J.; Rubner, M. F. *Macromolecules* **2009**, *42*, 8573.

(223) Sperling, R. a; Parak, W. J. *Philos. Trans. A. Math. Phys. Eng. Sci.* **2010**, *368*, 1333.

(224) Kango, S.; Kalia, S.; Celli, A.; Njuguna, J.; Habibi, Y.; Kumar, R. *Prog. Polym. Sci.* **2013**, *38*, 1232.

(225) Deng, X.; Friedmann, C.; Lahann, J. *Angew. Chem. Int. Ed.* **2011**, *50*, 6522.

(226) Kim, B. H.; Lee, D. H.; Kim, J. Y.; Shin, D. O.; Jeong, H. Y.; Hong, S.; Yun, J. M.; Koo, C. M.; Lee, H.; Kim, S. O. *Adv. Mater.* **2011**, *23*, 5618.

(227) Yang, S. H.; Kang, S. M.; Lee, K.-B.; Chung, T. D.; Lee, H.; Choi, I. S. *J. Am. Chem. Soc.* **2011**, *133*, 2795.

(228) Zhu, B.; Edmondson, S. *Polymer* **2011**, *52*, 2141.

(229) Ding, X.; Yang, C.; Lim, T. P.; Hsu, L. Y.; Engler, A. C.; Hedrick, J. L.; Yang, Y.-Y. *Biomaterials* **2012**, *33*, 6593.

(230) Chien, H. W.; Kuo, W. H.; Wang, M. J.; Tsai, S. W.; Tsai, W. B. *Langmuir* **2012**, *28*, 5775.

(231) Wei, Q.; Yu, B.; Wang, X.; Zhou, F. *Macromol. Rapid Commun.* **2014**, n/a.

(232) Black, K. C. L.; Liu, Z.; Messersmith, P. B. *Chem. Mater.* **2011**, *23*, 1130.

(233) Hong, S.; Lee, J. S.; Ryu, J.; Lee, S. H.; Lee, D. Y.; Kim, D.-P.; Park, C. B.; Lee, H. *Nanotechnology* **2011**, *22*, 494020.

(234) Ren, Y.; Rivera, J. G.; He, L.; Kulkarni, H.; Lee, D.-K.; Messersmith, P. B. *BMC Biotechnol.* **2011**, *11*, 63.

(235) Ku, S. H.; Lee, J. S.; Park, C. B. *Langmuir* **2010**, *26*, 15104.

(236) Frei, B. *Am. J. Med.* **1994**, *97*, 5S.

(237) Sabbahi, S.; Alouini, Z.; Jemli, M.; Boudabbous, A. *Water Sci. Technol.* **2008**, *58*, 1047.

(238) Bhattacharjee, S. *J. Bot.* **2012**, *2012*, 1.

(239) Darr, D.; Combs, S.; Dunston, S.; Manning, T.; Pinnell, S. *Br. J. Dermatol.* **1992**, *127*, 247.

(240) Simpson, J. A.; Cheeseman, K. H.; Smith, S. E.; Dean, R. T. **1988**, *254*, 519.

(241) Halliwell, B.; Gutteridget, J. M. C. *Biochem. J.* **1984**, *219*, 1.

(242) Du, X.; Li, L.; Li, J.; Yang, C.; Frenkel, N.; Welle, A.; Heissler, S.; Nefedov, A.; Grunze, M.; Levkin, P. A. *Adv. Mater.* **2014**, *47*, 8029.

(243) Bradshaw, M. P.; Prenzler, P. D.; Scollary, G. R. *Electroanalysis* **2002**, *14*, 546.

(244) Peng, Z.; Duncan, B.; Pocock, K. F.; Sefton, M. a. *Aust. J. Grape Wine Res.* **1998**, *4*, 127.

(245) Špalek, O.; Balej, J.; Paseka, I. *J. Chem. Soc. Faraday Trans.* **1982**, *78*, 2349.

(246) Smith, A. F.; Nicoll, W. D. *Ind. Eng. Chem.* **1955**, *47*, 2548.

(247) Kim, E.; Liu, Y.; Baker, C. J.; Owens, R.; Xiao, S.; Bentley, W. E.; Payne, G. F. **2011**, 880.

(248) Yang, J.; Cohen Stuart, M. a; Kamperman, M. *Chem. Soc. Rev.* **2014**, *43*, 8271.

(249) Morais, S.; Marco-Moles, R.; Puchades, R.; Maquieira, An. *Chem. Commun.* **2006**, 2368.

(250) Lee, E. J.; Chan, E. W. L.; Yousaf, M. N. *Chembiochem* **2009**, *10*, 1648.

(251) Bryant, S. J.; Cuy, J. L.; Hauch, K. D.; Ratner, B. D. *Biomaterials* **2007**, *28*, 2978.

(252) Hensarling, R. M.; Doughty, V. A.; Chan, J. W.; Patton, D. L. *J. Am. Chem. Soc.* **2009**, *131*, 14673.

(253) Pauloehrl, T.; Delaittre, G.; Winkler, V.; Welle, A.; Bruns, M.; Börner, H. G.; Greiner, A. M.; Bastmeyer, M.; Barner-Kowollik, C. *Angew. Chemie Int. Ed.* **2012**, *51*, 1071.

(254) Wang, Y.; Song, W.; Hu, W. J.; Lin, Q. *Angew. Chemie Int. Ed.* **2009**, *48*, 5330.

(255) Wu, H.; Ge, J.; Uttamchandani, M.; Yao, S. Q. *Chem. Commun.* **2011**, *47*, 5664.

(256) Arumugam, S.; Orski, S. V.; Locklin, J.; Popik, V. V. *J. Am. Chem. Soc.* **2012**, *134*, 179.

(257) Edahiro, J. I.; Sumaru, K.; Tada, Y.; Ohi, K.; Takagi, T.; Kameda, M.; Shinbo, T.; Kanamori, T.; Yoshimi, Y. *Biomacromolecules* **2005**, *6*, 970.

(258) Khetan, S.; Burdick, J. A. *Biomaterials* **2010**, *31*, 8228.

(259) DeForest, C. A.; Anseth, K. S. *Angew. Chemie Int. Ed.* **2012**, *51*, 1816.

(260) Rowan, S. J.; Cantrill, S. J.; Cousins, G. R. L.; Sanders, J. K. M.; Stoddart, J. F. *Angew. Chemie Int. Ed.* **2002**, *41*, 898.

(261) Whitesides, G. M.; Lees, W. J. *J. Org. Chem.* **1993**, *58*, 642.

(262) Fernandes, P. A.; Ramos, M. J. *Chem. A Eur. J.* **2004**, *10*, 257.

(263) Otsuka, H.; Nagano, S.; Kobashi, Y.; Maeda, T.; Takahara, A. *Chem. Commun.* **2010**, *46*, 1150.

(264) Amamoto, Y.; Otsuka, H.; Takahara, A.; Matyjaszewski, K. *Adv. Mater.* **2012**, *24*, 3975.

(265) Mclean, C. J. *J Accid. Emerg. Med.* **1997**, *14*, 40.

(266) Toriumi, D. M. M. D.; O'Grady, K.; Desai, D. M. D.; Bagal, A. M. D. *Plast. Reconstr. Surg.* **1998**, *102*, 2209.

(267) Matyjaszewski, K.; Coca, S.; Gaynor, S. G.; Wei, M.; Woodworth, B. E. *Macromolecules* **1998**, *31*, 5967.

(268) Serbutoviez, C.; Kloosterboer, J. G.; Boots, H. M. J.; Touwslager, F. J. *Macromolecules* **1996**, *29*, 7690.

(269) Sáfrány, Á.; Beiler, B.; László, K.; Svec, F. *Polymer* **2005**, *46*, 2862.

(270) Li, J. S.; Ueda, E.; Nallapaneni, A.; Li, L. X.; Levkin, P. A. *Langmuir* **2012**, *28*, 8286.

(271) Miwa, M.; Nakajima, A.; Fujishima, A.; Hashimoto, K. *Langmuir* **2000**, *16*, 5754.

(272) Chen, Z.; Guo, Y.; Fang, S. *Surf. Interface Anal.* **2010**, *42*, 1.

(273) Shu, D. G.; Morris, S. C.; Zhang, Z. F.; Liu, J. N.; Han, J.; Ling, C.; Zhang, L.; Zhang, X. L.; Yasui, K.; Li, Y. *Science* **2000**, *299*, 1377.